KONINKLIJK NEDERLANDS METEOROLOGISCH INSTITUUT

WETENSCHAPPELIJK RAPPORT
SCIENTIFIC REPORT

W.R. 81 - 1

F.T.M. Nieuwstadt

THE NOCTURNAL BOUNDARY LAYER
THEORY AND EXPERIMENTS

De Bilt 1981

Publikatienummer: K.N.M.I. W.R. 81-1 (FM)

Koninklijk Nederlands Meteorologisch Instituut,
Fysisch Meteorologisch onderzoek,
Postbus 201,
3730 AE De Bilt,
Nederland.

U.D.C.: 551.510.522

VRIJE UNIVERSITEIT TE AMSTERDAM

The Nocturnal Boundary Layer

Theory and Experiments

ACADEMISCH PROEFSCHRIFT

ter verkrijging van de graad van doctor in
de wiskunde en natuurwetenschappen aan
de Vrije Universiteit te Amsterdam,
op gezag van de rector magnificus
dr. H. Verheul,
hoogleraar in de faculteit der wiskunde en natuurwetenschappen,
in het openbaar te verdedigen
op woensdag 25 maart 1981 te 13.30 uur
in het hoofdgebouw der universiteit, De Boelelaan 1105

door

Franciscus Theodorus Marie Nieuwstadt
geboren te 's Gravenhage

K.N.M.I.
De Bilt

Promotor : Prof. dr. ir. H. Tennekes

Coreferent: Prof. dr. ir. J.A. Steketee
Dr. J.T.F. Zimmerman

Aan Marion

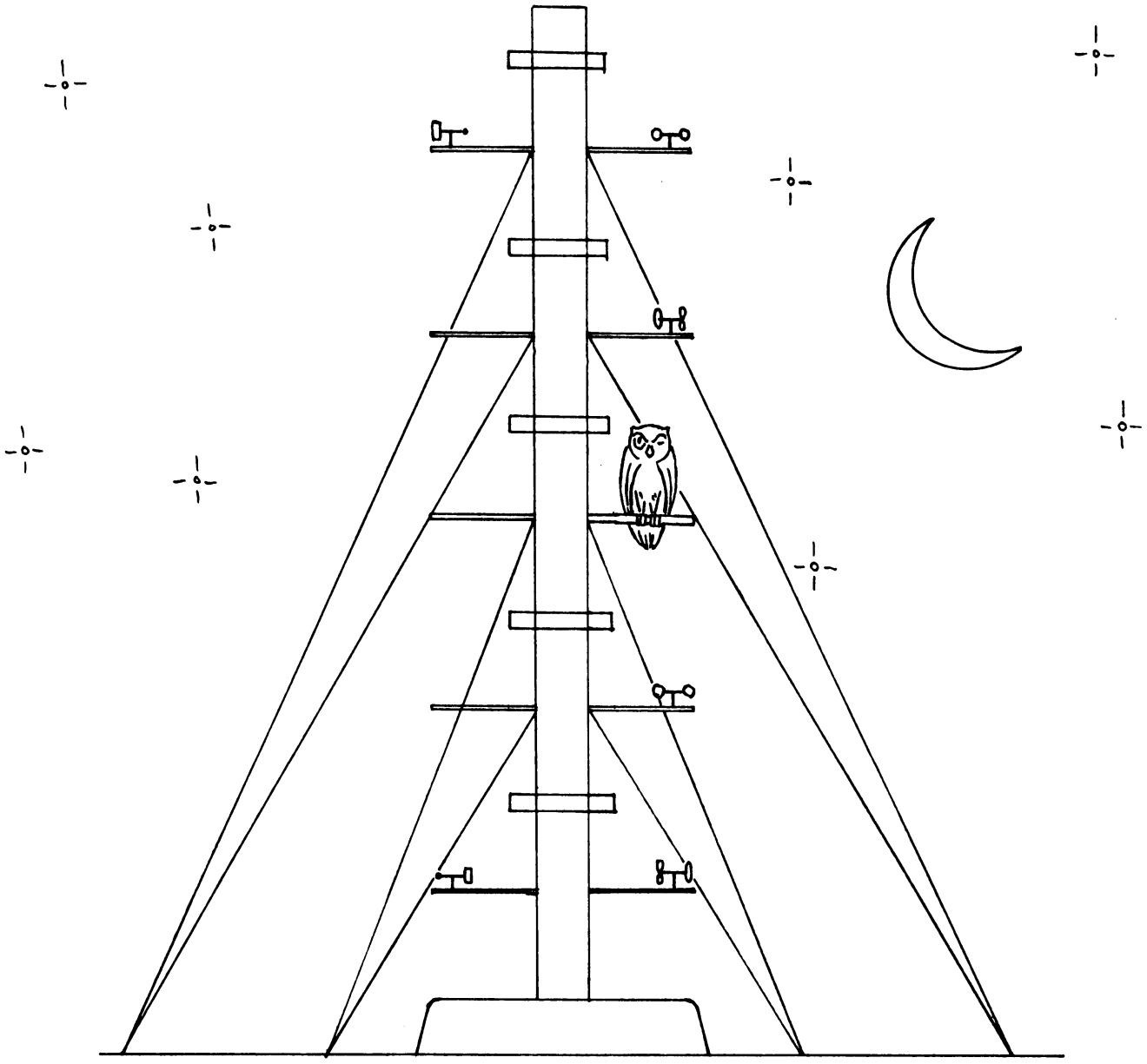

Contents

Voorwoord

Dit proefschrift vormt een afspiegeling van vier jaar onderzoek. Enerzijds is dit onderzoek uitvoerbaar geweest dankzij de faciliteiten die het KNMI mij heeft geboden. Dit geldt in het bijzonder de meteorologische meetmast te Cabauw, waarvan de meetresultaten de basis van mijn onderzoek hebben gevormd. Anderzijds is een dergelijk onderzoek alleen mogelijk door hetzij directe, hetzij indirecte, steun van vele collega's. Deze plaats biedt een uitstekende gelegenheid om iedereen te bedanken.

Met name bedank ik

mijn promotor, Henk Tennekes, die naast zijn veeleisende taak als direkteur Wetenschappelijk Onderzoek, deze studie heeft begeleid. In het bijzonder ben ik je dankbaar voor de uitgebreide en minutieuze kritiek op manuscripten, die niet alleen tot grotere redactionele vaardigheid leidde, maar vooral de diepgang van mijn onderzoek vergrootte;

al mijn collega's van de afdeling Fysische Meteorologie die via vele discussies tot mijn werk hebben bijgedragen: met name Han van Dop, Ad Driedonks, Aad van Ulden en Jaap Wisse;

de coreferenten prof. dr. ir. J.A. Steketee en dr. J.T.F. Zimmerman voor de tijd die zij aan mijn proefschrift hebben besteed. Het doet mij speciaal genoegen dat ik de hoogleraar, bij wie ik ben afgestudeerd, in een volgend stadium van mijn opleiding heb mogen betrekken;

al mijn collega's die rechtstreeks betrokken zijn geweest bij de controle en kwaliteitsbewaking van de Cabauw metingen;

de buitendienst en de medewerkers van Insa zonder wier inzet een meetproject als Cabauw niet mogelijk is;

de leden van de sectie FM voor assistentie op velerlei gebied;

de secretaresses van FM, wiens vak(type)werk hier is te bewonderen;

de tekenkamer, waarvan de uitstekende producten de volgende bladzijden sieren;

de drukkerij, die het vermenigvuldigen van dit proefschrift in prettige samenwerking heeft uitgevoerd.

I. General Introduction

This dissertation focuses on a specific branch of meteorology: the study of air flow in the lower part of the atmosphere, usually referred to as the atmospheric boundary layer. Its dominant processes are transport of heat, humidity and momentum between the surface and the overlying free atmosphere. As such the boundary layer acts as a source or sink of these quantities in the atmospheric circulation.

Apart from serving a direct meteorological interest, the boundary layer is also of particular significance because almost every human activity takes place in it. The results of this study are thus useful in a variety of fields such as aviation, air pollution dispersion, agriculture, wind engineering, wind energy, urban planning and air-sea interaction.

Our investigation is restricted to the boundary layer during the night. What may we expect in these conditions? To answer this question we start with a general description of meteorological phenomena in the atmospheric boundary layer.

Our point of departure is observation. The classical procedure in boundary-layer studies is to measure meteorological variables, such as temperature and wind, close to the ground. In recent years, however, observations at higher levels became available, creating a more complete picture of the atmospheric boundary layer.

An obvious method to obtain such observations is to extend the standard meteorological measurements along a mast. A good example is the meteorological mast near the village of Cabauw in the Netherlands. This mast has been operated by the Royal Netherlands Meteorological Institute since 1972. Here measurements are executed in the first 200 m of the atmospheric boundary layer. As we shall see in a later stage, these observations are in many cases sufficient to describe the basic structure of the nocturnal boundary layer.

Only very recently a new instrumental technique to probe the boundary layer was developed. Its principle of operation is based on the scattering of sound waves by temperature fluctuations.

Because of similarity with its electro-magnetic counterpart, the radar, this instrument is called Sodar (Sound detection and ranging). We shall use the Sodar primarily to measure the boundary-layer height. The observations from the mast and the Sodar constitute the basis of our study of the nocturnal boundary layer.

Before we start with a discussion on what these observations show, a few remarks should be devoted to atmospheric measurements in general. Many physical processes are simultaneously at work in the atmosphere. This makes the atmosphere a poor equivalent of a laboratory, where generally only one selected physical process is observed at the same time. On the other hand, theoretical studies of the atmosphere commonly concentrate on a small number of dominant processes. These are usually described in terms of idealized models. It must be clear that comparison of these models with atmospheric data leads unavoidably to scatter. Our results, especially in chapter III, corroborate that conclusion. This handicap of using atmospheric observations for comparison can only be compensated by careful interpretation.

One process apparent in all observations is the daily cycle. It is predominantly present in the boundary layer over a land surface, to which we shall restrict ourselves. The day-time boundary layer differs drastically from its night-time counterpart. To appreciate and understand the differences we shall describe the main characteristics of both boundary-layer types. As an additional restriction we assume clear sky conditions.

During the day-time the surface heated by the sun warms the adjacent air, which subsequently starts to rise. This process is known as convection; every glider pilot is familiar with it. Visible evidence of convection are the small cumulus clouds, which sometimes develop during the afternoon at the top of the boundary layer. Such an observation also enables us to estimate the height of the convective boundary layer to be ~1 km. Our mast observations in these conditions show that the wind is approximately constant with height. In other words, momentum is uniformly distributed across the boundary layer. The same goes for heat and humidity. Such distributions can only result from a strong vertical exchange. Inspection of the rapid dispersion of a chimney plume supports this statement.

During the night, however, the situation is reversed. The surface now cools due to radiation. The heat loss must partly be replenished by the atmosphere. This causes the development of an inversion, a condition when temperature increases with height. Profiles in the boundary layer are completely different from those in the day-time situation. Apart from an inversion mast observations also demonstrate that the wind changes considerably with height. The wind profile is non-uniform. Near the surface the wind is often light, while at the top of the boundary layer a strong wind prevails. Sodar observations estimate this top to be at a few hundred meters. The nocturnal boundary layer is thus relatively shallow. Its non-uniform profiles are symptoms of weak, vertical exchange. A chimney plume remains coherent for a long time.

So far for the mere observations. How to put them in physical terms? For that purpose we have to introduce two features of atmospheric fluid dynamics: turbulence and stratification.

Turbulent flow means that air motions are irregular in space and time, as opposed to smooth or laminar flow. The main property of turbulence is its effectiveness in transporting flow properties. As such it is far more effective than molecular processes. Within the atmospheric boundary layer turbulence is responsible for all transport of heat, humidity and momentum, the main transports in the boundary layer. Now that we have established the importance of turbulence, we continue by investigating how it is produced. Two production processes are significant: mechanical production and buoyancy production. The mechanism of the former is instability of a velocity gradient in large Reynolds number flow. These conditions are fulfilled in the boundary layer. Viscosity plays a minor role, which is equivalent to saying that the Reynolds number is large. A velocity gradient is present, because the surface retards the air flow above it. Mechanical production is thus always a source of turbulence in the atmospheric boundary layer. The other process, introduced as buoyancy production, is explained shortly.

Let us now turn to the second feature of atmospheric boundary-layer flow: stratification. By definition stratified flow is a flow affected significantly by the presence of density variations in a gravity field.

It manifests itself in the atmosphere by a temperature profile which deviates from the adiabatic or neutral profile amounting to $-1^{\circ}C$ per 100 m in dry conditions. Stratification has a profound influence on the structure of the boundary layer. Two cases must be distinguished: unstable and stable.

In an unstable atmosphere the temperature decreases faster with height than the neutral profile. The analogy in a liquid is a density profile which increases upward. Since denser liquid tends to sink any flow disturbance becomes unstable and is amplified. In terms of fluid motion this means that flow disturbances produce kinetic energy. The resulting energy is usually directly transformed into turbulence. This process we define as buoyancy production.

The opposite case, when the temperature decreases slower with height than the neutral profile, is called stable. Disturbances are attenuated. They consume energy because warm, lighter air is moved downward, while colder, denser air is carried up. The energy is taken from the turbulence, so that turbulence intensity decreases. This process is more appropriately referred to as buoyancy destruction.

Now we are ready to explain the observed characteristics of the day-time and night-time boundary layer in terms of the physical features mentioned above.

The day-time boundary layer is an example of the unstable case, because surface heating causes an unstable temperature profile. Flow disturbances, which in this case take the form of rising air motions, produce turbulent energy. Therefore, the unstable boundary layer is characterized by vigorous turbulence. This explains the large vertical exchange that we noticed in our observations.

We characterized the nocturnal boundary layer by a temperature inversion. Such a temperature profile clearly means that conditions are stable. The turbulence intensity is now small due to buoyancy destruction, which explains the small vertical exchange we have observed. But how is turbulence to survive in a stable boundary layer? The only source still remaining is mechanical production. We have seen that this type of production depends on shear. Consequently a strong vertical wind gradient must be present in the stable boundary layer. It is only possible to maintain such a velocity gradient over a limited depth. This explains the shallowness of the nocturnal boundary

layer found from our Sodar observations.

The general picture of the nocturnal boundary layer, the subject of this dissertation, now emerges: a shallow layer with small turbulence intensity sustained by a delicate balance between mechanical production and buoyancy destruction. The various aspects of the nocturnal boundary layer are the main subjects of the following chapters.

Chapter II presents a general discussion of the nocturnal boundary layer in terms of a numerical model. Our basic assumption in the model is horizontal homogeneity. This means that we neglect the contribution of horizontal transport to the rate of change of wind and temperature in the boundary layer. The only process taken into account is vertical, turbulent exchange.

Our model study shows that the wind and temperature profiles, measured along the mast, can only be simulated qualitatively. Good results, however, are obtained in predicting the height of the boundary layer.

The boundary-layer height represents a useful parameter in many problems. It gives, for instance, the depth to which contaminants can mix in the boundary layer: the so-called mixing height. The wind profile depends on the boundary-layer height because usually a wind speed maximum develops at the top of the boundary layer. The boundary-layer height is also frequently used as a scaling parameter in non-dimensional plots (cf chapter III). Therefore, we have further concentrated our study on the nocturnal boundary-layer height.

Our numerical results of chapter II seem to indicate that the boundary-layer height approaches a stationary value. This issue is pursued in chapter III. There we investigate whether the nocturnal boundary layer can be characterized as stationary. For that purpose a theoretical expression for the steady-state boundary-layer height is derived and compared with our Sodar observations. The thecretical expression is not confirmed. The conclusion must be that the stable boundary layer is not in a steady state but is continuously developing.

In chapter III we also discuss some problems related to the unambiguous definition of the stable boundary-layer height. It is here defined as the depth of the shallow turbulent layer. This definition must be distinguished from the widely used notion that the

boundary-layer height is connected to the inversion in the temperature profile. The differences between both definitions are discussed in more detail in chapter IV, where we consider in particular the influence of long-wave radiation on the temperature profile.

The question concerning the non-stationary boundary layer is taken up again in chapter V. Here we derive a time-dependent equation for the boundary-layer height. The point of departure in the derivation is the ratio of mechanical production to buoyancy destruction, stressed above as the processes affecting turbulence in the nocturnal boundary layer. The result takes the form of a linear relaxation equation. It predicts that the boundary-layer height converges to an equilibrium value. However, the time scale of this relaxation process becomes large: of the order of ten hours. This means that the boundary-layer height develops very slowly.

The main conclusions which result from these studies, can now be summarized as follows:

- Expressions for the boundary-layer height based on the hypothesis of stationary conditions do not agree with observations.
- Radiation influences the temperature profile directly, leading to a higher value of the inversion height compared with the turbulent layer thickness.
- The quasi-stationary behavior of the boundary-layer height apparent from our observations, must be attributed to the large time scale of the evolution process.

Finally a few editorial remarks. Chapters II-V have been individually published or submitted as journal articles. The general line should be apparent from this introduction. Some redundancy, however, in the subject matter of these chapters is unavoidable. There are also minor differences in notation from one chapter to the next. To underline the individual identity of each chapter we have used separate numbering of pages, equations and figures. At the end we have included chapter VI. It contains the mast and Sodar observations, on which our study is based.

II. The nocturnal boundary layer: a case study compared with model calculations[†]

Abstract

A case study of nocturnal boundary layer development is presented. The data include observations of turbulence and of profiles of wind and temperature. The measurements were done along a 200 m high meteorological mast.

The observations are interpreted in terms of the results of a one-dimensional boundary-layer model. The model is derived from the full set of equations governing the evolution of the nocturnal boundary layer by neglecting advection. The validity of this approximation is discussed.

From a comparison of observations and calculated results it follows that the influence of advection is important especially in the upper part of the boundary layer. Nevertheless we find that important characteristics of the nocturnal boundary layer such as its height can be reasonably well simulated by a one-dimensional model.

[†]Published in J. Appl. Meteor., 1979, 18, 1397-1405 with A.G.M. Driedonks as co-author.

1. Introduction

The boundary layer during a clear night contrasts with the convective boundary layer in the daytime. In the latter, turbulence is produced by buoyancy leading to large turbulent fluxes and to rapid vertical exchange. This means that the convective boundary layer is primarily locally determined. Advection plays a secondary role.

In the nocturnal boundary layer radiational cooling of the surface leads to a stable temperature gradient. Turbulence is then suppressed by negative buoyancy. In a shallow layer near the surface turbulence of small intensity can be maintained by mechanical production. Because vertical exchange in this layer is now small, advection quickly becomes important, as we will discuss in section 2.

A full solution of the nocturnal boundary layer including advection will lead to a 3-D mesoscale model. An adequate description of advection in such a model requires a high horizontal resolution resulting in a large computational effort. However, the results of such a complicated model will still be questionable, primarily because at the moment there are no initial and boundary conditions available of a compatible resolution.

To simulate the nocturnal boundary layer we have used here a one-dimensional model in which advection is neglected. With such a model vertical profiles are calculated as a function of time. The computation time is negligible compared to that required for the solution of a 3-D model. However, the usefulness of this model, in which terms known to be important are left out, must follow from a direct comparison with observations. This will be one of the major topics of this paper.

Above the boundary layer, where turbulent fluxes are zero, the solution of a one-dimensional model reduces to

the well-known inertial oscillation of the wind vector (Blackadar, 1957). Models based on this oscillation (Thorpe and Guymer, 1977) can explain the low-level wind maximum which is frequently observed in the nocturnal boundary layer. For the boundary layer itself models have been proposed by e.g. Delage (1974), Blackadar (1976), and Brost and Wyngaard (1978). Here we largely follow the approach taken by Delage (1974) as described in section 3.

For the night of 8/9 February 1975 a fairly complete set of data has been measured along the 200 m high meteorological mast at Cabauw in the Netherlands. Details of the experiments are given in section 4.

In section 5 and 6 these observations are discussed in terms of the characteristics of the nocturnal boundary layer. The measurements are compared with the results of our one-dimensional boundary layer model. The deviations between observed and calculated results can be attributed to the neglected advection terms; in our case mainly temperature advection. However, we will show that the major features of the nocturnal boundary layer are reasonably well represented by our simple model.

2. Equations of motion; the assumption of horizontal homogeneity

If the atmosphere is assumed to be in hydrostatic equilibrium, the continuity and momentum equations for the mean flow in the atmospheric boundary layer read (Busch, 1973)

$$\frac{\partial w}{\partial z} = - \nabla_H \cdot \underset{\sim}{u}_H \qquad (1)$$

$$\frac{\partial \underset{\sim}{u}_H}{\partial t} + \underset{\sim}{u}_H \cdot \nabla_H \underset{\sim}{u}_H + w \frac{\partial \underset{\sim}{u}_H}{\partial z} = \qquad (2)$$

$$- f \underset{\sim}{n} \times (\underset{\sim}{u}_H - \underset{\sim}{u}_g - \underset{\sim}{u}_{th}) + \frac{\partial}{\partial z} \underset{\sim}{\tau}_H / \rho ,$$

with $\underset{\sim}{u}_H = (u,v)$, $\nabla_H = (\frac{\partial}{\partial x}, \frac{\partial}{\partial y})$ and $\underset{\sim}{\eta} \times \underset{\sim}{u}_H = (-v,u)$, where $\underset{\sim}{u}_H$ is the horizontal mean wind vector, with components u in the x-direction and v in the y-direction, w is the vertical velocity component, $\underset{\sim}{\eta}$ the unit vector in the vertical direction, f is the Coriolis parameter, ρ the air density and $\underset{\sim}{\tau}_H$ the horizontal Reynolds stress vector (viscous stresses are neglected). The geostrophic wind at ground level $\underset{\sim}{u}_g$ and the thermal wind $\underset{\sim}{u}_{th}$ are defined by the equations

$$\underset{\sim}{u}_g = -\frac{1}{f}\,\underset{\sim}{\eta} \times \frac{1}{\rho}\,\nabla_H p_o \qquad (3)$$

$$\underset{\sim}{u}_{th} = \frac{g}{fT} \int_o^z \underset{\sim}{\eta} \times \nabla_H \theta \, dz, \qquad (4)$$

where p_o is the pressure at ground level; g is the gravitational acceleration and T is the absolute temperature in the boundary layer.
The potential temperature θ is governed by

$$\frac{\partial \theta}{\partial t} + \underset{\sim}{u}_H \cdot \nabla_H \theta + w \frac{\partial \theta}{\partial z} = -\frac{\partial}{\partial z} \frac{H}{\rho c_p}, \qquad (5)$$

in which H is the sensible heat flux and c_p the specific heat at constant pressure. Radiative terms have been neglected.

In order to simplify these equations of motion we will investigate whether the advection terms in (2) and (5) can be neglected in nocturnal boundary layers. A typical nocturnal boundary layer is characterized by a height h ~ 200 m, a cooling rate at ground level of ~1°C/hr and a geostrophic wind of ~10 m/s. The geostrophic velocity deficit, defined as $|\underset{\sim}{u}_H - \underset{\sim}{u}_g|$, is taken as 3 m/s. These values are comparable with our measurements discussed in section 6.

If all the terms in equations (2) and (5) are scaled with these values, we find that horizontal advection can only be neglected if $|\nabla_H \underset{\sim}{u}| \ll 3 \times 10^{-5} s^{-1}$ and $|\nabla_H \theta| \ll 3 \times 10^{-5}$ °C m^{-1}. In that case the thermal wind can also be neglected. These restrictions on the horizontal gradients are usually not met in reality. Moreover, in regions with

strong vertical gradients (e.g. a sharp inversion) even small vertical motions will cause a large contribution to the vertical advection. Therefore we must conclude that the advection terms in (2) and (5) cannot be neglected at first hand.

This means, that strictly speaking the complete set of equations (1)-(5) must be solved in order to simulate the nocturnal boundary layer. In such a three-dimensional model the horizontal and vertical grid spacing are interdependent, when advection and vertical diffusion are treated with equal weight (Barr and Kreitzberg, 1975). Summarizing their argument we express the influence of advection and vertical exchange in (2) in the following schematic way

$$\frac{\partial \underset{\sim}{u}_H}{\partial t} \sim \frac{\underset{\sim}{V}}{t_a} + \frac{\underset{\sim}{V}}{t_d} \quad , \tag{6}$$

where $\underset{\sim}{V}$ is a characteristic velocity, t_a the time scale for advection and t_d the time scale for diffusion. The solution for (5) can be treated in a similar way. The time scales are connected to characteristic length scales, which we take proportional to the horizontal and vertical grid spacing: Δx, Δz. A straightforward estimate of the time scale is given by

$$t_a \sim \frac{\Delta x}{|\underset{\sim}{V}|} \; , \; t_d \sim \frac{\Delta z^2}{K} \; , \tag{7}$$

where K is the vertical exchange coefficient to be discussed in the next section. As the height of the nocturnal boundary layer is of the order of 200 m, we take Δz to be 30 m.

Further characteristic values for K and $|\underset{\sim}{V}|$ in this case are 0.5 $m^2 s^{-1}$ and 10 ms^{-1}, respectively. This means that t_a and t_d are of the same order of magnitude when Δx is ~20 km. When a wider spacing between horizontal grid points is chosen, t_a will increase or, following from (6), the vertical diffusion terms will dominate. The solution at each point will then be effectively given by a one-dimensional model, in which advection is neglected.

A full three-dimensional solution of (1)-(5) with a horizontal grid of 20 km quickly becomes impracticable, even for a moderately sized region. Additionally, initial and boundary conditions of a compatible horizontal resolution are not available, so that a complete solution of (1)-(5) is not yet possible. Instead we used a one-dimensional model despite its limitations. A direct comparison with observations, as given in section 6, will show which characteristics can still be adequately simulated with such a model.

3. Description of the model

Our one-dimensional boundary layer model is similar to the models developed by Delage (1974), Bodin (1976) and Yu (1977). A brief description will suffice here.

Under the assumption of horizontal homogeneity (1)-(5) reduce to

$$\frac{\partial \underset{\sim}{u}_H}{\partial t} = - f \underset{\sim}{\eta} \times (\underset{\sim}{u}_H - \underset{\sim}{u}_g) + \frac{\partial}{\partial z} \frac{\underset{\sim}{\tau}_H}{\rho} \qquad (8)$$

$$\frac{\partial \theta}{\partial t} = - \frac{\partial}{\partial z} \frac{H}{\rho c_p} . \qquad (9)$$

The turbulent fluxes are expressed in terms of the gradients by the following equations:

$$\frac{\underset{\sim}{\tau}_H}{\rho} = K_M \frac{\partial \underset{\sim}{u}_H}{\partial z} \qquad (10)$$

$$- \frac{H}{\rho c_p} = K_M \frac{\partial \theta}{\partial z} . \qquad (11)$$

The exchange coefficients $K_{M,H}$ have the form (Delage, 1974)

$$K_{M,H} = \ell_{M,H} \sqrt{c\, e} \quad , \qquad (12)$$

where $\ell_{M,H}$ are the length scales for momentum and heat flux respectively, e is the turbulent kinetic energy per unit mass and c is a non-dimensional constant. We need an additional equation for the kinetic energy; it reads (Delage, 1974)

$$\frac{\partial e}{\partial t} = \frac{\tau_H}{\rho} \cdot \frac{\partial u_H}{\partial z} + \frac{g}{T} \frac{H}{\rho c_p} + \frac{\partial}{\partial z} K_M \frac{\partial e}{\partial z} - \frac{(c'e)^{3/2}}{\ell_M} \quad . \qquad (13)$$

In the limit as $z \to 0$, (13) reduces to a balance between mechanical production and dissipation. Consistency between (12) and (13) then leads to the requirement that $c' = c$. Following Yu (1977) and Bodin (1976) we take $c = 0.2$.

The system of equations (8)-(13) is closed by specifying the length scales ℓ_M and ℓ_H. Yu (1977) has examined a number of expressions for the length scales. Both he and Djolov (1974) obtain good results with the following formulation:

$$\ell_{M,H}^{-1} = \frac{\Phi_{M,H}(z/L)}{kz} + \frac{f}{\alpha |u_g|} \quad , \qquad (14)$$

where α is a constant taken here as 4×10^{-4} (Delage, 1974). The specification for the dimensionless velocity and temperature gradients Φ_M and Φ_H is adopted from Businger et al. (1971). In order to be consistent with their results, the von Karman constant is taken as 0.35. The gradients in (14) are taken as a function of the local Obukhov-length L, which is given by

$$L = - \frac{T c_p}{kg} \frac{|\tau_H|^{3/2}}{\rho^2 H} \quad . \qquad (15)$$

In order to solve (8)-(13) boundary and initial conditions must be specified. The upper boundary conditions are given at an arbitrary height z_J far above the top of the nocturnal boundary layer. They read

$$\left.\begin{aligned} u_H &= u_g \\ \frac{\partial \theta}{\partial z} &= 0, \quad \frac{\partial e}{\partial z} = 0 \end{aligned}\right\} \text{ for } z = z_J . \qquad (16)$$

The conditions at the lowest calculation level z_1 are

$$\left.\begin{aligned} u_H &= \frac{\tau_H}{k\sqrt{\rho |\tau_H|}} \ln(z/z_o) \\ \theta &= \theta_o - 0.74 \frac{H}{k\rho c_p \sqrt{\frac{|\tau_H|}{\rho}}} \ln(z/z_o) \\ \frac{\partial e}{\partial z} &= 0 \end{aligned}\right\} \text{ for } z = z_1 . \qquad (17)$$

The first condition relates the stress to the velocity in a way that is consistent with (10), (12) and (14). It states that for small values of z the wind velocity must follow a logarithmic profile and that the velocity is parallel to the stress. The external parameter z_o in this equation is the roughness length. The second condition states that the temperature must follow a logarithmic law for small values of z consistent with (11), (12) and (14). The temperature θ_o at roughness height must be specified to describe the surface cooling. It may follow from measurements or it must result from a model in which the radiation processes near the earth's surface are treated. Here the former approach is used.

To obtain initial profiles for all variables we use the following procedure. Taking a neutral temperature profile, which is usually found at the beginning of the night, we run the model without changing external parameters and without temperature forcing until a nearly steady state is reached (small inertial oscillations in the solution remain present). This solution is then used as the initial condition. In this way a stable method of starting the calculations is obtained. However, the actual conditions at the beginning of the night might be far from stationary. This means that errors will be introduced due to the choice of initial conditions. In section 6 we will discuss these errors; we will show there that they might have a considerable influence on the solution at a later stage, especially at higher levels.

A solution to this system of equations is sought by applying Newton's method. The resulting linear set of equations is solved on a non-uniform grid $z_j (j = 1, ...J)$ by the box scheme. This is an implicit difference method particularly suited for parabolic equations (Keller, 1971). The grid size varies from 3 m near the surface to 400 m near the upper boundary. The time step is taken as 360 s.

4. Experimental data

The experimental data were obtained at the 200 m high meteorological mast at Cabauw in the Netherlands (Driedonks et al., 1978).

The profile measurements comprise the wind speed, wind direction and temperature (Table 1). Measurements of turbulence were carried out simultaneously at three levels: 20, 80 and 200 m. Wind fluctuations were measured by a trivane (Wieringa, 1967) and temperature fluctuations by fast-response thermocouples (Driedonks, et al., 1978). The sampling frequency was 1 Hz. From these data the turbulent momentum and heat fluxes (averaged over 30 min.) were obtained after removal of a linear trend in the data. The height of the turbulent boundary layer was monitored with the help of an acoustic sounder (Sodar).

Table 1

Continuously measured wind and temperature data at the 200 m mast at Cabauw, the Netherlands, for the period of February 1975.

element	instrument	height (m)	sampling time (s)	recording device
wind speed	cup anemometers	2, 10, 20, 40 80, 120, 160 200	120	paper tape
wind direction	wind vane	10, 80, 200	120	paper tape
temperature	ventilated thermocouples	2, 10, 20, 40 80, 120, 160, 200	120	paper tape
boundary-layer height	acoustic sounder	0-1000		facsimile recorder

For the measuring period the geostrophic wind was calculated from the pressure data at 19 meteorological stations in the Netherlands by a method based on principal component analysis of a time series of pressure data measured at these stations (Cats, 1977).

Measurements were performed during the night of 8/9 February 1975. Table 2 gives a summary of the data obtained during that night.

Table 2

Data set for the night-period 8/9 February 1975 (times in GMT, which is one hour earlier than local time).

Data set	Time-period
30 min. averaged mean profiles and acoustic sounder recording	14.30-03.00
30 min. averaged turbulence statistics and correlations	18.30-03.30
geostrophic wind	14.00-03.00

The synoptic situation showed a stationary high pressure area over central Europe leading at the experimental site to a prevailing southeasterly wind of approximately 10 m/s.

From the synoptic pressure distribution an estimate can be found for the vertical velocity w_h at the top of the boundary layer. First, we apply the operator $\nabla_h \times$ to both sides of (8). Then, after using (10) and the continuity equation (1), the equation for w_h becomes

$$w_h = \frac{K_M}{f} \left(\frac{\partial \zeta}{\partial z}\right)_{z = 0}, \qquad (18)$$

where $\zeta = \partial v_H/\partial x - \partial u_H/\partial y$ is the vertical component of the vorticity. In the derivation of (18) we assume that ζ is stationary, consistent with the meteorological situation.

The $(\partial\zeta/\partial z)_{z=0}$ is estimated as ζ_h/h where ζ_h is the vorticity at the top of the boundary and h the boundary-layer height. In our case the boundary layer height is 200 m (see section 6), which is approximately the height of the 1000 mbar plane. The ζ_h is calculated with the quasi-geostrophic approximation, which reads (Haltiner, 1971)

$$\zeta_h = \frac{g}{f} \nabla^2 z_h, \qquad (19)$$

where z_h is the height of the 1000 mbar plane and ∇^2 the Laplace operator. From the weather maps we estimate $\zeta_h \sim 3 \times 10^{-5}\ s^{-1}$. With a characteristic value of $K_M \sim 0.5\ m^2 s$ we then find $w_h \sim 10^{-3}$ m/s. Considering the error bounds of our estimation procedure this value does not differ significantly from zero. Therefore we will neglect the influence of the vertical velocity.

5. Consistency of closure assumptions

Since measurements of turbulent fluxes and mean profiles are available we can verify the consistency of the closure assumptions in our model. By substituting the observed values of τ_H, H, e, $\frac{\partial \underset{\sim}{u}_H}{\partial z}$ and $\frac{\partial \theta}{\partial z}$ into (10), (11) and (12) we can determine the observed values for the length scales $\ell_{M,H}$. These must be compared with the result of (14). A comparison for ℓ_M at 80 m is shown in Fig. 1. The results found at the 20 m measuring level are similar (200 m is excluded, because turbulent fluxes are practically zero there). A similar agreement between observed and calculated values is found for ℓ_H. From these results we conclude that the flux-gradient relationships (10), (11), (12) and (14) are consistent with our observations.

It is also useful to check for consistency in the value of the constant c in (12). As $c = \tau_H/(\rho e)$ for $z \to 0$ (Delage, 1974), we evaluate its value from our turbulence measurements at 20 m. An average value of 0.18 is found. This agrees well with the value 0.2 used in our model (section 3).

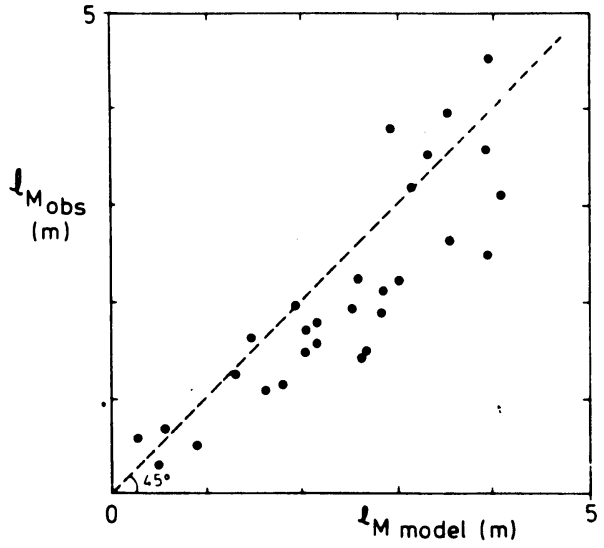

Fig. 1. The comparison between the observed ℓ_M and the ℓ_M following from Eq. 14 for a height of 80 m.

6. Results and discussion

In our observations the cooling of the air near the surface started at 14.30 GMT (15.30 local time). We take this as the beginning of the night. Sunset occured at 16.30 GMT.

The calculations were started at 14.30 GMT. The temperature profile along the mast was neutral at that time. The initial conditions were determined following the method described in section 3. We obtained the surface temperature θ_o, which is an external parameter in (17), from a logarithmic extrapolation of the measured temperature at 9 and 2 m. The roughness length z_o was taken as 0.2 m (Van Ulden et al., 1976).

Fig. 2 shows the observed and calculated heights of the nocturnal boundary layer. We define the boundary layer height in the model calculations as the height where the turbulent heat flux has decreased to 10% of its value at ground level. It is not clear whether the height where heat flux vanishes is completely equivalent to the boundary layer height found from the acoustic sounding registration. This equivalence has been discussed for the daytime boundary layer by Frisch and Clifford

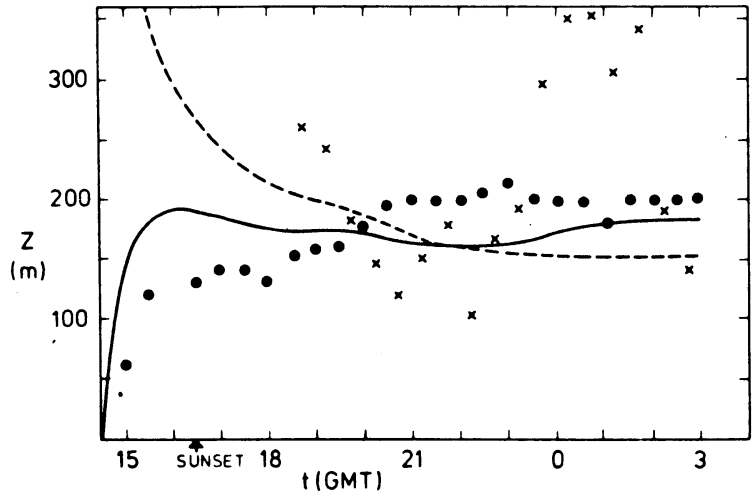

Fig. 2. The height of the nocturnal boundary layer as a function of time; • for observed boundary layer height; x for the height given by (20); —— for the height where the calculated heat flux decreases to 10% of its surface value; ---- for the height where the calculated stress decreases to 10% of its surface value.

(1974). However, the agreement between the observed and calculated values is reasonable.

In Fig. 2 we also give the height where the calculated stress decreases to 10% of its value at ground level. Brost and Wyngaard (1978) define the boundary layer height in this way. This height also approaches a stationary value comparable to the observed results.

Several simple parametric expressions for the stationary boundary-layer height were reviewed by Yu (1978). The most important is a similarity relation proposed by Zilitinkevitch (1975) and by Businger and Arya (1974). It reads

$$h^2 = 0.16 \frac{L}{f} \sqrt{\frac{|\underset{\sim}{\tau}_H|}{\rho}} , \qquad (20)$$

where both $\underset{\sim}{\tau}_H$ and L are evaluated in the surface layer ($z \to 0$). The constant 0.16 has been proposed by Brost and Wyngaard (1978). The results calculated with (20) are shown in Fig. 2. In this

case (20) poorly predicts the nocturnal boundary-layer height.

In Fig. 3 the calculated and observed potential temperatures at different levels are given as functions of time. The measured and calculated temperatures agree very well at 2 and 9 m. This is not surprising, because the forcing temperature

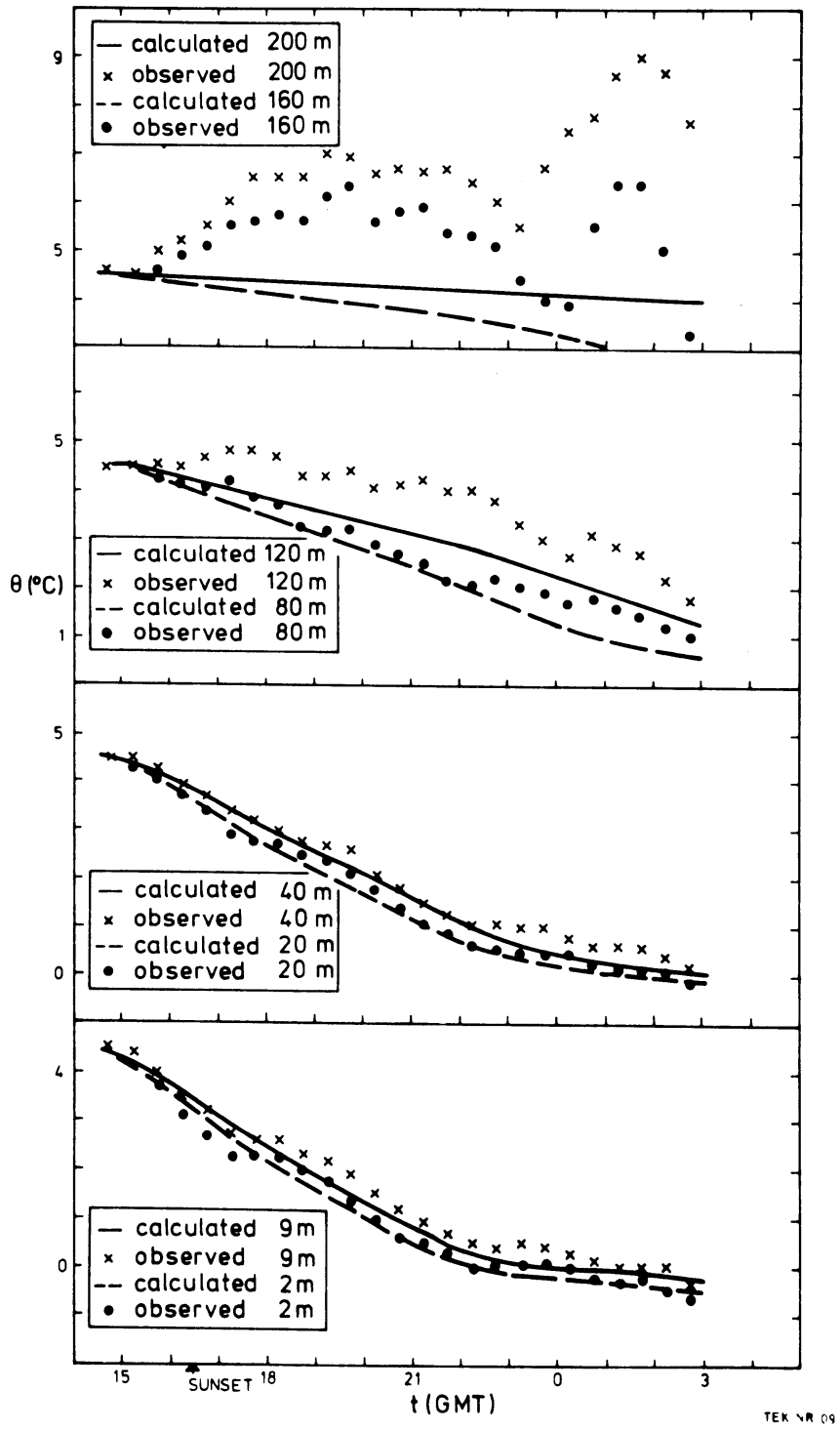

Fig. 3. Measured and calculated potential temperature as a function of time for six observation heights.

θ_o in the model is obtained from the measured values at these levels. Here the temperature decreases almost linearly till about 22.00 GMT and remains approximately constant after that time. This behavior seems to be inconsistent with the stationary boundary layer height found in Fig. 2, because according to Brost and Wyngaard (1978) the boundary layer height can only be truly stationary if there is a persistent constant cooling rate.

Temperature changes due to long wave radiation have been calculated following the method given by Elzasser and Culbertson (1960). They are given for some height intervals in Table 3. These results are based on the temperature and humidity profile measured along the mast, and on the data of the closest radiosonde launching. They show that the temperature change due to radiation is small inside the boundary layer.

Therefore the difference between model results and observations are caused primarily by neglecting the effects of advection, which were discussed in section 2. The influence of advection increases with height, because the turbulent fluxes and therefore

Table 3

Temperature changes due to long-wave radiation at 00.00 GMT.

Δh (m) height interval	$\frac{\partial \theta}{\partial t}$ (°C/s) temperature change in Δh
0-20	2.5×10^{-7}
20-80	1.1×10^{-5}
80-200	2.6×10^{-5}
200-500	-2.6×10^{-5}

the vertical exchange decreases with height (Barr and Kreitzberg, 1975). This effect is clearly visible in Fig. 3.

At 200 m the measurements show an average increase of $0.3^{\circ}C/hr$. Since this level is above the boundary layer, the temperature change can only be caused by advection. The horizontal advection can be estimated as follows. In the afternoon the potential temperature is uniform with height over a mixed layer of considerable depth. Therefore horizontal gradients in this layer can be obtained from surface data. In our case the horizontal gradient was calculated from the surface meteorological observations at 15.00 GMT to be $1 \times 10^{-5}\ ^{\circ}C\ m^{-1}$ with a southeasterly direction. As the influence of surface cooling during the night remains confined to the boundary layer which is less than 200 m, we assume that this horizontal gradient does persist above the nocturnal boundary layer. With a measured wind of ~10 m/s also with a southeasterly direction this results in an advective temperature change of $\sim 0.3^{\circ}C/hr$, in agreement with the mean temperature change at 200 m.

The wind speed as a function of time is shown in Fig. 4. The initial conditions for the model do not match the measurements indicating that a stationary neutral condition is not a suitable starting condition in this case. The initial conditions are very important for the solution of (8) at heights where during the night turbulent fluxes vanish (in this case 200 m). There the solution of the model equations is dominated by an inertial oscillation. The phase and amplitude of this oscillation follow directly from the difference between the initial wind vector and the geostrophic wind (Blackadar, 1957).

We have calculated such an inertial oscillation for the wind vector at 200 m starting from the measured value at 16.00 GMT (around sunset) and using a constant geostrophic wind of 10 m/s with a direction of 125°. The results are a wind maximum of 13.5 m/s at about 22.00 GMT and a wind speed equal to the geostrophic wind at about 01.30 GMT. The data of Fig. 4 show that this inertial oscillation describes the measured wind speeds at 200 m reasonably well.

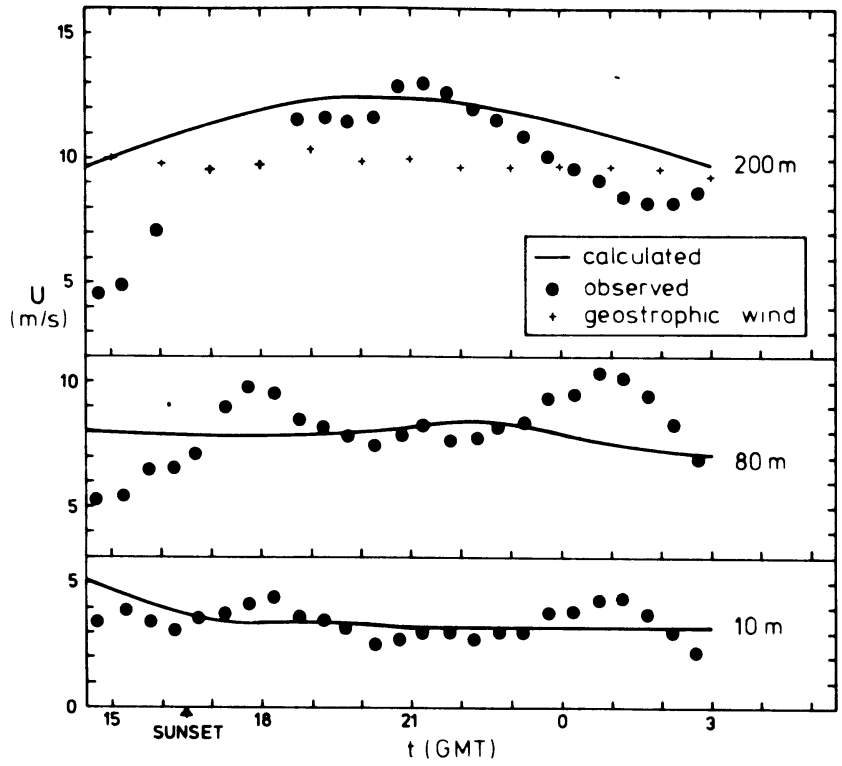

Fig. 4. Measured and calculated wind speed as a function of time for three observation heights.

The model calculations at 200 m also show an oscillation. This can be considered an inertial oscillation from the time that the calculated fluxes at 200 m are negligible (approximately 18.00 GMT). Due to the initial conditions the agreement of calculated results with measurements in the first part of the night is poor.

The wind speeds at 20 and 80 m are on the average well simulated by the model. However, the measurements show an oscillation with a period of ~7 hours, which is much smaller than the period $2\pi/f$ of an inertial oscillation. From Fig. 3 it follows that this oscillation occurs also simultaneously in the temperature at 200 m. The calculated results do not show these oscillations, because our model does not contain any processes with a time scale of 7 hours. We have found similar oscillations in the observations during another night period.

The wind direction α as a function of time is shown in Fig. 5. An inertial oscillation would lead to a veering wind direction

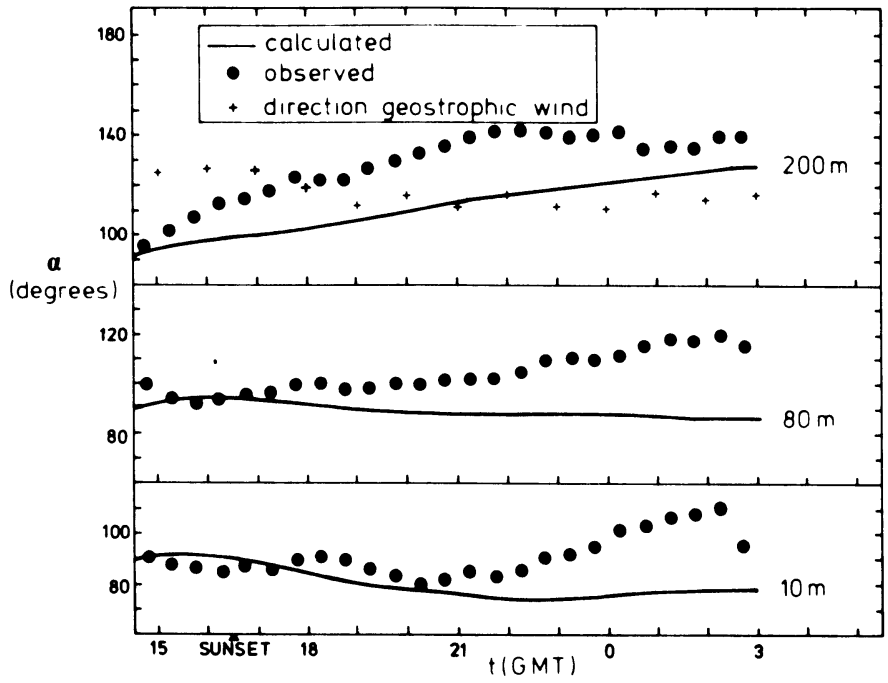

Fig. 5. Measured and calculated wind direction as a function of time for three observation heights.

in the first part of the night and a wind direction equal to the geostrophic direction when the maximum wind speed is reached. This is approximately true for the calculated results at 200 m. However, the measured wind direction at this height veers with respect to the calculations at a rate of 2°/hr until 22.00 GMT and then remains approximately constant. Therefore the veering in the measured wind direction cannot altogether be attributed to an inertial oscillation. At 80 m the measured direction veers also at a rate of 2°/hr with respect to the calculated result, which is almost constant. These differences must be attributed to the neglected advection terms. From synoptic surface data we estimate that the horizontal temperature gradient inside the nocturnal boundary layer is of the order of 3×10^{-5} °C m^{-1} in a south-easterly direction. A thermal wind can then be calculated from (4). Since the observed wind is also in a south-easterly direction, the thermal wind will be perpendicular to the observed wind vector. The influence of the thermal wind will result in a

change of wind direction. Using (2) this change can be approximated at a height z as $f|\underset{\sim}{u}_{th}(z)|/|\underset{\sim}{u}_{H}(z)|$. For 80 m this leads to a value of ~2°/hr for the wind direction change in accordance with the observed results. At 200 m we find ~4°/hr, which is somewhat larger than the veering of the observed wind direction with respect to the calculation. We therefore conclude that the difference between the measured and calculated wind direction can be attributed in this case principally to temperature advection.

At 10 m the measured and calculated wind directions are in good agreement in the first part of the night. The veering in the observed values after 22.00 GMT is probably related to the veering at higher levels.

The measured and calculated turbulent fluxes are shown in Fig. 6. The fluxes at 200 m are not shown, because they are

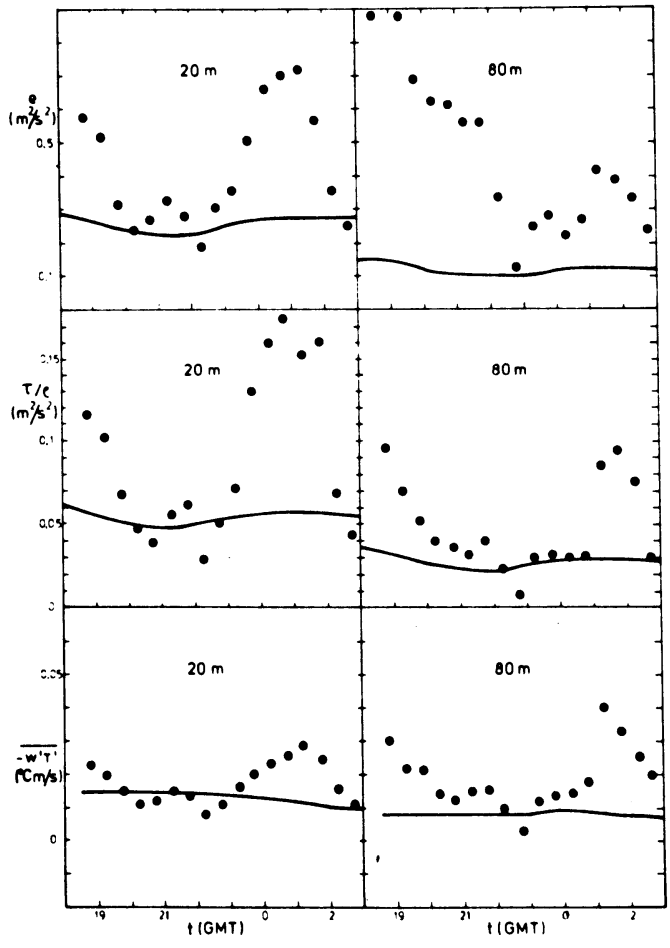

Fig. 6. Measured and calculated turbulent fluxes as a function of time for two observation heights; —— for the calculations; • for the observations.

negligible for most of the night. High levels of turbulence not found in the calculated results are present in the measurements. They occur simultaneously with oscillations in the wind speed and temperature, which were discussed in connection with Fig. 4. Because of the large timescale of this burst of turbulence (~3 hours), we do not believe that it is caused by breaking gravity waves, which are known to produce intermittent high levels of turbulence in a stable boundary layer (Sethu Raman, 1977). These high observed values of turbulence are responsible for the poor agreement between (20) and the observed boundary layer height (Fig. 2).

As the time histories shown in Figs. 3, 4 and 5 give a poor impression of the vertical profiles, we show in Fig. 7 some characteristic profiles of the wind speed and the temperature. They indicate that the overall features of the observed profiles are reasonably well simulated by the model results.

7. Conclusions

Data obtained during a case study are compared with the results of a one-dimensional boundary layer model. In this model turbulent fluxes are parameterized with the help of exchange coefficients. This parameterization is found to be consistent with the measurements.

The height of the turbulent nocturnal boundary layer grows to a stationary value of approximately 200 m. This height is reasonably well simulated by our model.

Above the boundary layer the flow is dominated by an inertial oscillation both in the observations and in the calculations. Differences between the observed and calculated results at this height could be explained in our case in terms of temperature advection.

Inside the boundary layer turbulent fluxes have to be taken into account. The observations are reasonably well simulated by our model. Differences between model results and measurements are caused by advection. They increase with height.

Advection can have a considerable influence on the evolution of the nocturnal boundary layer. Its contribution was estimated in our observed results. However, we conclude that a one-dimensional boundary layer model in which advection is neglected, can reasonably well simulate the boundary-layer height and the profiles of wind and temperature inside the nocturnal boundary layer.

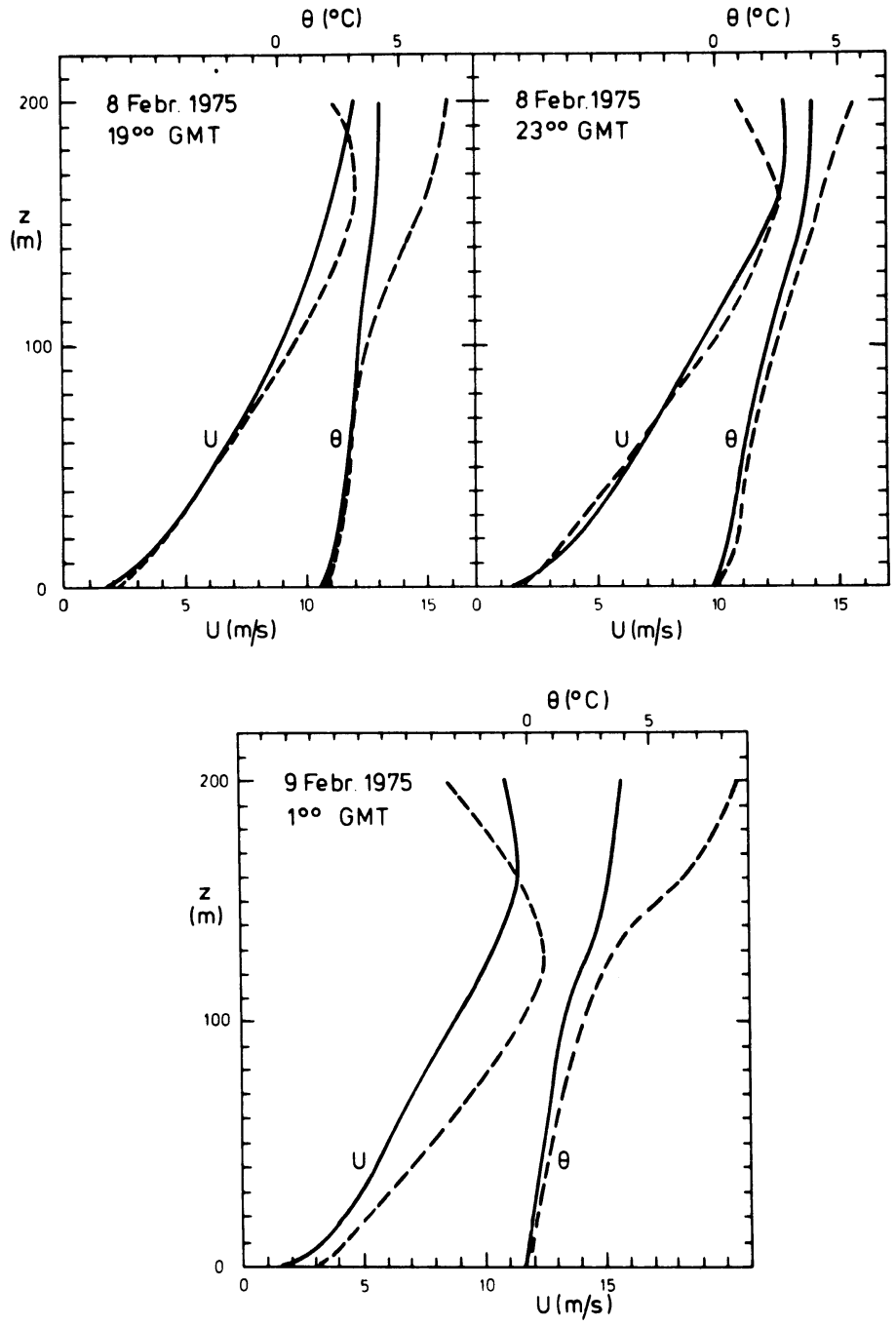

Fig. 7. Vertical profiles of measured and calculated wind speed and potential temperature; —— for the calculation; ---- for the observations.

III. The steady-state height and resistance laws of the nocturnal boundary layer: Theory compared with Cabauw observations.†

Abstract

An expression is derived for the height of the stationary, stable boundary layer. It satisfies the conventional limits for neutral conditions and for large values of stability. Comparison with acoustic sounder observations near the meteorological mast at Cabauw (the Netherlands) shows that the steady-state height is not attained for large stability values. The observations are also used to investigate how the similarity functions A and B in the resistance laws depend on the stability parameters $\mu_o = u_*/fl$ and $\mu = h/L$. The function B shows a clear trend as a function of stability, which can be described in terms of μ. The dependence of A is masked by scatter in the data points. The general conclusion leads to the concept of a non-steady stable boundary layer.

†To appear in the December issue, 1980, of Bound.-Layer Meteor.

1. Introduction

Similarity theory is a powerful tool in the study of the atmospheric boundary layer. It describes the structure of the boundary layer in terms of local characteristic parameters only, and neglects all dependence on the upstream history or time evolution of the flow. A review of several applications of similarity theory in the atmospheric boundary layer was given recently by Arya and Sundararajan (1976). Here we will confine ourselves to the stable nocturnal boundary layer.

An essential parameter in the application of similarity theory is the boundary-layer height. Zilitinkevich (1972) showed that for stationary conditions the stable boundary-layer height, h, can be expressed in terms of the other characteristic boundary-layer parameters, which are the friction velocity u_*, the Obukhov length L and the Coriolis parameter f. The relation for h as proposed by Zilitinkevich is only valid in very stable conditions. In section 2 we extend his formula to all stable cases.

A well-known result of similarity theory in the atmospheric boundary layer is the logarithmic resistance law (section 3). It follows from matching velocity profiles valid in different parts of the boundary layer. The matching procedure leads to similarity functions A and B in the resistance law, which are in general functions of two stability parameters $\mu_o = u_*/fL$ and $\mu = h/L$ (Zilitinkevich, 1975). A simplification results when the boundary-layer height can be expressed in terms of the other characteristic parameters as discussed above for steady-state conditions. In that case μ and μ_o are interdependent, so that theoretically A and B can be described in terms of only one stability parameter. Such a procedure has been followed by many authors (Clarke and Hess, 1974; Melgarejo and Deardorff, 1974; Zilitinkevich and Deardorff, 1974; Zilitinkevich, 1975 and Yamada, 1976).

The question whether the stable boundary-layer height can be expressed in terms of the other boundary-layer parameters is investigated here empirically. Therefore we introduce in section 4 two sets of experimental data obtained during clear nights along the meteorological mast at Cabauw in the Netherlands (Driedonks et al., 1978). In these observations the height of the stable turbulent boundary layer was measured directly with an acoustic sounder. This gives a more accurate value of the boundary-layer height than the more usual indirect estimate from e.g. the temperature profile.

A comparison of the observations with the theoretical results of sections 2 and 3 is discussed in section 5. In particular we investigate whether the observed boundary-layer height attains its steady-state value and how the similarity functions A and B can be described as functions of stability.

2. The height of the stationary, stable boundary layer

The equations of motion for a homogeneous, steady, atmospheric boundary layer read

$$f(v-v_g) + \frac{\partial}{\partial z}\left(K \frac{\partial u}{\partial z}\right) = 0 \,, \qquad (1)$$

$$-f(u-u_g) + \frac{\partial}{\partial z}\left(K \frac{\partial v}{\partial z}\right) = 0 \,,$$

where u and v are the mean velocity components in the x and y directions, u_g and v_g are the components of the geostrophic wind and f is the Coriolis parameter. The turbulent stresses in (1) are modeled with an eddy viscosity K. For a constant value of K Equation (1) yields the well-known Ekman spiral. The boundary-layer height of this Ekman spiral is given by

$$h = c\sqrt{K/f} \,, \qquad (2)$$

where c is a constant of proportionality.

Its numerical value depends on the way in which the boundary-layer height is defined, e.g. as the height where the stress is reduced to a certain proportion of its surface value.

In reality K is not independent of height. Numerical simulations of the steady, stable boundary layer led Brost and Wyngaard (1978) to propose the following expression for the vertical profile of K

$$\frac{K}{k\, u_* h} = \frac{(z/h)(1-z/h)^{1.5}}{1 + 4.7(z/L)} \quad , \tag{3}$$

where the friction velocity u_* and the Obukhov length L are defined by

$$u_* = \sqrt{\tau_o/\rho} \quad , \tag{4}$$

$$L = -\rho\, c_p\, u_*^3 \,/\, k\, \beta\, H \quad . \tag{5}$$

Here, τ_o and H are the turbulent momentum and heat flux at the surface respectively, ρ is the air density, c_p is the specific heat at constant pressure and β is the buoyancy parameter g/T. The Von Karman constant k is taken here as 0.35.

Zilitinkevich (1972) proposed that (2) remains applicable when K is a function of height. An effective value for the eddy viscosity K must then be substituted in (2). We assume here that this effective value for K can be obtained from (3) for a fixed value of z/h. We then derive from (2) and (3)

$$h/L = \frac{0.3\, u_*/fL}{1 + 1.9\, h/L} \tag{6}$$

In the derivation the constant c in (2) was chosen such that in the neutral limit ($L \to \infty$) (6) reduces to $h = 0.3\, u_*/f$ (Tennekes, 1973a). At the same time we substituted 0.4 for the value of z/h at which the effective value of K is obtained from (3). Equation (6) then agrees with the model results of Brost and Wyngaard for the limit of

large stability ($L \to 0$), which reads

$$h = 0.4 \sqrt{u_* L/f} \,. \qquad (7)$$

This is similar to the expression found by Zilitinkevich (1972) and Businger and Arya (1974). The latter authors, however, find a value of 0.72 for the constant of proportionality in (7). This is probably caused by the fact that they define h as the height where the stress has decreased to 1% of its surface value, whereas Brost and Wyngaard use the 5% level.

We conclude that (6) approaches the appropriate limits for $L \to 0$ and $L \to \infty$. It therefore gives an expression for the height of the stationary, stable boundary layer valid for all values of $L > 0$.

3. Resistance laws for stable conditions

The resistance laws of a homogeneous and stationary boundary layer are derived by matching a velocity-defect profile in the upper part of the boundary layer to a surface layer profile in the lower part (Blackadar and Tennekes, 1968; Hess, 1973). They read

$$G/u_* \cos \alpha = 1/k \, (\ln(Ro \, u_*/G) - B), \qquad (8)$$

$$G/u_* \sin \alpha = -1/k \, A, \qquad (9)$$

where G is a reference velocity for the boundary layer and α the angle between this reference velocity and the wind direction in the surface layer. $Ro = G/f\, z_o$ is the Rossby number based on the surface roughness parameter z_o.

The equations of motion (1) suggest a velocity-defect profile in the form of a geostrophic departure law. In that case G becomes equal to the geostrophic wind (Hess, 1973, Arya, 1975).

In contrast, Melgarejo and Deardorff (1974) and also Zilitinkevich (1975) take the wind at the top of the boundary layer as a reference velocity. The former authors

argue that the main reasons for this choice are:

(1) results are applicable closer to the equator;

(2) results account better for differences between the actual wind and the geostrophic wind at the top of the boundary layer;

(3) the wind velocity can be observed more accurately than the geostrophic wind.

Clarke and Hess (1974) compare values for the functions A and B in the resistance laws obtained with both reference velocities. They find similar results except for large stability, when, due to a low-level maximum, the wind at the top of the boundary layer greatly exceeds the geostrophic velocity.

Here we use the geostrophic wind for G, because the wind at the top of the boundary layer was not always measured during the experiments to be discussed in the next section.

When the geostrophic wind varies with height or equivalently when baroclinic effects are important, Arya and Wyngaard (1975) and Yamada (1976) show that the appropriate reference velocity becomes the vertically averaged geostrophic wind. For stable conditions Arya (1978) estimates that the variation in A and B due to these baroclinic effects will be 30% for a geostrophic wind shear of $|\partial v_g/\partial z| \sim 10^{-2}$ s^{-1}. The geostrophic wind shear in our experiments was estimated to be less than this value. Therefore we neglect baroclinic effects in the following, and adopt the geostrophic wind at the surface as the reference velocity G.

The matching theory, on which (8) and (9) are based, predicts that the similarity functions A and B can only depend on the following parameters: h, u_*, f, and L. From these quantities only two independent dimensionless parameters can be formed (Zilitinkevich, 1975).

$$\mu = h/L \tag{10}$$

$$\mu_o = u_*/f\,L\ . \tag{11}$$

Therefore in general $A = A(\mu,\mu_o)$ and $B = B(\mu,\mu_o)$.

From calculations with a second-order closure model Brost and Wyngaard (1978) obtain explicit expressions for A and B. They read

$$B = 1.1 - \ln(\mu/\mu_o) - 2.2\,\mu \tag{12}$$

$$A = -0.56\,\mu_o/\mu\ . \tag{13}$$

As discussed in the preceding section, μ and μ_o are related by (6) if the boundary layer can be considered stationary and homogeneous. When μ and μ_o are interdependent, A and B can be expressed as a function of only one stability parameter (Zilitinkevich and Deardorff, 1974; Zilitinkevich, 1975).

In this case the relations (12) and (13) for A and B simplify. For large values of the stability (μ and $\mu_o \to \infty$) this leads to (Brost and Wyngaard, 1978)

$$B = 2.0 + \ln \mu_o^{\frac{1}{2}} - 0.9\,\mu_o^{\frac{1}{2}} \tag{14}$$

$$A = -1.4\,\mu_o^{\frac{1}{2}}\ . \tag{15}$$

Rao and Snodgrass (1979) have tabulated similar expressions for A and B, which are based on model simulations by several authors.

For neutral conditions (μ and $\mu_o \to 0$) (12) and (13) reduce to

$$B = 2.3\ ,\quad A = -1.9\ . \tag{16}$$

This result is in reasonable agreement with the neutral values for A and B proposed by Tennekes (1973a), Clarke and Hess (1974) and Yamada(1976).

4. Experimental data

To check the theoretical results of the preceding sections we need observations of the parameters G, α, h, u_* and L for stable conditions. We obtained such data from measurements during clear nights at the meteorological mast at Cabauw in the Netherlands. This mast is situated in flat and reasonably homogeneous terrain with an average roughness length of 0.2 m (Van Ulden et al., 1976). A full description of the site and the instrumentation of the mast is given by Driedonks et al. (1978).

Two data sets are available. The first, denoted as Cabauw, 1977, consists of observations during fifteen clear nights in 1977, which were selected on the condition of a synoptically stationary situation. The surface layer parameters u_* and L in this data set were calculated from the results of a profile method (Nieuwstadt, 1978). This method obtains u_* and $\theta_* = -H/\rho c_p u_*$ from wind and temperature profiles, which had been observed between 2 and 20 m.

The second data set, denoted as Cabauw 1975, consists of measurements during four clear nights in February 1975. During these nights u_* and L were obtained from direct turbulence measurements of τ_o and H. A case study of one of these night periods was described by Nieuwstadt and Driedonks (1979).

Conditions around sunset are highly non-stationary. It is unlikely that resistance laws are then applicable. Therefore we started our data sets at approximately two hours after sunset when the nocturnal boundary is considered to be fully developed. The observations were continued until sunrise.

The geostrophic wind for both data sets is calculated from hourly pressure data at 19 meteorological stations in the Netherlands by a method based on principal com-

ponent analysis of a time series of pressure data measured at these stations (Cats, 1977).

For several nights in both data sets the wind direction difference α shows fluctuations as a function of time, which do not occur in the other parameters of the boundary layer. These fluctuations are mainly caused by slow excursions in the surface wind direction. At this stage we can only attribute this to mesoscale advection processes. It will lead to a considerable amount of scatter in the comparison of results which depend strongly on the value of α. This will become apparent in the next section.

For both data sets the height of the boundary layer is determined from the registration of an acoustic sounder (Sodar), on which the nocturnal inversion can be clearly seen if sufficient turbulence is present. The top of the analog registration of this instrument is taken as the boundary-layer height. The inaccuracies in this procedure are estimated to be within the instrumental error of ~30 m. This value is related to the length of the sound pulse emitted by the Sodar.

Often the height of the boundary layer is estimated as the thickness of the ground-based inversion in the temperature profile (e.g. Melgarejo and Deardorff, 1974). However, the height of the turbulent layer, which is taken here as representative of the boundary-layer height, is usually smaller than the inversion thickness due to the influence of advection and radiation on the temperature profile (Nieuwstadt and Driedonks, 1979; Nieuwstadt, 1980). This is confirmed by the model simulations of Brost and Wyngaard (1978) and by observations analyzed by Mahrt et al. (1979).

Our experimental data allow a comparison between both estimates of the boundary-layer height for those cases in which the temperature profile measured along the mast includes the whole surface-based inversion. The inversion thickness is then determined as the height to which significant cooling extends (Melgarejo and Deardorff, 1974). The results are compared in Figure 1 with the heights obtained from the Sodar-registration. Indeed we find that the height obtained from the temperature profile is generally larger than the height measured by the Sodar. Moreover, the correlation between the two heights is poor. Based on the arguments given above we therefore prefer the height measured by the Sodar as the estimate of the nocturnal boundary-layer height. Such a choice was also recommended by Arya and Sundarajan (1976).

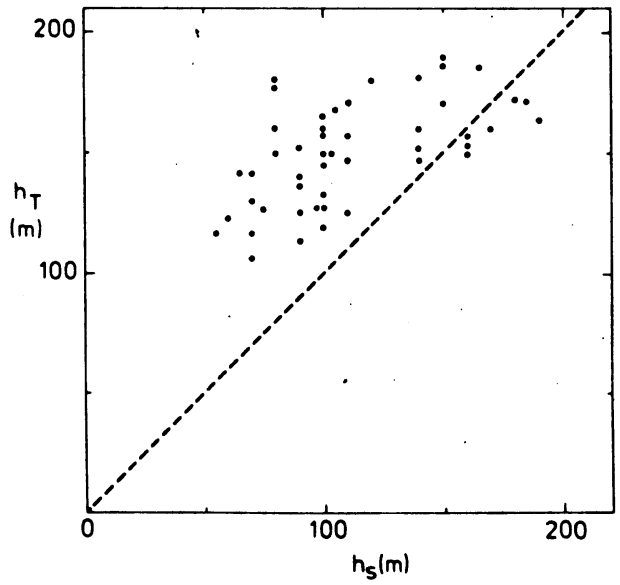

Fig. 1. Comparison of the boundary-layer height defined from the temperature profile (h_T) with the boundary-layer height observed with an acoustic sounder (h_s).

5. Discussion

We have shown in section 2 that the height of the stationary boundary layer can be expressed in terms of the other characteristic parameters. This leads to a relation between μ and μ_o given by (6).

The expression of Zilitinkevich (7), which follows from (6) for large values of the stability, has been checked against measurements by Yamada (1976), Arya and Sundarajan (1976) and Yu (1978). They found a poor agreement of the experimental results with (7). Moreover, (7) seemed to underestimate the actual boundary-layer height considerably. In these studies the height of the boundary layer was based primarily on the temperature profile. Therefore these results must be approached cautiously, because we have shown in section 4 that the height obtained in this way is poorly correlated with the more preferable estimate from the Sodar-registration. However, our results seem to support the conclusions of the authors mentioned above, as we shall see shortly.

Our data are shown in Figure 2, together with equation (6). The experimental data show a dependence between μ and μ_o, but they do not fit the curve given by (6) except for small values of μ_o, which indicate near-neutral conditions. A choice of other constants in (6) would not lead to a better agreement with the observations, because the data rather support a linear relation between μ and μ_o. However, a dimensionless plot like Figure 2, which is commonly used in atmospheric boundary-layer research, may show artificial correlation effects (Hicks, 1978). Artificial correlation leads to relationships between dimensionless parameters, which have no physical cause and only follow from the definition of the parameters. A discussion on the influence of artificial correlation is usually

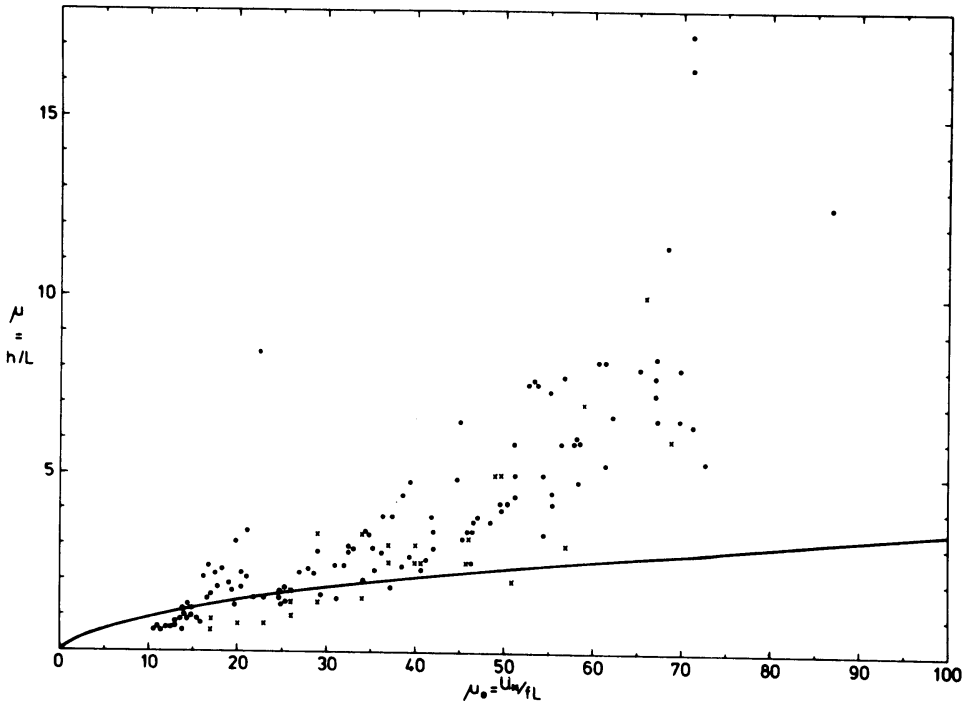

Fig. 2. Comparison of observations of the stability parameters μ *and* μ_o *in the stable boundary layer; the dots denote the data set Cabauw 1977 and the crosses the data set Cabauw 1975; the drawn line follows from Equation (6).*

omitted in a presentation of dimensionless plots. Therefore we will elaborate on its appearance in our results for μ and μ_o, shown in Figure 2, in an appendix. There we show that the data still support a linear relation between μ and μ_o when the influence of artificial correlation is largely eliminated.

Such a linear relationship would imply that for all values of the stability the boundary-layer height will have the same form as for neutral conditions. This means that the height will no longer depend directly on L, which is hard to believe. Furthermore, an estimate of the proportionality constant in the linear relation, apparent in Figure 2, leads to a value of about 0.1. This is smaller than the value of 0.3 usually found for neutral conditions, so that a linear

relation between μ and μ_o must lead to an incorrect neutral limit. Another aspect is that the scatter in the data, which is small in near-neutral conditions when the agreement with (6) is good, increases for larger stabilities.

Therefore we are tempted to conclude that the boundary layer does not attain a steady state during the course of the night. Hence the boundary-layer height is not determined by local parameters but it is a function of its history. This means that the boundary-layer height can only be obtained from an appropriate rate equation.

Such a rate equation was recently derived by Yamada (1979) by integrating the temperature equation across the boundary layer. He finds a good agreement with observations. However, Nieuwstadt (1980) shows that his equation does not describe the evolution of the turbulent boundary-layer height. For this height Zeman (1979) proposes a rate equation based on the energy budget of the mean flow. He gives no comparison with observations, but his results show good agreement with the model simulations of Brost and Wyngaard (1978). It will be the subject of further study whether the application of such a rate equation can explain our observations shown in Figure 2.

As a digression we may mention that a complete analogy can be found in the convective boundary layer. In that case the boundary-layer height follows also from a rate equation (Tennekes, 1973b; Carson, 1973) rather than from local parameters.

We now turn to a comparison of the similarity functions A and B with our experimental data. However, the validity of the resistance laws and thus of the functions A and B in a non-stationary boundary layer can be questioned. We will assume here that these laws

remain applicable if the boundary can be considered self-similar. This means that the turbulent structure of the boundary layer at each time is only dependent on local, characteristic parameters and not on the time history of the flow. The time dependence of the flow is only reflected in the time evolution of the characteristic parameters themselves. Except possibly near sunset, when conditions change very rapidly, self-similarity seems to be a reasonable assumption for the structure of the nocturnal boundary layer (Caughey et al., 1979).

In the non-stationary case, when the boundary-layer height follows from a rate equation, μ_o and μ are independent stability parameters. As discussed in section 3, this means that the similarity functions must be expressed in their general form A (μ, μ_o) and B (μ, μ_o). To facilitate a comparison with observations, we will assume here that the expressions (12) and (13) for B and A remain valid. An important consequence of (12) is that B will depend primarily on μ, because μ_o enters only in a logarithmic function.

In Figures 3 and 4 we have plotted the observed

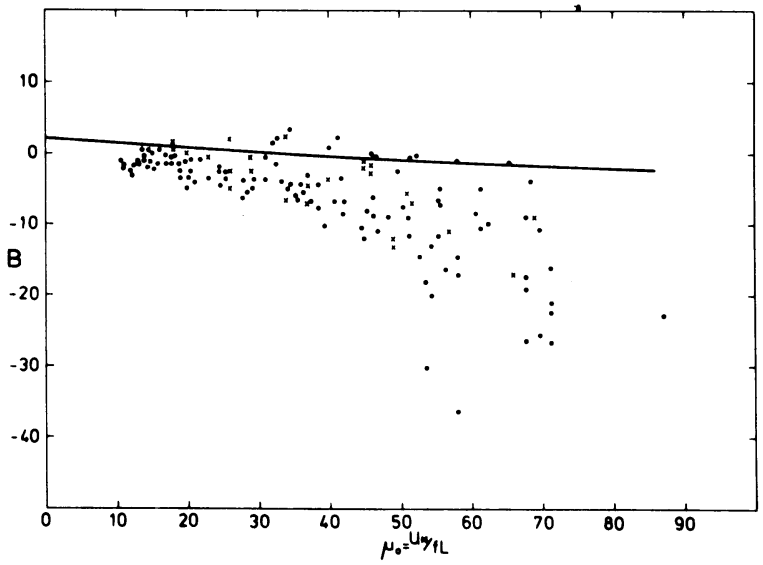

Fig. 3. The observed similarity function B in the resistance laws as a function of the stability parameter μ_o; the dots and crosses are defined as in Figure 2; the drawn line follows from Equations (6) and (12).

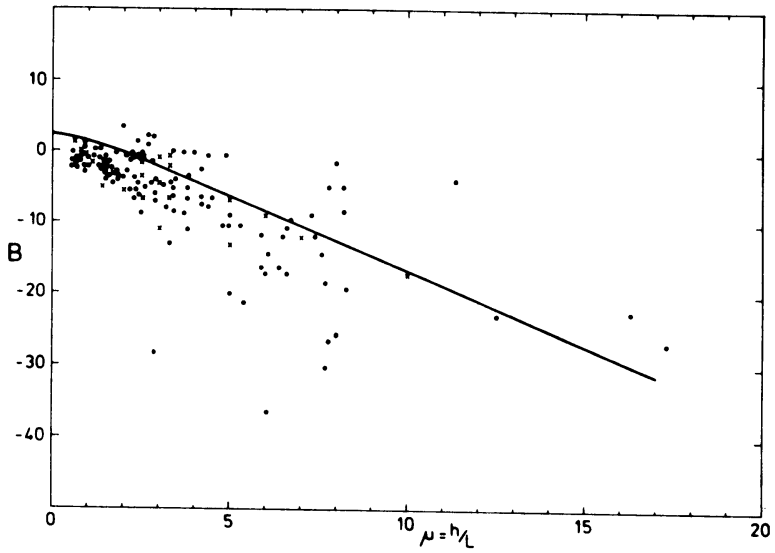

Fig. 4. Same as Figure 3, but as a function of the stability parameter μ.

values of B against the parameters μ_o and μ respectively. In these figures we have also drawn (12), which is expressed as a function of either μ_o or μ with the aid of (6). This curve predicts the trend in the data points better in Figure 4, where B is shown as a function of μ. Together with the condition given above that B must depend primarily on μ, this result leads us to conclude again that (6) is not valid. This confirms our hypothesis that the stable boundary layer must be considered non-stationary.

However, we have argued that in the non-steady case B must be considered a function of both stability parameters rather than a function of either μ_o or μ. This means that the data on B must be compared with (12), in which the observed values of both μ and μ_o are substituted. We can expect, however, the same agreement as shown in Figure 4 because of the dominant dependence of B on μ.

Next, we discuss the similarity function A. In Figures 5 and 6 the observed data on A are plotted against μ_o and μ respectively. In both figures the theoretical curve defined by (13) and (6) is also shown. In this case the trend in the data is better predicted by the theoretical curve in Figure 5, where the data are shown as a function of μ_o.

In both figures a trend in the data points is unfortunately masked by a very large scatter for the whole range of the stability parameter. This scatter must be attributed primarily to the slow wind direction fluctuations mentioned in section 4. These will influence A more than B because of the sine function in the definition of A (9) as opposed to the cosine function in the expression for B (8).

Due to this large scatter no detailed conclusions can be drawn from Figures 5 and 6.

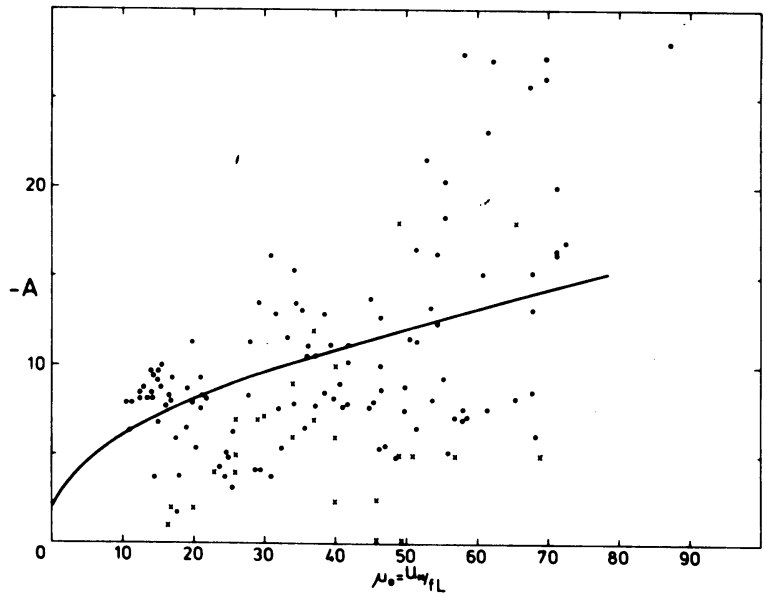

Fig. 5. The observed similarity function A in the resistance laws as a function of the stability parameter μ_o; the dots and crosses are defined as in Figure 2; the drawn line follows from Equations (6) and (13).

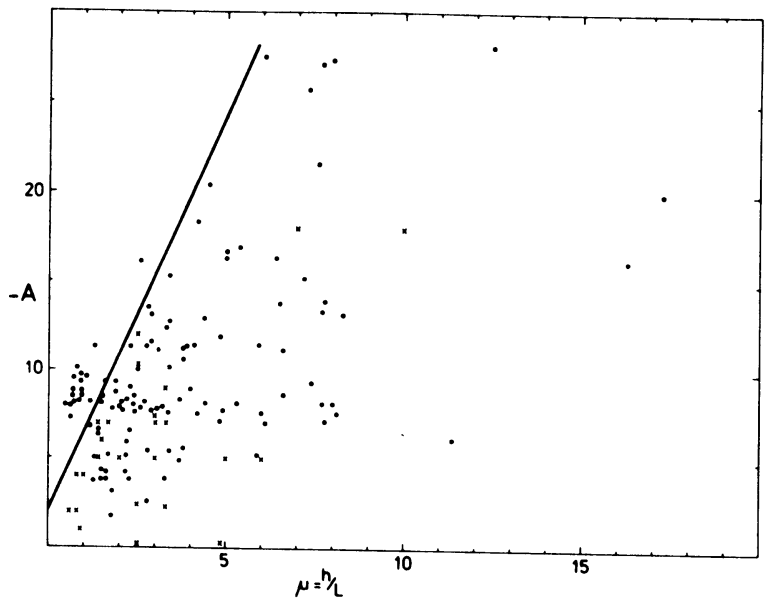

Fig. 6. Same as Figure 5, but as a function of the stability parameter μ.

6. Summary and conclusions

We have collected a large number of experimental data for clear nights. These data show that for large values of the stability the boundary-layer height does not attain a steady-state value as for instance expressed by the equation of Zilitinkevich.

The similarity functions A and B in the resistance law for a homogeneous stationary boundary layer are summarized for the stable case. The values of B obtained from observations show a clear trend with stability. This dependence can be described in terms of an expression which primarily depends on μ. A trend in A with stability is largely obscured by scatter in the data, which is caused by large time-scale fluctuations in the wind direction.

Our results lead to a non-steady boundary layer for large values of the stability. The height of such a boundary layer cannot be determined in terms of local, characteristic parameters. It must follow from a rate equation which describes the time evolution of the boundary-layer height. Examples of a rate equation are discussed by Yamada (1979), Zeman (1979) and Nieuwstadt (1980). It will be the subject of further study, whether the application of these rate equations can explain the observations discussed here.

7. Appendix

Plots of dimensionless quantities are frequently used to organize empirical data. In this respect they are very useful, because they may lead to universal scaling laws in terms of which data points obtained from different experiments can be collapsed. However, such dimensionless plots may suffer from artificial correlation if the dimensionless quantities contain common scaling variables. This may lead to apparent relationships between these quantities which have not any physical cause (Hicks, 1978).

As an example, we direct our attention to the dimensionless plot of $\mu = h/L$ against $\mu_o = u_*/Lf$ for the data set Cabauw 1977 (see Figure 2). In this data set the parameters, which can be considered independently obtained, are u_*, h and θ_* (see section 4). Because both μ and μ_o depend on u_* and θ_*, artificial correlation may appear in the plot of μ against μ_o.

We investigate this by constructing a second data set of h, u_* and θ_*, which is derived by generating random values within the ranges observed in the Cabauw 1977 data set. These ranges are $0.1 < u_* < 0.55$ m/s, $50 < h < 400$ m and $0.04 < \theta_* < 0.12$ °C. A plot of the dimensionless

quantities μ and μ_o, obtained from this random data set with the aid of (5), (10) and (11), is shown in Figure 7. This figure is strikingly similar to Figure 2, which is obtained with the measured Cabauw data. In both figures a positive correlation between μ and μ_o is apparent. In Figure 7 this must be a symptom of artificial correlation, which in this case is principally caused by the parameter u_* due to its large range of variation. It follows directly that the dependence of both μ and μ_o on u_*, will induce the relationship: $\mu \sim \mu_o^2$. The data in Figure 7 seem to follow such a dependence quite well.

From this we must not directly conclude that the results shown in Figure 2 are worthless because of artificial correlation. At this stage we have only shown that a plot of μ against μ_o is not very suitable to reveal physical relationships, despite the fact that the individual parameters μ and μ_o seem physically meaningful.

The responsible parameter, which primarily caused the artificial correlation in this case, was identified as u_*. Therefore it would seem advantageous to define

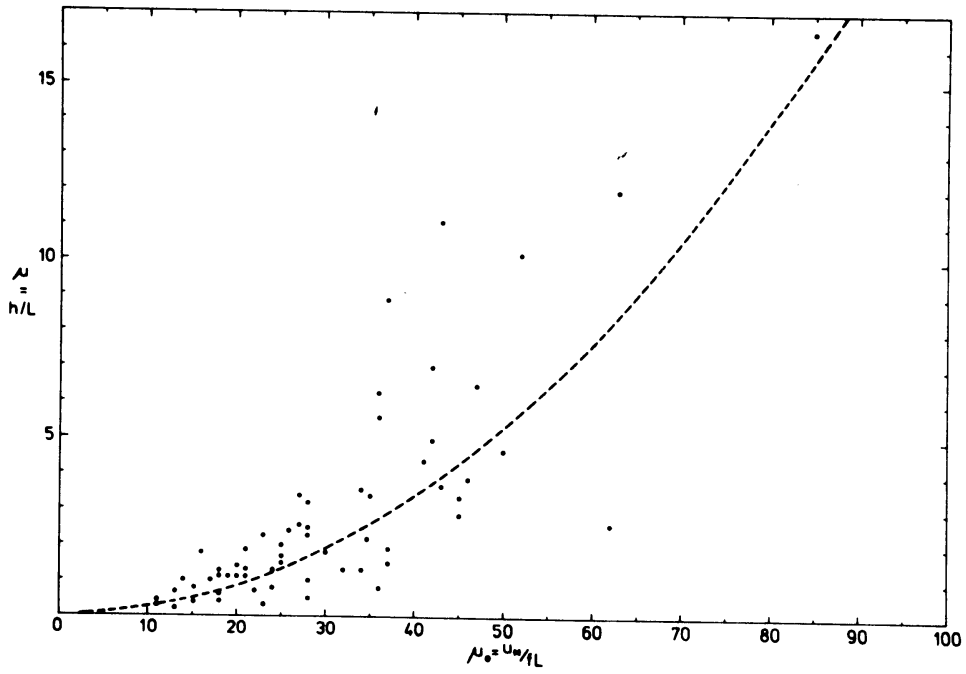

Fig. 7. Comparison of the stability parameters μ_o and μ for a random data set; the dotted line is $\mu = \mu_o^2$.

a new dimensionless quantity, which does not contain u_*, e.g. u_*^2/f^2hL. For our random data set we have plotted this quantity as a function of μ_o in Figure 8. This figure has undeniably the appearance of a random data plot. Despite the fact that in this case θ_* is common to both quantities, the large range of variation in the u_* and h eliminates any artificial dependence.

When we plot this new dimensionless quantity for our data set Cabauw 1977, the result is completely different as shown in Figure 9 (note the change of vertical scale compared to Figure 8). Here, a correlation between both dimensionless quantities becomes apparent, which cannot be an artificial one. It shows that the data rather follow a linear dependence than the theoretical relation (6) als shown in this figure. This is in

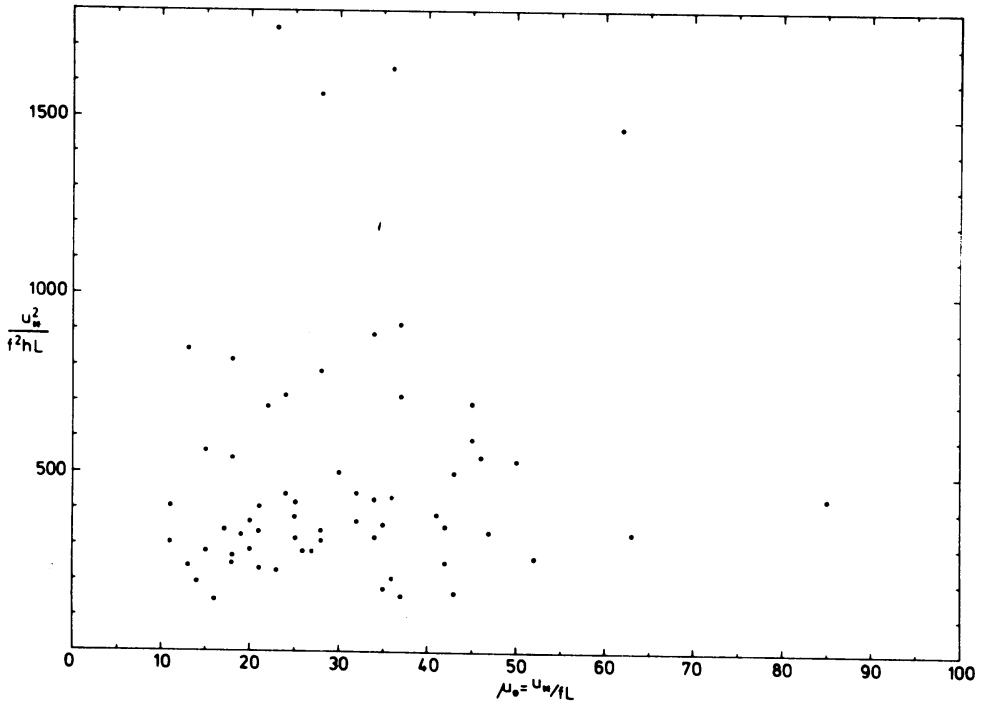

Fig.8. Comparison of the parameter u_*^2/f^2hL with the stability parameter μ_o for a random data set.

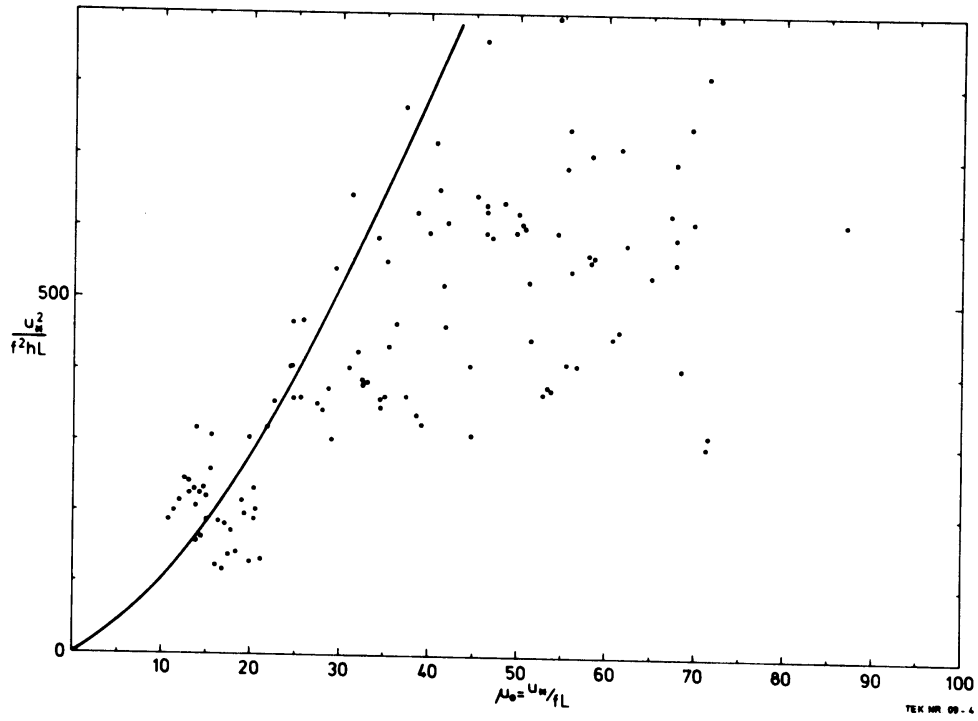

Fig. 9. Comparison of the parameter u_*/f^2hL *with the stability parameter* μ_o *for the data set Cabauw 1977; the drawn line follows from Equation (6).*

agreement with the results of Figure 2, because a linear relationship in Figure 9 is equivalent to a linear dependence between the original parameters μ and μ_o. These results confirm completely our discussion in connection with Figure 2. They also illustrate that plotting of dimensionless quantities should be handled with care.

IV. A rate equation for the inversion height in a nocturnal boundary layer[†]

Abstract

The application of a self-similar profile in the integration of the temperature equation across the stable boundary layer leads to a rate equation for the inversion height. An analytic solution of the resulting equation is derived. Its behavior is determined by two processes: cooling by turbulent mixing and cooling by internal radiation, which is parameterized in terms of the surface cooling rate. This parameterization, which attributes the temperature change in the boundary layer close to the surface completely to internal radiation, leads to a monotonic growth of the inversion depth. When the radiation term is neglected and only the turbulent heat flux is taken into account, the solution is governed by a relaxation process.

[†]To appear in the December issue, 1980, of J. Appl. Meteor.

1. Introduction

Most studies of the nocturnal boundary-layer height concentrate on diagnostic equations. Such equations describe the boundary-layer height in terms of local parameters only (i.e. surface heat and momentum flux). For large values of the stability an expression for the boundary-layer height was derived by Zilitinkevich (1972) by assuming quasi-steady conditions. Comparison with observations, however, shows poor agreement (Yu, 1978; Nieuwstadt, 1980).

Recent studies (Brost and Wyngaard, 1978; Caughey et al., 1979) show that the stable boundary layer in the atmosphere is continuously evolving. This means that its structure cannot be described by steady-state equations. Therefore the height of the boundary layer should not be expressed in terms of a diagnostic equation but in terms of a prognostic equation, which describes the time evolution of the boundary layer.

Rate equations for the stable boundary-layer height were recently derived by Yamada (1979) and Zeman (1979). These equations require a definition of the boundary layer height. Zeman (1979), following Brost and Wyngaard (1978), defines it as the height where the turbulent fluxes have decreased to a small proportion of their surface value. On the other hand, Yamada (1979) refers to the temperature profile and defines the boundary-layer height as the inversion height, i.e. the depth to which significant cooling has extended. These two definitions are not equivalent (Brost and Wyngaard, 1978; Mahrt et al., 1979; Nieuwstadt, 1980).

Here, we shall follow Yamada and consider a rate equation for the inversion depth. It is derived by integrating the temperature equation. In section 2 we summarize the derivation for a more general temperature profile than used by Yamada. In section 3 we give the exact solution of this equation and we investigate some of its properties.

2. A rate equation for the inversion depth

We confine ourselves to horizontally homogeneous conditions. The equation for the potential temperature θ in the boundary layer then reads

$$\frac{\partial \theta}{\partial t} = \frac{\partial}{\partial z}(-\overline{w\theta}) + C\left(\frac{\partial \theta}{\partial t}\right)_r, \qquad (1)$$

where t is time and z is the vertical coordinate. This equation states that the temperature change in the boundary layer is caused by two processes: turbulent mixing, represented by the gradient of the turbulent heat flux $\overline{w\theta}$, and the divergence of longwave radiation, represented by the term $(\partial\theta/\partial t)_r$. For convenience we have included a constant C, which is set equal to one when radiation effects are taken into account and equal to zero when radiation is neglected.

We assume, following Yamada, that the temperature profile within the boundary layer is given by the similarity expression

$$\theta = \theta_h - \Delta\theta(1 - z/h)^{\alpha}. \qquad (2)$$

Here, θ_h is the temperature at $z = h$, where h is the height of the inversion. The temperature difference across the boundary layer is defined as $\Delta\theta = \theta_h - \theta_s$, where θ_s is the surface temperature. The value of the exponent α is still not clear. Yamada (1979) presents evidence for $\alpha = 3$, but he cautions against applying these results to other locations. Zeman (1979) uses $\alpha = 1$. Here, we will only assume that $\alpha \geq 1$.

Following Yamada, the internal radiation term in (1) is parameterized as

$$\left(\frac{\partial \theta}{\partial t}\right)_r = \frac{d\theta_s}{dt}(1 - z/h), \qquad (3)$$

which shows that the cooling of the boundary layer for $z = 0$ is completely attributed to radiation. This means

that the influence of turbulent mixing is neglected, which puts on the turbulent heat flux the constraint that $\partial\overline{w\theta}/\partial z = 0$ for $z = 0$, when radiation is included. The parameterization given by (3) will have a large influence on the solution as we shall show in the next section.

Using profiles (2) and (3) we can integrate the temperature equation (1) across the boundary layer. In this integration we assume that the turbulent heat flux at the top of the boundary layer is negligible and that the temperature θ_h is independent of time. The integration then leads to a rate equation for h. It reads (Yamada, eq. 11)

$$\frac{dh}{dt} = \frac{(1 - \frac{\alpha+1}{2} C)d\theta_s/dt}{(\theta_h - \theta_s)} \left[h - \frac{\alpha+1}{1 - \frac{\alpha+1}{2} C} \frac{\overline{w\theta_s}}{d\theta_s/dt} \right], \qquad (4)$$

where $\overline{w\theta_s}$ is the heat flux at the surface. This equation must be completed by an initial condition, which is taken as $h = h_o$ for $t = t_o$.

3. Results

An analytic solution of the rate equation (4) with the initial condition $h = h_o$ for $t = t_o$ is possible. It reads

$$h = h_e(t) + \frac{F(t_o)}{F(t)} \{h_o - h_e(t_o)\} - \frac{1}{F(t)} \int_{t_o}^{t} F(t') \frac{dh_e(t')}{dt'} dt' \qquad (5)$$

with

$$F(t) = \{\theta_h - \theta_s(t)\}^{1 - \frac{\alpha+1}{2} C} \qquad (6)$$

and

$$h_e(t) = \frac{\alpha+1}{1 - \frac{\alpha+1}{2} C} \frac{\overline{w\theta_s}}{d\theta_s/dt} \qquad (7)$$

The first term on the right-hand side of (5) represents an equilibrium height, defined by (7). The term equilibrium

is based on the condition that $dh/dt = 0$ for $h = h_e$, which follows directly from (4). h_e can be interpreted as the height for which the temperature change, integrated across the boundary layer, is completely balanced by the radiative and turbulent processes.

The second term describes the influence of the initial conditions on the solution. This term decreases as a function of time if the exponent in (6) is greater than zero. For $\alpha. \geq 1$, considered here, this can happen for $C = 0$ only, which means no radiation (recall that $C = 0$ or $C = 1$). If radiation is included, i.e. if $C = 1$, the exponent will be negative and this term will increase with time, leading to a growing h. As we shall see shortly, this behavior is a consequence of the radiation parameterization and follows also directly from (4), because $C = 1$ and $\alpha > 1$ in this equation always lead to $dh/dt > 0$. The result of a growing inversion height is confirmed by the model simulations by André et al. (1978) and also by observations (Yamada, 1979; Mahrt et al., 1979).

The last term on the right-hand side of (5) describes the influence of a non-stationary h_e. It shows that solution depends on the complete time history of h_e and not only on values at time t. This illustrates the difference of this solution with a diagnostic equation for h.

To gain more insight in the properties of the rate equation (4) and its solution (5) it is illustrative to examine separately the influence of the different effects in this equation. We shall distinguish two cases: (a) radiation, but no turbulent heat flux, and (b) turbulent mixing, but no radiation. It should be stressed that by radiation we mean here the direct cooling of the boundary layer by internal, long-wave radiation. The cooling of the surface, which is also due to long-wave radiation loss, is always present as the driving force in establishing a stable temperature profile in the boundary layer.

a. No turbulent heat flux ($C = 1$ and $\overline{w\theta}_s = 0$). The solution (4) now reduces to

$$h = h_o \left[\frac{\theta_h - \theta_s(t)}{\theta_h - \theta_s(t_o)} \right]^{\frac{\alpha-1}{2}} \qquad (8)$$

This shows that for $d\theta_s/dt < 0$ and $\alpha > 1$, h is an increasing function of t. For $\alpha = 1$, h becomes stationary. This result explains to a large extent the non-decreasing behavior of the complete solution (4) discussed above.

We can understand this behavior if we observe that $\int_o^h (\partial\theta/\partial t)_r dz$ is proportional to the amount of heat which is removed from the boundary layer by internal radiation. If we parameterize the radiation by a linear profile, as given by Yamada (1979), and if we require that the temperature profile must always satisfy (2), conservation of energy as expressed by (1) then leads automatically to an increasing inversion height for $\alpha > 1$.

However, the parameterization of the radiation, which essentially determines this property of the solution, must be considered rather crude in this case. It is, for instance, not clear that the radiation profile can be chosen independently of the temperature profile, as was done here.

b. No radiation ($\overline{w\theta}_s \neq 0$ and $C = 0$). First we note that these conditions seem incompatible with the previous cases where radiation is included. There, the temperature decrease at $z = 0$ is completely caused by radiation leading to a zero divergence of the heat flux, whereas in this case cooling is only possible when $\partial\overline{w\theta}/\partial z \neq 0$ for $z = 0$. However, we consider only the bulk properties of the boundary layer in terms of an integral method, so that these local inconsistencies may be neglected.

The solution (5) has now a completely different behavior than in the case where radiation was taken into account.

This can best be illustrated by rewriting (4) as

$$\frac{dh}{dt} = -\frac{1}{T_D}\{h - h_e(t)\} \quad , \tag{9}$$

where

$$T_D = \frac{-\{\theta_h - \theta_s(t)\}}{d\theta_s/dt} \quad . \tag{10}$$

and where $h_e(t)$ is given by (7) for $C = 0$.

Equation (9) can be characterized as a relaxation equation, which describes a process in which h is forced towards an equilibrium value h_e. The time scale T_D involved in this relaxation process is given by (10). It will be clear that this time scale increases with time because $d\theta_s/dt < 0$. This means that the boundary-layer height evolves at a decreasing rate. In our case this results in an algebraic approach of h towards h_e rather than an exponential approach, as would be the behavior of a usual relaxation process. The algebraic approach can be easily verified from the full solution (5).

Equation (9) allows stationary and decreasing solutions of h, which do not occur when the radiation term is included, as we have seen above. This behavior resembles the evolution of the turbulent layer depth in a stable boundary layer, which according to observations may approach a quasi-stationary value (Nieuwstadt and Driedonks, 1979; Mahrt et al., 1979). Such results are also found by Zeman (1979) and Brost and Wyngaard (1978), who considered models for the height of the turbulent, stable boundary layer in which the radiational effects were neglected.

The latter authors also show that the boundary-layer height approaches a stationary state when $d\theta_s/dt$ is constant. This means that h and also $\overline{w\theta_s}$ approach constant values. Such behavior is confirmed by the rate equation (9). It shows that for this case h approaches the then constant value h_e. The expression (7) for h_e correlates well with the model results of Brost and Wyngaard (1978).

4. Summary and conclusions

Following Yamada (1979) we have derived a rate equation for the inversion depth in a nocturnal boundary layer by integrating the temperature equation.

A simple parameterization of the internal radiation term in this equation leads to a solution which increases as a function of time. This behavior agrees with model calculations and observations of the nocturnal inversion height.

The influence of internal radiation and of turbulent mixing is investigated separately. Taking only radiation into account we find a solution for the inversion height which is non-decreasing with time. It appears that the parameterization of the radiation is primarily responsible for the monotonic growth found for the solution of the complete equation. Omission of the radiation term, which means that only the turbulent heat flux is taken into account, leads to a relaxation equation. This type of equation can lead to stationary and decreasing solutions. That behavior is more in agreement with model calculations and observations of the turbulent layer depth in a stable boundary layer.

An approach to a rate equation for the height of the turbulent layer is the subject of a present investigation. It gives rise to a relaxation equation that is similar to the one discussed here.

V. A rate equation for the nocturnal boundary-layer height†

Abstract

A rate equation is derived which describes the development of the boundary-layer height under stable conditions as a function of time.

It takes the form of a linear relaxation equation; its solution is forced toward an equilibrium value. The equilibrium height is connected to the work done by the ageostrophic wind in the boundary layer. The time scale of the relaxation process increases monotonically from a few hours shortly after sunset to a value of the order of ten hours later on. This means that the boundary-layer height evolves very slowly, which may lead to the unwarranted impression that stationary conditions have been reached. The main features of the rate equation are confirmed by comparison with the results of computer simulations and with field observations of the boundary-layer height during clear nights.

†Submitted to J. Atmos. Sci. with H. Tennekes as co-author.

1. Introduction

The nocturnal boundary-layer height is the depth of the shallow turbulent boundary layer, which develops under stable conditions. Previous studies (Yu, 1978; Nieuwstadt and Driedonks, 1979; Nieuwstadt, 1980b) have shown that it cannot be described by a diagnostic equation, which expresses this height in terms of local, characteristic parameters. Therefore a prognostic equation is needed to describe the evolution of the boundary-layer height as a function of time. The goal of this paper is to construct such an equation.

Rate equations for the nocturnal boundary-layer height have been considered by Deardorff (Yu, 1978), Smeda (1979) and Mahrt (1981). They attempt to find an equation, which simulates the characteristic behavior of the nocturnal boundary layer. However, in their studies ad hoc assumptions are necessary to determine some important parameters. Here, we shall avoid such assumptions. Instead, we shall derive the rate equation directly from the equations governing the development of the stable boundary layer. The resulting equation turns out to be similar to that proposed by the authors mentioned above. An advantage of our approach is that the physical processes contributing to the development of the boundary-layer height can be more easily recognized.

Another kind of rate equation has been developed by Yamada (1979). He derives an equation for the evolution of the inversion height in stable conditions. However, his results are not applicable to our problem because the height of the turbulent boundary layer is not necessarily equal to the inversion depth. We return to this issue in section 2. The difference between the results obtained by Yamada and the type of rate equation derived in this paper is discussed in more detail by Nieuwstadt (1980a).

Yet another approach has been proposed by Zeman (1979). He uses an integral method to construct a complete model of the nocturnal boundary layer. This leads to a rather com-

plicated rate equation for the boundary-layer height in terms of other unknowns, which in turn are expressed by additional time-dependent equations. Here, we aim to develop a more simple rate equation, which allows a straightforward interpretation.

In section 2, we derive the rate equation by considering sources and sinks of turbulent kinetic energy in a stable boundary layer. The analytic solution of this equation and its properties are discussed. The characteristic behavior is described by a relaxation process. The equilibrium height which occurs in the equation is discussed in section 3, where also a simple expression for this height is proposed. The time scale of the relaxation process and its influence on the solution is discussed in section 4. A comparison with observations obtained during clear nights at the meteorological mast at Cabauw in the Netherlands is given in section 5.

2. Rate equation for the stable boundary-layer height

We base the rate equation on a consideration of production and destruction of turbulent kinetic energy inside a stable boundary layer. For that purpose we introduce a modified flux Richardson number defined as the ratio of the production and destruction term averaged across the boundary layer. We consider the evolution of this Richardson number as a function of time by deriving equations for its numerator and denominator which are evaluated with the aid of self-similar boundary-layer profiles. Substitution of these equations in the expression for the modified Richardson number then leads to the rate equation.

Before beginning with our derivation we first consider the definition of the nocturnal boundary-layer height. We assume here that it is the height, at which the turbulent shear stress and heat flux become negligibly small (Brost and Wyngaard, 1978; Zeman, 1979). Other studies (Yu, 1978; Yamada, 1979) relate the boundary-layer height to the inversion

depth. However, Mahrt et al. (1979) and Nieuwstadt (1980b) have shown that these two definitions are not equivalent. The temperature profile is not only influenced by turbulent mixing but also by other processes such as radiation. Therefore the inversion height is not a reliable indicator of the turbulent layer depth.

As the starting point of our analysis we take the turbulent kinetic energy budget. Since the nocturnal boundary layer is stable, the only source term in this budget is the mechanical or shear production $\underset{\sim}{\tau}/\rho \cdot \partial \underset{\sim}{v}/\partial z$, where $\underset{\sim}{\tau} = (\tau_x, \tau_y)$ is the Reynolds stress and $\partial \underset{\sim}{v}/\partial z$ the gradient of the horizontal wind $\underset{\sim}{v} = (u,v)$. The buoyancy flux $g/T\ \overline{w\theta}$ suppresses turbulence, because $\overline{w\theta}$ is generally negative at night. The ratio of these two effects, which plays an important role in the dynamics of the stable boundary layer, is given by the flux Richardson number. It reads

$$Ri_f = - \frac{\frac{g}{T}\,\overline{w\theta}}{\frac{\underset{\sim}{\tau}}{\rho} \cdot \frac{\partial \underset{\sim}{v}}{\partial z}} \quad . \tag{1}$$

We base our investigation of the stable boundary-layer height on this parameter.

Model calculations (Wyngaard, 1975) show that in a stable boundary layer the value of Ri_f is of the order of 0.2. This means that only a small fraction of the turbulent kinetic energy is destroyed by buoyancy. The remaining part is lost through viscous dissipation, because the other terms in the energy budget such as the transport term and the time derivative, are negligible in a stable boundary layer (Brost and Wyngaard, 1978).

The thickness of the turbulent boundary layer must be related to the shear production and the buoyancy destruction averaged across the boundary layer. Therefore we introduce as

a new parameter $\overline{Ri_f}$, which is defined as

$$\overline{Ri_f} = - \int_0^h \frac{g}{T} \overline{w\theta}\, dz \Big/ \int_o^h \frac{\underset{\sim}{\tau}}{\rho} : \frac{\partial \underset{\sim}{v}}{\partial z}\, dz \qquad (2)$$

where h is the boundary-layer height.

An expression for $\overline{Ri_f}$ in terms of other boundary-layer parameters is necessary in the subsequent discussions. It is obtained by assuming the following self-similar profiles

$$\overline{w\theta} = \overline{w\theta}_o\, f_1\,(z/h) \qquad (3a)$$

$$\underset{\sim}{\tau}/\rho = u_*^2\, \underset{\sim}{f}_2\,(z/h) \qquad (3b)$$

$$\underset{\sim}{v} = U_h\, \underset{\sim}{f}_3\,(z/h), \qquad (3c)$$

where the friction velocity u_* is defined as $u_* = \sqrt{|\underset{\sim}{\tau}_o|/\rho}$. The indices o and h denote the value of the variable at the surface and at the top of the boundary layer, respectively. It is then obvious that the following conditions must be satisfied:

$$f_1(0) = 1,\ |\underset{\sim}{f}_2(0)| = 1,\ |\underset{\sim}{f}_3(0)| = 0$$

and

$$f_1(1) = 0,\ |\underset{\sim}{f}_2(0)| = 0,\ |\underset{\sim}{f}_3(0)| = 1.$$

For the flux profiles self-similarity is confirmed by the data of Caughey et al.(1979). Their data can be well approximated by the following expressions

$$f_1(z/h) = (1-z/h)^3 \qquad (4a)$$

$$|\underset{\sim}{f}_2(z/h)| = (1 - z/h)^{1.5} \qquad (4b)$$

Self-similarity as expressed by (3c) is not so clear for the velocity profile. Yamada (1976) presents some evidence in favor of self-similarity although the scatter in his data is rather large. Caughey et al. (1979) argue that mean profiles in the stable boundary layer may be far out of equilibrium

with the local turbulent boundary-layer structure, so that self-similarity is destroyed. Furthermore, (3c) cannot be valid in the surface layer, where a description of the velocity profile in terms of u_* and the roughness length z_o is more appropriate. The surface layer can be treated separately (Zeman, 1979), but a simple formulation is then no longer possible. We must, therefore, consider (3c) as a rather restrictive assumption. It is only justified, because we consider here an integral method which treats bulk properties of the boundary layer. This means that detailed specification of the profiles is not necessary, because they are only applied in integrals across the boundary layer. To facilitate an easy evaluation of integrals we tentatively assume

$$|\underset{\sim}{f}_3(z/h)| = z/h, \qquad (4c)$$

which denotes a linear velocity profile in the boundary layer. This is a consistent extrapolation of the log-linear profile valid in the surface layer for stable conditions (Wyngaard, 1973).

To resume our discussion of an alternative expression for $\overline{Ri_f}$ substitution of (3a), (3b) and (3c) into (2) leads to

$$\overline{Ri_f} = c_1 \frac{h}{L} c_D^{1/2}, \qquad (5)$$

where the Obukhov length L is defined as

$$L = - \frac{u_*^3 T}{gk \overline{w\theta}_o} . \qquad (6)$$

The Von Karman constant k is taken here equal to 0.35. The drag coefficient c_D is defined as $c_D = (u_*/U_h)^2$. The integrals in (2) can be evaluated for the functions given by (4a), (4b) and (4c). This leads to a value 1.8 for the nondimensional constant c_1.

For comparison we give the results of Brost and Wyngaard (1978). Their expressions for the geostrophic drag law

which applies to stationary conditions reduce for large values of h/L to

$$\frac{G}{u_*} \sin \alpha = 10 \frac{h}{L} \qquad (7)$$

$$\frac{G}{u_*} \cos \alpha = \frac{2.2}{k} \frac{h}{L} , \qquad (8)$$

where α is the angle between the geostrophic wind G and the surface wind direction. Assuming $U_h \approx G$ we find from (7) and (8) that $c_D^{1/2}\, h/L = 0.085$. Substitution of this result into (5) leads to a value of $\overline{Ri_f}$ equal to 0.15, which seems a reasonable value in comparison with our earlier estimate for Ri_f. However, we must stress that this result is only valid for the stationary conditions and large values of h/L considered in this paragraph.

A rate equation for the boundary-layer height h is now obtained by considering $\overline{Ri_f}$ for non-stationary conditions. In that case $\overline{Ri_f}$ becomes a function of time. This time dependence is found by specifying separate equations for the numerator and the denominator of (2). We proceed from the horizontally homogeneous equations for the mean velocity components u, v and for the mean potential temperature θ. These read

$$\frac{\partial u}{\partial t} = f\, v + \frac{\partial}{\partial z} (\tau_x/\rho), \qquad (9a)$$

$$\frac{\partial v}{\partial t} = - f\, (u - G) + \frac{\partial}{\partial z} (\tau_y/\rho), \qquad (9b)$$

$$\frac{\partial \theta}{\partial t} = - \frac{\partial}{\partial z} \overline{w\theta} . \qquad (9c)$$

Here the x-axis is taken along the geostrophic wind G; f is the Coriolis parameter and $\overline{w\theta}$ is the vertical turbulent temperature flux. The divergence of long-wave radiation is neglected in (9c), because we assume that the height of the turbulent boundary layer, considered here, is primarily influenced by dynamical processes (Brost and Wyngaard, 1978; Zeman, 1979). Such an assumption, however, cannot be made when

the evolution of the inversion height is considered (André et al., 1978; Yamada, 1979; Nieuwstadt, 1980a).

An expression for the denominator of $\overline{Ri_f}$ is obtained from (9a) and (9b) by constructing an equation for the mean kinetic energy $E = 1/2\ (u^2 + v^2)$. Integrating the resulting equation across the boundary layer and applying the boundary conditions $u = v = 0$ for $z = 0$ and $\tau_x = \tau_y = 0$ for $z = h$, we find

$$\int_0^h \frac{\underset{\sim}{\tau}}{\rho} \cdot \frac{\partial \underset{\sim}{v}}{\partial z}\, dz = h\, P + E_{z=h}\, \frac{dh}{dt} - \frac{d}{dt} \int_0^h E\, dz, \qquad (10)$$

where the production term P is defined as

$$P = {}^1/h \int_0^h f\, G\, v\, dz. \qquad (11)$$

This term represents the work done on the ageostrophic velocity component by the pressure gradient $\partial p/\partial y$, which is related to the geostrophic wind by

$$G = -\frac{1}{\rho f} \frac{\partial p}{\partial y}\,. \qquad (12)$$

Since P is indirectly the main source of turbulent kinetic energy in a stable boundary layer, it is not surprising that it is an important parameter in the development of the turbulent layer depth. We return to a further discussion of P in section 3.

If we substitute the velocity profile (3c) and (4c), equation (8) reduces to

$$\int_0^h \frac{\underset{\sim}{\tau}}{\rho} \cdot \frac{\partial \underset{\sim}{v}}{\partial z}\, dz = h\, P + c_2\, U_h^{\,2}\, \frac{dh}{dt}\,. \qquad (13)$$

Evaluation of the integrals leads to $c_2 = 1/4$. We have assumed that U_h is stationary. A non-stationary behavior can be incorporated in (10) by specifying a separate equation for U_h (Zeman, 1979). We will, however, not pursue this here.

Next we derive an equation for the numerator of (2) by multiplying the temperature equation (9c) with the coordi-

nate z and integrating the resulting expression across the boundary layer. With the aid of Leibnitz's rule we find

$$\int_0^h \overline{w\theta}\, dz = -\frac{d}{dt}\int_0^h z\,(\theta_h-\theta)dz + {}^1/2\, h^2\, d\theta_h/dt, \qquad (14)$$

where θ_h is the temperature at the top of the boundary layer. This temperature will change as function of time due to advection and long-wave radiation. We neglect these processes here and assume that θ_h is constant in time. This means that the last term in (14) is neglected. Non-stationary behavior of θ_h requires a separate rate equation (Zeman, 1979), which we will not pursue here.

Consistent with (3) we assume that the temperature distribution is given by the following self-similar profile

$$\theta_h - \theta = (\theta_h - \theta_o)\, f_4(z/h), \qquad (15)$$

where θ_o is the temperature at the surface. It should be mentioned that the arguments concerning self-similarity discussed earlier are also applicable here. The function $f_4(z/h)$ should always satisfy the constraints $f_4(1) = 0$ and $f_4(0) = 1$. In our calculations an explicit expression for $f_4(z/h)$ is needed. Yamada (1979) presents some evidence for a behavior according to a cubic power law. Here we use a linear profile following Zeman (1979)

$$f_4(z/h) = 1 - z/h\,. \qquad (16)$$

After substitution of the profiles (15) and (16) into (14) we find

$$\int_0^h \overline{w\theta}\, dz = c_3\, h^2 \frac{d\theta_o}{dt} - 2\, c_3\, (\theta_h-\theta_o)\, h \frac{dh}{dt}\,, \qquad (17)$$

where the integration constant c_3 becomes equal to 1/6. Note that in a stable boundary layer generally $d\theta_o/dt < 0$, which indicates cooling of the surface.

Substitution of (13) and (17) into (2) then results in the following rate equation for h

$$2\left[1 - \frac{c_2}{2c_3}\frac{\overline{Ri_f}}{Ri_B}\right]\frac{dh}{dt} = \frac{1}{T}\left[h_e - h\right], \qquad (18)$$

where

$$T = -\frac{(\theta_h - \theta_o)}{d\theta_o/dt} \qquad (19)$$

and

$$h_e = -\frac{\overline{Ri_f}\, P}{c_3 \frac{g}{T}\frac{d\theta_o}{dt}}\,. \qquad (20)$$

The bulk Richardson number Ri_B is defined as

$$Ri_B = \frac{g}{T}\frac{(\theta_h - \theta_o)h}{U_h^2} \qquad (21)$$

We first direct our attention to the ratio $\overline{Ri_f}/Ri_B$, which with the aid of (5), (6) and (21) can be transformed to

$$\frac{\overline{Ri_f}}{Ri_B} = c_1\, k\, \frac{c_H}{c_D}\,, \qquad (22)$$

where c_H is defined by $\overline{w\theta_o} = c_H\, U_h(\theta_o - \theta_h)$. c_D was defined earlier (see text following (5)). In order that (18) has a physically realistic solution, which remains bounded for all times, the following constraint must be satisfied: $\overline{Ri_f}/Ri_B < 2c_3/c_2$. With $c_1 = 1.8$, $c_2 = 1/4$, $c_3 = 1/6$, as derived above, and with (22) this condition leads to $c_H/c_D < 2.1$. It means that c_H must not be much larger than c_D, or heat must not be transported more effectively than momentum. This condition is certainly met in a stable boundary layer, where observations indicate that $c_H \sim c_D$

(Arya, 1977)†. Substitution of this observational result into (22) leads to a constant ratio $\overline{Ri_f}/Ri_B$ equal to 0.63. We stress that this does not imply that $\overline{Ri_f}$ is also constant. As we have seen above, $\overline{Ri_f}$ = const. occurs for stationary conditions and large values of h/L.

With this result for $\overline{Ri_f}/Ri_B$ and using the values for c_2 and c_3, discussed above, we find $2(1 - (c_2/2c_3)\overline{Ri_f}/Ri_B) \sim 1$. Equation (18) now is simplified to

$$\frac{dh}{dt} = \frac{1}{T}(h_e - h). \qquad (18a)$$

This equation can be characterized as a linear relaxation equation, for which the solution evolves in time toward an equilibrium value h_e. The term equilibrium height is chosen because (18a) shows that dh/dt = 0 for $h = h_e$. The equilibrium height is discussed in section 3. The rate of approach of h toward h_e is governed by the time scale T, which is discussed in section 4.

An equation similar to (18a) was also proposed by Deardorff (Yu, 1978), Smeda (1979) and Mahrt (1981). However, their expressions for T and h_e are different from (19) and (20). We shall return to these differences in the next sections.

With the initial condition $h = h_o$ for $t = t_o$ equations (18a), (19) and (20) allow an analytic solution. It reads

$$h = h_e(t) + \frac{F(t_o)}{F(t)}\{h_o - h_e(t_o)\} + \\ - \frac{1}{F(t)} \int_{t_o}^{t} F(s) \frac{dh_e}{ds}\, ds, \qquad (23)$$

---

†Several authors (e.g. Melgarejo and Deardorff, 1974) use the definition $\overline{w\theta_o} = c_H u_* (\theta_o - \theta_H)$. In that case (22) becomes $\overline{Ri_f}/Ri_B = c_1 k c_H/c_D 1/2$. Equivalently the results of Melgarejo and Deardorff indicate $c_H \sim c_D^{1/2}$.

where

$$F(t) = \{\theta_h - \theta_o(t)\}. \qquad (24)$$

The first term on the righthand side of (23) shows the limit condition of a relaxation process when h becomes equal to h_e. The second term gives the influence of the initial condition. This term decays as a function of time because F(t) is a monotonic increasing function (remind that we take $d\theta_o/dt < o$ in a stable boundary layer). The last term shows that the solution for h depends on the complete time history of h_e. This illustrates the difference between this solution and a diagnostic equation for which h(t) can only depend on the values of parameters at time t. Also note that this term vanishes for constant h_e, to which we shall return in the next section.

Equation (23) is singular for $\theta_o(t_o) = \theta_h$ because T then becomes equal to zero. Such an initial condition applies to the boundary layer shortly before sunset, when the potential temperature is constant with height. The boundary-layer height then collapses from its convective value of ~1 km to its nocturnal value which is of the order of a few hundred meters. This transition region, which takes a few hours (Caughey et al., 1979), is poorly understood.

Conditions are highly non-stationary leading to rapidly changing profiles so that integral methods are probably not applicable. Therefore, it is not surprising that our rate equation, which is based on integral methods, shows a singular behavior in the transition period. This means in our opinion that (18a) only describes the development of the stable boundary-layer height after the sunset transient has decayed.

3. The equilibrium height

In this section the equilibrium height h_e given by (20) is discussed in more detail and compared with results found by other authors.

We can interpret (20) as a diagnostic equation for h. Diagnostic equations are applicable in stationary conditions. They express the boundary-layer height in terms of local parameters (Zilitinkevich, 1972; Nieuwstadt, 1980b). Such an interpretation for h_e is consistent with the rate equation (18), because the solution (23) shows that for stationary conditions h approaches the then constant h_e for $t \to \infty$. This means that a diagnostic expression for the boundary-layer height must be considered as an asymptotic limit for the special circumstances that steady-state conditions prevail. Equation (20) shows, that stationary conditions are only possible for a constant cooling rate , $d\theta_o/dt$ = const. This condition is also argued by Brost and Wyngaard (1978).

We proceed to derive a simplified expression for h_e, which is constructed by specifying an approximate expression for P in (20). Recalling the discussion following (11), we note that P represents the work done by the ageostrophic wind component v. This velocity component must be proportional to G sin α so that as a first approximation $P \sim f G^2 \sin \alpha$ seems suitable. It shows that P, and therefore h_e, increases when the cross-isobaric angle α increases.
However, P must satisfy another constraint, which can be derived by integrating the stationary form of (9a) across the boundary layer. It reads

$\int_0^h f v \, dz = u_*^2 \cos \alpha$, where we have used the fact that the surface stress is parallel to the surface wind. Substitution of this result in (11) shows that P must also be proportional to cos α. As a convenient interpolation formula, which combines both dependences of P on α, we propose $P \sim f G^2 \sin \alpha \cos \alpha$. Substitution into (20) leads to our final result

$$h_e = c_4 \frac{f G^2 \sin \alpha \cos \alpha}{\frac{g}{T} \left| \frac{\partial \theta_o}{\partial t} \right|} \quad , \qquad (25)$$

where $\overline{Ri_f}$ and c_3 have been absorbed in the constant c_4, whose magnitude will be estimated in the next section.

Expression (25) is attractive because it does not contain turbulent fluxes. However, the angle α is an internal boundary-layer parameter, which is usually obtained from a resistance law (Melgarejo and Deardorff, 1974; Arya, 1977). Unfortunately, the estimates of α with these laws show much scatter when compared with observations (Nieuwstadt, 1980b). Nevertheless in our opinion (25) is illustrative, because it shows clearly the influence of wind direction change in a stable boundary layer.

A diagnostic equation for the boundary-layer height is not confirmed by observations (Nieuwstadt and Driedonks, 1979; Nieuwstadt, 1980b). The reasons are: stationary conditions cannot be attained in practice because the cooling rate is seldom constant for an extended period of time (cf. the case study shown in section 5) and, more important, because time scales in the stable boundary layer become very large. This means, as we will show in the next section, that the asymptotic value represented by (25) generally cannot be reached during the course of a night.

Therefore, it is not possible to check (25) by comparison with observations and the only thing we can do is to compare it with expressions derived by other authors. We assume large values of h/L so that (7) and (8) are valid.

Brost and Wyngaard (1978) propose

$$h \sim \frac{u_*^2}{f\, G \sin \alpha} \qquad (26)$$

They show that (26) is confirmed by model calculations for the stationary boundary layer. To show its consistency with (25) we use $d\theta_o/dt \sim \overline{w\theta_o}/h$, which can be derived by integrating (9c) across the boundary layer if conditions are stationary. Substitution of this result in (25) and the use of (8) then lead to (26).

A well known equation for the height of the stationary boundary layer has been derived by Zilitinkevich (1972). It

reads

$$h = c_5 \left(\frac{u_* L}{f}\right)^{1/2} . \qquad (27)$$

Numerous model calculations (e.g. Businger and Arya, 1974) confirm this expression. However, the value of c_5 found by different authors varies appreciably. Here we shall use $c_5 = 0.4$ proposed by Brost and Wyngaard (1978).

In the derivation of (27) an assumption is made concerning the turbulent transfer coefficient in a stable boundary layer. This contrasts with the derivation of (25) and (26) which is based only on the equations (9a), (9b) and (9c) for the mean values. This additional assumption must be taken into account in a comparison with (25). If we use $(\partial\theta/\partial z)_o \sim (\theta_h - \theta_o)/h$ as follows from (15), the relation for $d\theta_o/dt$, discussed above, can be extended to $d\theta_o/dt \sim \overline{w\theta}_o/h \sim -K(\theta_h - \theta_o)/h^2$. A reasonable assumption for the turbulent transfer coefficient in the stable boundary layer is $K \sim u_* L$, which is consistent with a linear wind speed profile in the surface layer. Substitution of these results in (25), application of (7) and (8) and also the use of the results on c_D and c_H discussed in the preceding section then show that (25) and (27) are equivalent.

Another expression for the equilibrium height has been proposed by Deardorff (Yu, 1978) and Smeda (1978). This reads

$$h \sim u_*/f . \qquad (28)$$

It shows that the stationary, stable boundary-layer height is not directly dependent on stability. Instead, (28) implies that it is proportional to the neutral boundary-layer height (Tennekes, 1973). This result is clearly in contradiction with Zilitinkevich's expression (27).

Mahrt (1981) assumes that the equilibrium height can be described in terms of a critical value of the bulk Richardson

number (21). In our notation this leads to

$$h = Ri_{cr} \frac{G^2}{\frac{g}{T}(\theta_h - \theta_o)} \qquad (29)$$

where the critical Richardson number Ri_{cr} is estimated to be equal to 0.5. This approach is in contradiction with the results of Brost and Wyngaard (1978), who show that no unique value is found for the bulk Richardson number in a stable boundary layer. On the other hand our result (22) with $c_H/c_D \sim 1$ and $\overline{Ri_f} \sim 0.2$, as derived in the previous section for stationary conditions, leads to $Ri_B \sim 0.3$ close to the value proposed by Mahrt. Therefore, the question whether (29) is valid in a stable boundary layer is still unresolved.

Summarizing we conclude that the height of the steady, turbulent, stable boundary layer is given by (25), (26) or (27), which were shown to be equivalent for large values of h/L.

4. The time scale

The time scale T in (18a) governs the rate at which the solution is forced toward the equilibrium height. We shall examine the consequences of expression (19) for this time scale.

An important aspect of (19) is that the time scale increases monotonically as a function of time. In other words the boundary-layer height evolves at a decreasing rate. In terms of the analytic solution (23) this means that the dependence of the boundary-layer height on time is algebraic rather than exponential as would be the dependence in a relaxation process with fixed time constant.

An estimate for T is readily obtained from (19). At the beginning of the night, when $\theta_h - \theta_o$ is still small, and for a reasonable value of $d\theta_o/dt \sim -1^{\circ}C/hr$ T becomes equal to a few hours. Later in the night, when $\theta_h - \theta_o$ is large, the

time scale can easily become of the order of ten hours. A similar estimate is also given by Caughey et al. (1979). This leads to the important conclusion that the nocturnal boundary-layer height adjusts very slowly to a change in external conditions.

This large time scale leads to the practical consequence that a night period is generally too short for the boundary-layer height to reach its equilibrium value. We illustrate this by presenting a few examples of the time evolution of the boundary-layer height as described by (18a) for a constant value of $d\theta_o/dt$ when $h \to h_e$ for $t \to \infty$. A comparison is made with the results of Brost and Wyngaard (1978), who present model calculations of the time evolution of h for several values of $d\theta_o/dt$. This can also be considered as a comparison with the model of Zeman (1979), who claims a good agreement with the results of Brost and Wyngaard. The data of these authors on α, which are tabulated for the case G = 10 m/s, are used in the expression (25) to evaluate h_e. In Figures 1

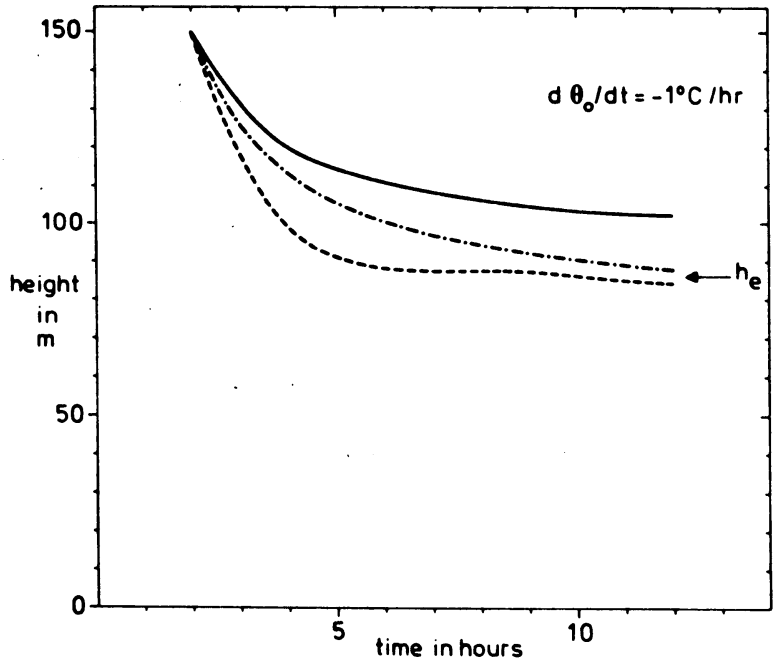

Fig. 1. A comparison of the solution of the rate equation (18a) with the calculations of Brost and Wyngaard (1978) for the case $d\theta/dt = -1^{\circ}C/hr$; *drawn line: the solution of (18a) with* h_e *equal to the result of Brost and Wyngaard, which is also indicated in the figure; dashed line: the results of Brost and Wyngaard; dashed-dotted line the solution of (18a) with* $c_4 = 0.15$ *in (25).*

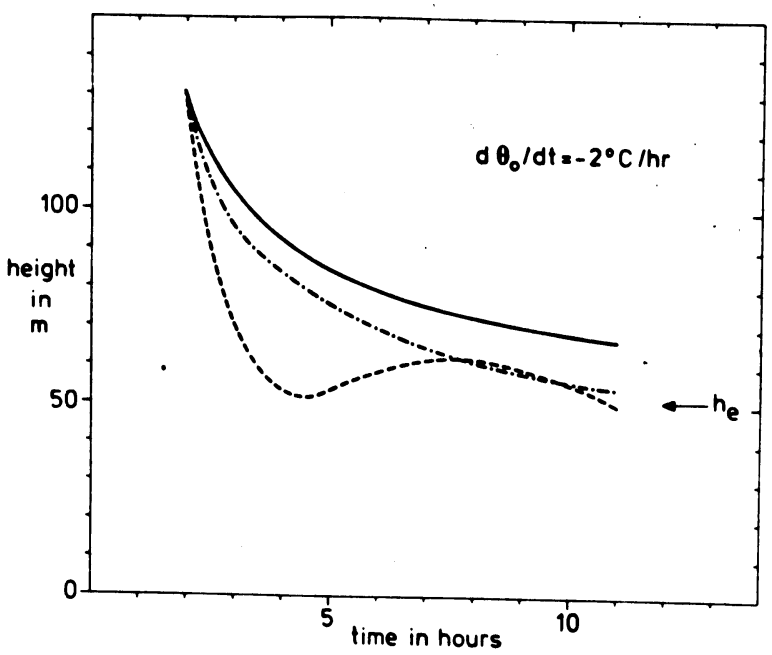

Fig. 2. The same as Figure 1 for $d\theta_o/dt = -2^oC/hr$.

and 2 we show results for $d\theta_o/dt = -1$ and $-2^oC/hr$, respectively. For one set of curves shown in these figures we have adjusted the constant c_4 from 0.18 to 0.21 in order to make our value of h_e equal to the stationary boundary-layer height given by Brost and Wyngaard. These results show clearly that even after a time period of ten hours the boundary layer is still considerably higher than the equilibrium height h_e, despite the fact that the small rate of change of the solution seems to suggest that such an equilibrium condition has been reached. Therefore, the assumption that the boundary-layer height may reach its equilibrium value within a few hours, which underlies the application of diagnostic equations, is unwarranted. The boundary layer seems quasi-stationary only because its time scale is very large.

Adopting the view that the boundary layer is still evolving after a time period of ten hours, we now look for a value of c_4 that leads to the best overall agreement with the results of Brost and Wyngaard. As indicated by the second set of

curves in the Figures 1 and 2 this is obtained for $c_4 = 0.15$. This value is suggested to calculate the equilibrium height from (25) and will be used in the remainder of this paper.

As another consequence of the large time scale in the nocturnal boundary layer the influence of the initial condition on the solution of (18a) decays only very slowly. We may illustrate this memory effect by solutions of (18a) for different initial conditions which are shown for the case $d\theta_o/dt = -2^oC/hr$ in Figure 3. In the calculation we have arbitrarily assumed that (18a) becomes valid two hours after the time that $\theta_o = \theta_h$. Even after ten hours the curves in Figure 3, which asymptotically must become equal to the indicated value of h_e, differ substantially.

This result means that the transient condition around sunset, which determines the initial condition for our rate equation (cf. section 2), has an important influence on the

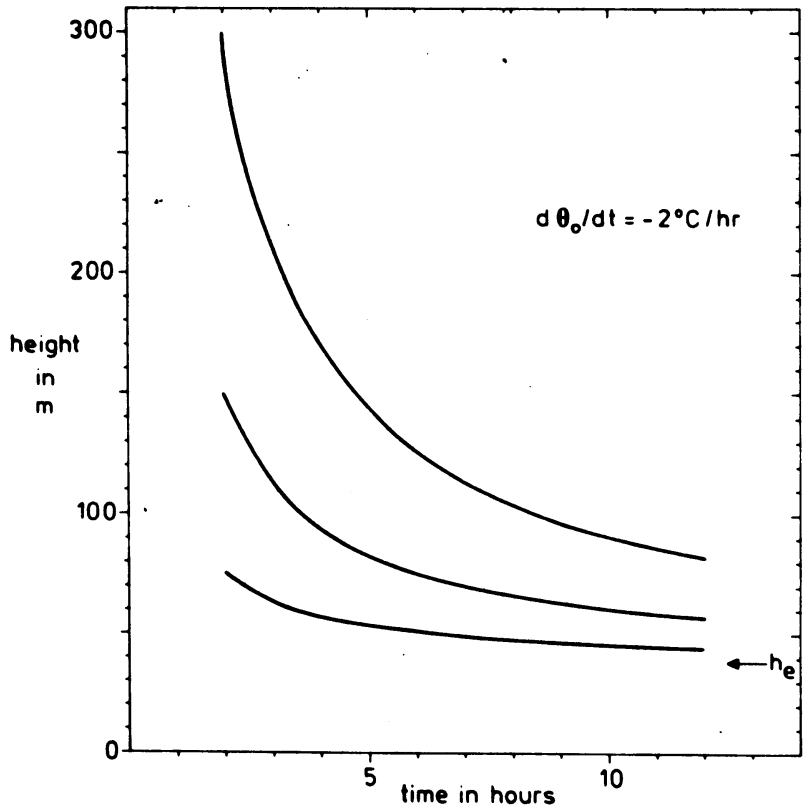

Fig. 3. The solution of (18a) for $d\theta_o/dt = -2^oC/hr$ *and with* $c_4 = 0.15$ *in (25) for several initial conditions. The value of* h_e *is also indicated.*

boundary layer later in the night. Therefore, the successful prediction of the boundary-layer height for an entire night period depends strongly on our ability to describe its evolution around sunset. A simple model for this is yet to be found and must be the subject of further study.

Deardorff (Yu, 1978), Smeda (1979) and Mahrt (1981) use another expression for the time scale T in their rate equations. They propose $T \sim h/u$, where the velocity scale u is usually taken equal to u_*. The actual magnitude of these time scales varies strongly (Mahrt, 1981).

5. Observations

To compare our model with observations we use measurements during clear nights, when a shallow turbulent boundary layer has developed near the surface. We have obtained such data with the meteorological mast at Cabauw in the Netherlands. An extensive description of the mast is given by Driedonks et al. (1978). Our data set consists of observations of G, α, L, u_*, θ_o and h during the course of several nights in 1977. The parameters G, α and θ_o are directly measured. u_* and L are obtained indirectly with the aid of a profile method (Nieuwstadt, 1978). We recall that the boundary-layer height h is the height to which turbulence extends. Therefore we use the observations made with an acoustic sounder to estimate this height. An additional discussion of this data set is presented by Nieuwstadt (1980b).

We have stated several times that the stable boundary-layer height cannot be described in terms of a diagnostic equation. This point is now illustrated by a comparison with our observations. Several equivalent expressions for a diagnostic equation of the nocturnal boundary-layer height were discussed in section 3. Because equation (27), derived by Zilitinkevich (1972), is widely used, we have chosen it for our comparison.

The results are shown in Figure 4. The agreement between this equation and the Cabauw observations is undoubtedly poor. It cannot be attributed to a wrong value of the proportionality constant in (27). Therefore, the conclusion that diagnostic equations are not appropriate in this case is confirmed.

To compare the observations with a prognostic equation we solve the rate equation (18a) by substituting the observed values of G, α and $d\theta_o/dt$ in (19) and (25). Here, θ_h is taken equal to the boundary-layer temperature at the beginning of the night, when the temperature profile is neutral. The calculation is started at approximately 2 hours after sunset to avoid the initial development of the boundary layer (cf. section 2). At this time usually the first clear observation of the boundary-layer height is obtained from the acoustic sounder. This value is applied as the initial condition in

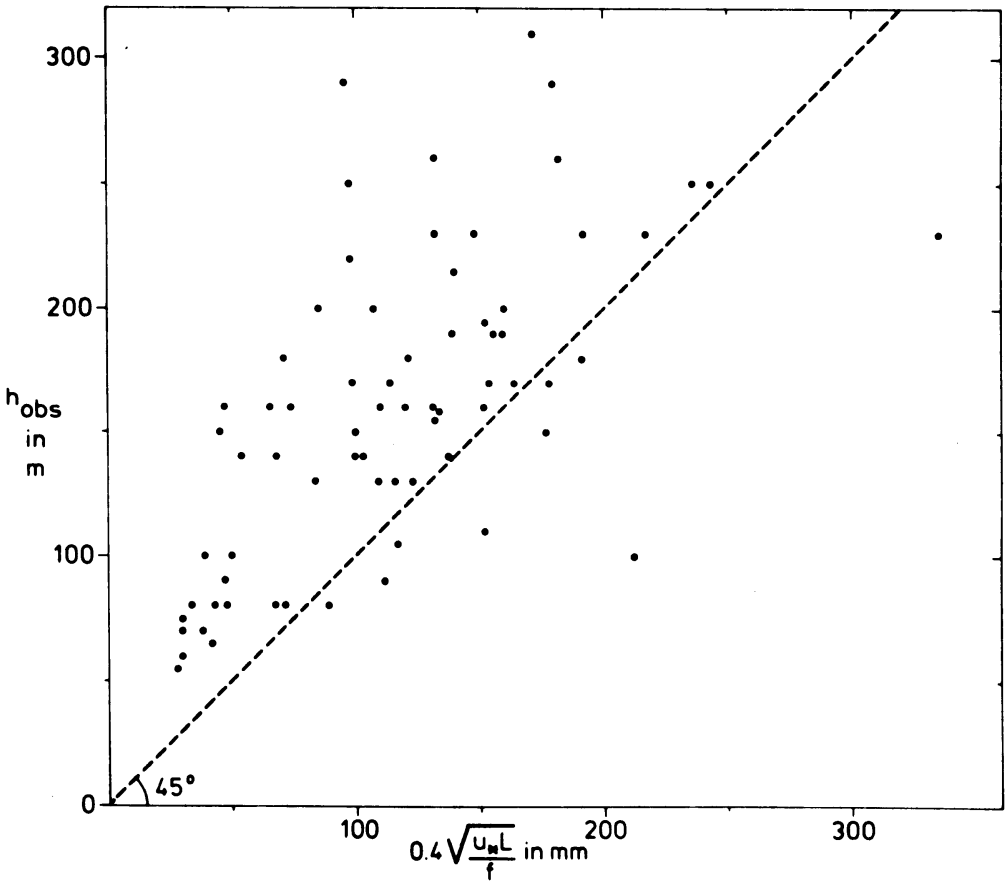

Fig. 4. A comparison of the observed values of the boundary-layer height with the diagnostic expression of Zilitinkevich (27).

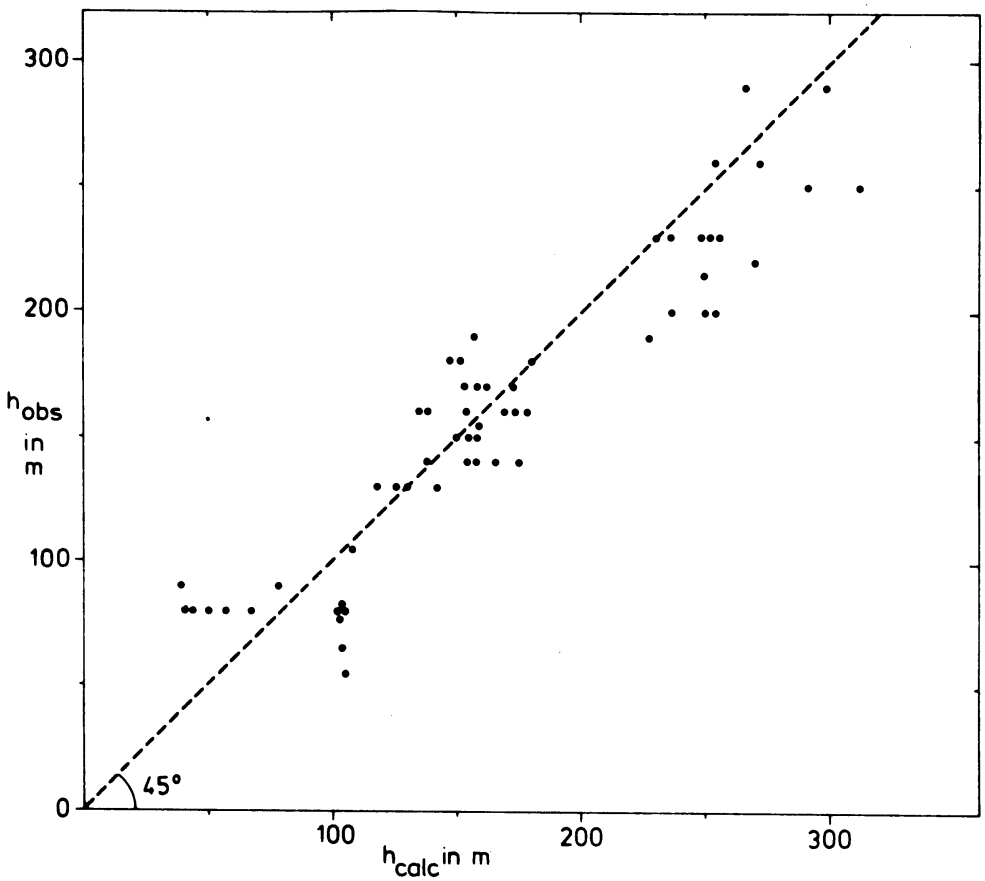

Fig. 5. A comparison of the observed values of the boundary-layer height with the solution of the rate equation (18a).

the solution of (18a). The results are shown in Figure 5. The agreement between observations and calculations is much better than that in Figure 4. The main reason is persistence of the initial conditions both in the observed and calculated results. This confirms the influence of the large time scale discussed in section 4.

As an additional example we show a case history of nocturnal boundary-layer development. The parameters G, α and θ_o are shown in Figure 6 as a function of time. The boundary-layer height is given in Figure 7. The results of the prognostic equation agree better with the observations than the results of the diagnostic equation.

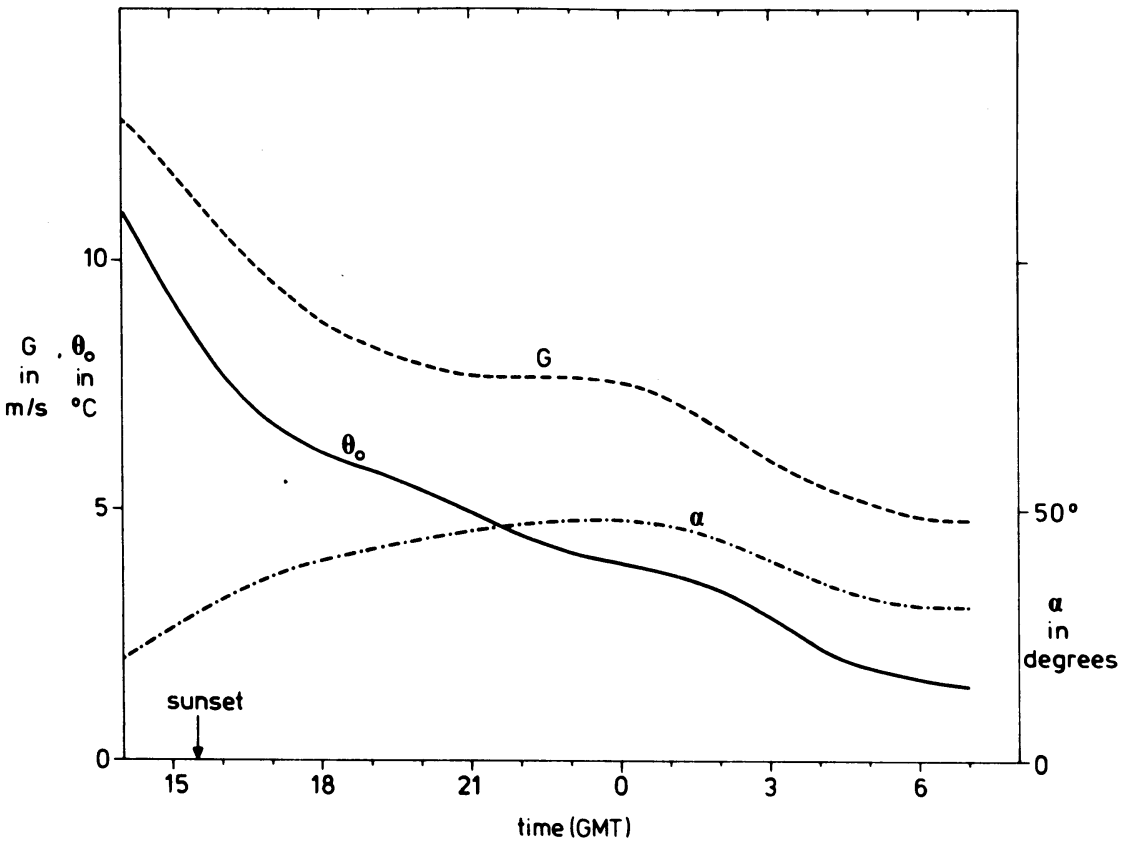

Fig. 6. An observed stable night period. The parameters G, θ_o and α as a function of time.

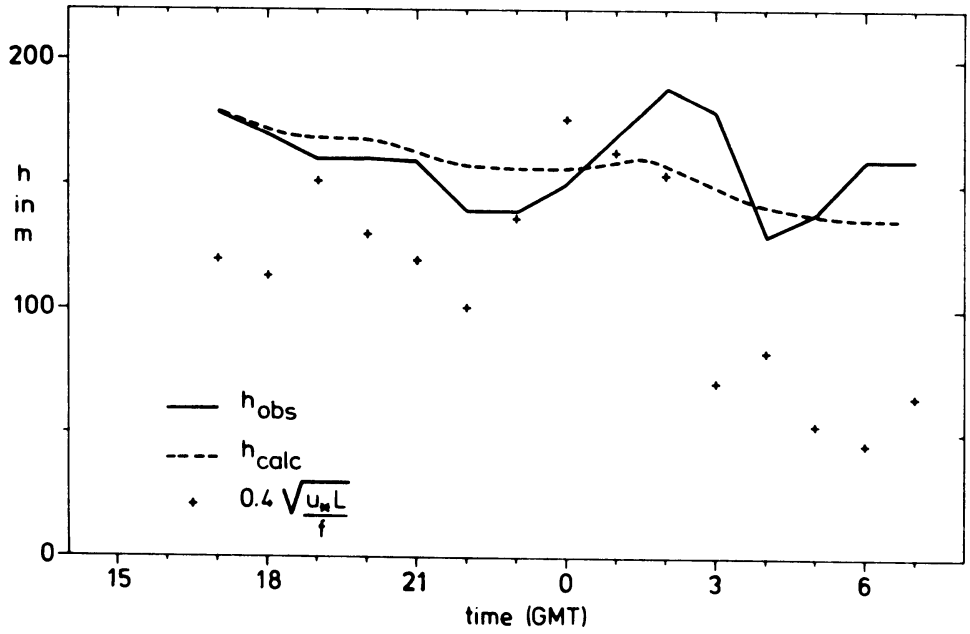

Fig. 7. The time evolution of the boundary-layer height for the night period shown in Figure 6; drawn line: the observed value; dashed line: the solution of the rate equation (18a); plus signs: the values obtained from Zilitinkevich's expression (27).

6. Conclusions

Using self-similar velocity, temperature and flux profiles we have derived a rate equation for the nocturnal boundary-layer height by means of an integral method. The equation has the form of a linear relaxation equation. It shows how the boundary layer is forced toward an equilibrium height. The equation cannot describe the transient conditions around sunset.

The equilibrium height, which can be considered as a diagnostic expression for the boundary-layer height, is the asymptotic solution of the rate equation for a constant cooling rate. It is directly related to the energy produced by the ageostrophic wind component against the pressure gradient. An estimate of this production term leads to a simplified expression for the equilibrium height. This is shown to be equivalent to other diagnostic expressions of the nocturnal boundary-layer height.

The rate of change of the boundary-layer height is governed by a time scale that increases monotonically as a function of time. It varies from a few hours in the beginning of the night to a value of about ten hours as sunrise approaches. This means that the stable boundary-layer height evolves very slowly and the equilibrium height is generally not attained during the course of a night. Another consequence of the large time scale is that the influence of the initial condition on the solution of the rate equation decays slowly.

A comparison with observations shows that the results obtained with the rate equation are superior to those which follow from diagnostic equations.

VI. Observations of the nocturnal boundary layer during clear nights measured with the meteorological mast at Cabauw in the Netherlands.

Legenda (all times are in Greenwich Mean Time)

$T_{0.6}$	Temperature at a height of 0.6 m in °C	given as half-hour averages over the time-periods indicated
$T_{1.5}$	Temperature at a height of 1.5 m in °C	
T_{200}	Temperature at a height of 200 m in °C	
U_{10}	Wind speed at a height of 10 m in m/s	
U_{200}	Wind speed at a height of 200 m in m/s	
α_{20}	Wind direction at a height of 20 m in degrees	
α_{200}	Wind direction at a height of 200 m in degrees	
u_*	Friction velocity in m/s (obtained with a profile method F. Nieuwstadt (Bound.-Layer Meteor., 1978, 14, 235-246).	
T_*	Temperature scale in °C	
G	Geostrophic wind speed in m/s	given as obsrvations on each whole hour
α_G	Geostrophic wind direction in degrees	
h	Boundary-layer height in m from an acoustic sounder	

29/30 March 1977. Sunset at 18^{08} GMT. Sunrise at 5^{21} GMT.

Time	$T_{0.6}$	$T_{1.5}$	T_{200}	U_{10}	U_{200}	α_{20}	α_{200}	u_*	T_*	G	α_G	h
15^{30}-16	3.6	3.4	1.4	6.3	7.5	341	355	.54	-.06	9.8	62	-
16-16^{30}	3.2	3.1	1.3	6.1	7.8	334	349	.50	-.03			
16^{30}-17	2.2	2.3	1.2	5.2	7.7	333	356	.44	.01	10.3	59	-
17-17^{30}	1.5	1.6	1.0	4.2	8.3	343	2	.33	.04			
17^{30}-18	1.0	1.2	1.1	4.1	8.2	347	10	.29	.07	8.9	63	-
18-18^{30}	.2	.5	1.1	4.2	7.5	349	14	.36	.10			
18^{30}-19	- .3	.1	.9	3.7	6.5	346	22	.25	.10	8.2	73	-
19-19^{30}	-1.0	- .4	.8	2.9	5.1	351	37	.19	.10			
19^{30}-20	-1.5	- .2	.8	2.1	5.0	359	52	.11	.06	8.9	74	-
20-20^{30}	-1.6	- .5	.8	2.2	5.5	17	48	.12	.07			
20^{30}-21	-1.6	- .6	.7	2.1	5.9	25	55	.09	.06	9.7	76	-
21-21^{30}	-1.7	- .7	.8	1.8	6.2	33	57	-	-			
21^{30}-22	-1.8	- .9	.6	1.7	6.2	46	60	-	-	7.6	83	-
22-22^{30}	-2.0	-1.3	.4	1.6	6.1	53	68	-	-			
22^{30}-23	-2.2	-1.3	.7	1.7	6.2	53	76	-	-	7.6	83	-
23-23^{30}	-1.9	-1.1	.7	2.1	7.0	63	83	.08	.06			
23^{30}-24	-1.7	-1.0	.8	2.3	7.2	63	87	.12	.07	7.6	87	140
0-0^{30}	-2.1	-1.3	.5	2.1	8.6	60	90	.13	.06			
0^{30}-1	-2.7	-1.8	.2	2.2	7.9	75	114	.11	.06	8.2	97	110
1-1^{30}	-2.4	-1.6	.3	2.4	7.3	84	129	.14	.07			
1^{30}-2	-2.8	-1.9	.2	2.2	7.2	84	129	.11	.06	7.9	97	100
2-2^{30}	-3.0	-2.1	- .0	2.3	7.2	86	128	.12	.06			
2^{30}-3	-2.9	-1.9	- .1	2.3	7.0	91	127	.13	.06	7.7	109	100
3-3^{30}	-2.5	-1.9	- .4	2.6	7.5	96	128	.17	.07			
3^{30}-4	-2.7	-2.1	- .5	2.6	7.6	95	123	.17	.07	8.1	108	100
4-4^{30}	-3.3	-2.3	- .6	2.0	7.6	89	116	.11	.05			
4^{30}-5	-3.5	-2.4	-1.0	1.9	7.3	88	116	.09	.05	8.9	101	100
5-5^{30}	-3.4	-2.4	-1.1	1.7	7.5	90	117	.07	.04			

30/31 March 1977. Sunset at 18^{09} GMT. Sunrise at 5^{29} GMT.

Time	$T_{0.6}$	$T_{1.5}$	T_{200}	U_{10}	U_{200}	α_{20}	α_{200}	u_*	T_*	G	α_G	h
15^{30}-16	4.1	3.8	1.5	5.5	8.1	82	86	.50	-.05	12.1	96	-
16-16^{30}	3.9	3.8	1.6	5.0	7.0	84	83	.44	-.02			
16^{30}-17	3.4	3.4	1.4	4.7	8.0	87	89	.41	.01	11.3	100	-
17-17^{30}	2.7	2.9	1.2	4.4	8.7	99	100	.38	.03			
17^{30}-18	1.9	2.2	1.0	3.7	9.4	100	101	.30	.06	11.1	98	-
18-18^{30}	1.1	1.5	.9	3.4	10.1	95	97	.26	.07			
18^{30}-19	.4	1.0	.7	3.1	10.5	87	94	.23	.07	11.7	96	-
19-19^{30}	- .2	.4	.4	2.8	9.8	77	90	.21	.08			
19^{30}-20	- .7	- .1	.2	2.8	9.9	74	90	.20	.08	11.8	97	190
20-20^{30}	- .9	- .3	.0	2.8	10.6	76	92	.20	.08			
20^{30}-21	- .8	- .4	- .3	3.4	11.9	75	94	.27	.07	12.1	92	185
21-21^{30}	-1.0	- .6	- .9	3.4	12.2	79	94	.28	.07			
21^{30}-22	-1.3	- .9	-1.3	3.4	12.2	84	99	.26	.06	11.3	98	165
22-22^{30}	-1.5	-1.1	-1.4	3.4	12.5	91	105	.27	.06			
22^{30}-23	-1.8	-1.5	-1.6	3.4	12.6	95	110	.27	.06	9.1	114	140
23-23^{30}	-2.2	-1.9	-1.7	3.1	12.8	97	114	.24	.06			
23^{30}-24	-2.5	-2.1	-1.9	3.0	12.6	100	119	.24	.06	9.9	120	150
0- 0^{30}	-2.6	-2.3	-1.9	3.6	12.7	102	126	.29	.06			
0^{30}-1	-3.0	-2.6	-1.8	2.9	12.4	107	133	.22	.06	8.3	127	150
1-1^{30}	-2.9	-2.6	-1.9	3.2	11.5	117	142	.25	.05			
1^{30}-2	-3.0	-2.7	-2.0	3.5	10.5	118	150	.28	.05	9.1	140	120
2-2^{30}	-3.4	-3.0	-2.1	3.0	10.6	116	156	.23	.06			
2^{30}-3	-3.6	-3.2	-2.2	3.0	11.4	114	156	.23	.05	8.5	146	110
3-3^{30}	-3.7	-3.3	-2.1	3.0	11.5	119	160	-	-			
3^{30}-4	-3.9	-3.5	-2.1	3.0	11.1	120	160	.23	.06	7.9	140	100
4-4^{30}	-4.4	-3.9	-2.3	2.7	10.4	123	161	.19	.06			
4^{30}-5	-4.3	-3.9	-2.4	2.9	10.4	119	156	.21	.06	7.5	139	90
5-5^{30}	-4.4	-3.9	-2.5	9.8	10.1	123	157	.20	.06			

9/10 April 1977. Sunset at 18^{26} GMT. Sunrise at 4^{56} GMT.

Time	$T_{0.6}$	$T_{1.5}$	T_{200}	U_{10}	U_{200}	α_{20}	α_{200}	u_*	T_*	G	α_G	h
16^{30}-17	4.4	4.4	2.2	6.8	9.8	26	28	.62	-.01	11.1	58	-
17-17^{30}	3.8	3.9	2.1	6.1	9.8	27	28	.55	.02			
17^{30}-18	3.1	3.4	2.0	5.3	9.3	11	19	.49	.04	12.8	55	-
18-18^{30}	1.9	2.3	2.0	3.8	9.2	23	36	.30	.08			
18^{30}-19	1.1	1.5	1.7	4.1	10.8	29	38	.34	.09	12.1	61	-
19-19^{30}	.7	1.1	1.3	4.3	11.1	30	37	.36	.09			
19^{30}-20	.2	.6	.9	4.0	10.9	31	42	.33	.09	12.0	59	-
20-20^{30}	- .5	.0	.6	3.5	10.2	34	46	.28	.09			
20^{30}-21	- .9	- .4	.2	3.5	9.6	31	48	.27	.09	10.6	63	110
21-21^{30}	-1.3	- .9	- .1	3.3	9.9	30	49	.25	.09			
21^{30}-22	-1.7	-1.3	- .3	3.1	10.5	31	50	.24	.08	10.8	61	105
22-22^{30}	-2.2	-1.7	- .4	2.7	10.4	31	52	.18	.07			
22^{30}-23	-2.5	-2.1	- .5	2.8	9.8	24	54	.19	.08	9.7	54	80
23-23^{30}	-2.8	-2.3	- .2	2.5	10.0	23	56	.16	.07			
23^{30}-0	-3.2	-2.5	- .1	2.4	10.1	22	57	.15	.07	10.6	53	80
0-0^{30}	-3.2	-2.6	- .1	2.4	9.9	24	62	.14	.07			
0^{30}-1	-3.5	-2.8	- .1	2.0	8.8	27	60	.10	.05	9.3	54	80
1-1^{30}	-4.2	-3.1	- .2	1.7	8.7	21	58	-	-			
1^{30}-2	-4.3	-3.3	- .2	1.9	8.1	17	58	.08	.05	9.9	54	80
2-2^{30}	-4.8	-3.7	- .3	2.0	8.0	12	62	.08	.06			
2^{30}-3	-4.5	-3.4	- .3	2.1	7.5	24	65	.10	.07	9.7	53	65
3-3^{30}	-4.5	-3.3	- .2	2.0	7.1	21	55	.09	.05			
3^{30}-4	-5.1	-3.9	- .2	2.0	6.9	13	46	.08	.06	8.9	52	55
4-4^{30}	-5.1	-4.2	- .2	1.6	6.4	27	45	-	-			
4^{30}-5	-5.5	-4.2	- .5	1.9	5.2	14	46	-	-	7.9	44	55
5-5^{30}	-5.4	-4.5	- .7	2.5	5.2	353	46	-	-			

18/19 May 1977. Sunset at 19^{31} GMT. Sunrise at 3^{41} GMT.

Time	$T_{0.6}$	$T_{1.5}$	T_{200}	U_{10}	U_{200}	α_{20}	α_{200}	u_*	T_*	G	α_G	h
17^{30}-18	17.9	18.3	-	5.4	11.2	68	70	.53	.07	16.5	83	-
18-18^{30}	17.4	17.8	-	5.0	11.5	68	72	.47	.09			
18^{30}-19	16.5	17.0	-	4.6	11.8	64	70	.44	.10	18.2	79	-
19-19^{30}	15.1	15.7	-	3.7	11.8	57	69	.33	.12			
19^{30}-20	14.2	14.9	-	3.3	11.6	48	64	.25	.12	18.6	79	-
20-20^{30}	12.1	13.0	-	2.9	10.4	29	59	.19	.11			
20^{30}-21	11.8	12.3	-	3.8	10.9	23	56	.31	.12	18.3	82	230
21-21^{30}	11.8	12.2	-	4.1	12.1	22	51	.36	.09			
21^{30}-22	11.8	12.1	-	4.7	13.7	28	51	.43	.08	18.6	79	230
22-22^{30}	11.7	12.0	-	4.4	14.5	36	57	.40	.08			
22^{30}-23	10.9	11.3	-	3.6	14.5	37	64	.31	.10	18.3	79	230
23-23^{30}	10.8	11.2	-	3.9	14.9	39	70	.33	.11			
23^{30}-0	10.3	10.7	-	3.6	14.2	34	71	.30	.11	18.0	82	260
0-0^{30}	9.9	10.3	-	3.6	14.0	36	69	.31	.10			
0^{30}-1	9.6	10.0	-	3.9	14.6	36	67	.33	.10	17.3	84	250
1-1^{30}	10.2	10.6	-	4.1	15.1	49	70	.36	.09			
1^{30}-2	10.1	10.6	-	4.3	16.1	59	76	.41	.10	18.1	85	250
2-2^{30}	9.5	10.0	-	3.5	13.9	56	72	.32	.10			
2^{30}-3	8.4	9.0	-	2.6	12.8	45	70	.18	.09	18.1	82	250
3-3^{30}	7.3	7.8	-	3.0	12.0	32	68	.21	.10			
3^{30}-4	6.9	7.3	-	3.0	12.1	34	67	.23	.10	17.9	79	230
4-4^{30}	6.9	7.2	-	3.4	12.8	35	71	.30	.08			

22/23 May 1977. Sunset at 19^{37} GMT. Sunrise at 3^{36} GMT.

Time	$T_{0.6}$	$T_{1.5}$	T_{200}	U_{10}	U_{200}	α_{20}	α_{200}	u_*	T_*	G	α_G	h
17^{30}-18	16.1	16.2	-	6.2	10.9	20	25	.61	.02	15.2	72	-
18-18^{30}	15.3	15.6	-	5.4	11.2	24	28	.49	.04			
18^{30}-19	14.3	14.6	-	4.5	10.8	23	29	.41	.06	15.0	72	-
19-19^{30}	13.3	13.6	-	3.9	11.4	28	33	.34	.07			
19^{30}-20	12.3	12.7	-	3.4	11.3	29	36	.28	.08	15.0	71	-
20-20^{30}	11.5	11.9	-	3.2	10.7	30	42	.27	.08			
20^{30}-21	11.1	11.5	-	3.7	10.4	25	44	.31	.09	13.9	68	-
21-21^{30}	10.6	11.0	-	3.2	10.8	22	47	.26	.09			
21^{30}-22	10.2	10.6	-	3.1	10.8	23	51	.25	.09	14.2	64	-
22-22^{30}	9.6	10.0	-	2.8	10.4	24	56	.21	.09			
22^{30}-23	9.2	9.6	-	3.0	10.6	28	64	.23	.09	13.8	68	230
23-23^{30}	9.1	9.4	-	3.0	10.5	33	64	.24	.09			
23^{30}-0	8.8	9.1	-	3.2	10.1	29	61	.27	.09	13.0	70	230
0-0^{30}	8.5	8.9	-	3.0	10.2	34	68	.24	.08			
0^{30}-1	8.2	8.6	-	3.1	10.5	36	74	.25	.09	13.0	70	215
1-1^{30}	7.9	8.3	-	2.8	10.7	36	84	.23	.08			
1^{30}-2	7.6	7.9	-	2.8	10.0	32	92	.23	.07	12.9	72	200
2-2^{30}	7.4	7.7	-	3.1	9.5	29	94	.27	.08			
2^{30}-3	7.3	7.6	-	2.9	9.7	32	96	.25	.07	12.8	76	195
3-3^{30}	7.1	7.4	-	2.5	9.3	32	97	.21	.06			

23/24 May 1977. Sunset at 19^{38} GMT. Sunrise at 3^{34} GMT.

Time	$T_{0.6}$	$T_{1.5}$	T_{200}	U_{10}	U_{200}	α_{20}	α_{200}	u_*	T_*	G	α_G	h
17^{30}-18	17.0	17.2	16.5	2.6	4.4	25	53	.22	.04	13.0	83	-
18-18^{30}	16.1	16.4	16.3	2.9	4.2	17	53	.25	.05			
18^{30}-19	15.4	15.9	16.6	3.1	4.0	12	67	.24	.08	12.6	83	-
19-19^{30}	13.9	14.5	16.7	2.7	3.9	12	72	.20	.09			
19^{30}-20	13.0	13.6	16.7	2.9	4.4	17	73	.21	.09	13.3	87	-
20-20^{30}	12.3	12.9	16.7	2.8	5.1	20	75	.21	.10			
20^{30}-21	11.6	12.3	16.7	2.6	5.7	26	75	.17	.09	12.8	90	-
21-21^{30}	11.7	12.1	16.6	3.3	6.9	34	74	.27	.11			
21^{30}-22	11.7	12.2	16.6	3.3	8.8	43	74	.26	.11	14.2	86	160
22-22^{30}	11.9	12.4	16.1	3.2	11.4	48	72	.24	.10			
22^{30}-23	12.1	12.6	15.8	3.3	14.6	55	78	-	-	14.7	84	180
23-23^{30}	12.0	12.5	15.5	3.6	14.2	65	78	.32	.11			
23^{30}-0	11.5	12.0	15.5	3.3	14.8	65	78	.28	.11	14.1	89	170
0-0^{30}	11.0	11.5	15.1	3.3	15.0	60	79	.29	.12			
0^{30}-1	10.7	11.2	15.4	3.6	14.5	57	84	.32	.12	14.2	89	170
1-1^{30}	10.5	10.9	16.0	3.5	12.9	58	88	.31	.11			
1^{30}-2	10.1	10.6	16.2	3.2	11.5	63	89	.26	.11	13.3	89	155
2-2^{30}	9.6	10.1	16.1	2.9	9.9	65	95	.23	.10			
2^{30}-3	9.2	9.7	15.6	3.0	9.1	58	103	.24	.11	12.5	88	160
3-3^{30}	8.3	8.9	15.5	2.6	8.0	46	105	.18	.09			

24/25 May 1977. Sunset at 19^{39} GMT. Sunrise at 3^{33} GMT.

Time	$T_{0.6}$	$T_{1.5}$	T_{200}	U_{10}	U_{200}	α_{20}	α_{200}	u_*	T_*	G	α_G	h
17^{30}-18	19.9	20.3	19.1	3.3	8.1	90	94	.30	.06	13.8	100	-
18-18^{30}	19.1	19.7	19.0	2.5	7.6	89	92	.20	.06			
18^{30}-19	18.1	18.9	19.0	2.6	8.3	82	86	.20	.08	14.1	97	-
19-19^{30}	16.8	17.9	18.8	2.3	8.1	76	78	.14	.08			
19^{30}-20	15.9	17.2	18.7	2.4	9.8	72	75	.14	.09	13.5	93	-
20-20^{30}	14.0	15.1	18.5	2.0	10.2	53	75	-	-			
20^{30}-21	13.0	14.3	18.3	1.7	10.6	57	75	-	-	14.1	88	-
21-21^{30}	12.3	14.0	18.0	2.0	11.0	54	75	-	-			
21^{30}-22	12.3	13.4	18.0	2.4	11.3	52	77	.10	.09	14.4	89	150
22-22^{30}	11.7	12.8	17.9	2.6	11.7	42	80	.13	.10			
22^{30}-23	11.0	12.0	17.7	2.7	12.0	32	83	.14	.10	15.1	88	160
23-23^{30}	10.2	10.9	17.2	2.9	12.5	33	83	.19	.11			
23^{30}-0	10.1	10.7	17.6	3.0	11.5	35	84	.21	.11	15.3	89	150
0-0^{30}	9.5	10.1	17.8	2.8	10.4	37	83	.20	.11			
0^{30}-1	9.4	10.1	17.5	2.6	10.9	41	89	.16	.10	14.0	95	140
1-1^{30}	8.8	9.6	16.5	2.3	11.0	38	91	.14	.08			
1^{30}-2	9.0	9.5	15.9	2.9	10.7	46	95	.22	.10	14.4	98	140
2-2^{30}	8.9	9.5	16.3	2.6	8.9	50	104	.19	.10			
2^{30}-3	8.6	9.3	16.0	2.6	8.5	54	104	.18	.10	13.8	98	170
3-3^{30}	8.6	9.1	16.3	2.8	8.0	55	104	.22	.10			

25/26 May 1977. Sunset at 19^{41} GMT. Sunrise at 3^{32} GMT.

Time	$T_{0.6}$	$T_{1.5}$	T_{200}	U_{10}	U_{200}	α_{20}	α_{200}	u_*	T_*	G	α_G	h
17^{30}-18	21.6	22.1	21.3	3.0	8.7	91	96	.27	.07	15.1	101	-
18-18^{30}	20.7	21.4	21.3	2.6	8.7	81	88	.20	.08			
18^{30}-19	19.4	20.4	21.4	2.7	10.0	75	83	.19	.10	15.2	102	-
19-19^{30}	18.0	19.0	21.2	2.7	10.4	66	79	.18	.11			
19^{30}-20	17.0	18.0	20.8	2.9	11.4	66	76	.20	.12	15.5	98	-
20-20^{30}	16.7	17.6	20.4	3.3	12.3	64	76	.26	.14			
20^{30}-21	16.5	17.1	20.0	3.6	13.7	64	80	.30	.14	15.2	102	-
21-21^{30}	16.2	16.9	19.7	3.5	14.9	67	83	.30	.13			
21^{30}-22	16.2	16.9	19.6	3.6	15.8	71	90	.30	.12	16.3	100	200
22-22^{30}	15.8	16.4	19.1	3.3	14.8	68	90	.26	.11			
22^{30}-23	14.9	15.4	18.2	3.6	13.2	59	78	.32	.13	17.3	99	230
23-23^{30}	14.8	15.2	17.9	4.1	14.9	59	83	.37	.12			
23^{30}-0	14.9	15.2	17.1	4.7	16.0	66	84	.45	.10	17.0	107	270
0-0^{30}	14.9	15.3	16.2	4.7	16.6	72	87	.45	.09			
0^{30}-1	14.8	15.2	15.7	5.0	16.7	76	90	.48	.09	17.8	103	360
1-1^{30}	14.5	14.9	15.0	4.5	15.2	75	89	.42	.08			
1^{30}-2	14.1	14.5	14.5	4.5	14.6	75	87	.42	.08	17.2	109	360
2-2^{30}	13.6	14.0	14.0	4.2	14.3	75	87	.39	.08			
2^{30}-3	13.2	13.5	13.4	4.2	14.1	76	87	.40	.08	18.1	112	300
3-3^{30}	12.8	13.1	12.8	4.2	13.5	75	85	.40	.08			

4/5 July 1977. Sunset at 20^{02} GMT. Sunrise at 3^{27} GMT.

Time	$T_{0.6}$	$T_{1.5}$	T_{200}	U_{10}	U_{200}	α_{20}	α_{200}	u_*	T_*	G	α_G	h
17^{30}-18	24.5	24.8	23.4	3.5	6.9	51	62	.34	.04	14.4	89	-
18-18^{30}	23.6	23.9	22.9	3.5	7.9	37	52	.31	.04			
18^{30}-19	22.6	23.0	22.5	4.1	9.1	35	46	.38	.06	14.5	90	-
19-19^{30}	21.7	22.1	22.3	3.6	9.2	34	49	.31	.07			
19^{30}-20	20.8	21.2	22.1	3.2	9.1	37	56	.27	.09	14.5	88	-
20-20^{30}	20.0	20.5	21.3	3.4	10.3	38	55	.28	.09			
20^{30}-21	19.6	20.1	20.6	3.0	10.9	51	65	.27	.08	12.2	84	-
21-21^{30}	18.9	19.4	19.9	3.2	10.5	52	65	.28	.09			
21^{30}-22	17.9	18.5	19.2	2.7	10.8	50	65	.20	.08	12.6	80	-
22-22^{30}	17.1	17.7	18.8	2.4	11.1	50	68	.16	.08			
22^{30}-23	16.6	17.2	18.5	2.8	11.9	48	68	.20	.09	11.7	81	-
23-23^{30}	16.1	16.7	18.2	2.5	11.8	46	68	.18	.08			
23^{30}-0	15.6	16.2	17.9	2.6	12.2	45	71	.18	.08	12.2	79	200
0-0^{30}	15.6	16.1	18.7	2.6	12.4	49	75	.20	.07			
0^{30}-1	15.0	15.6	18.6	2.1	12.0	51	73	.15	.06	11.3	81	200
1-1^{30}	14.4	15.0	18.2	2.4	12.2	42	75	.17	.07			
1^{30}-2	13.8	14.3	18.2	2.7	12.1	37	74	.20	.08	12.5	83	190
2-2^{30}	13.8	14.2	17.9	3.0	12.0	39	74	.26	.07			
2^{30}-3	13.5	13.7	17.9	3.3	12.6	39	76	.29	.08	11.9	91	190
3-3^{30}	13.0	13.4	17.9	2.6	12.8	40	79	.20	.08			

13/14 October 1977. Sunset at 16^{52} GMT. Sunrise at 6^{02} GMT.

Time	$T_{0.6}$	$T_{1.5}$	T_{200}	U_{10}	U_{200}	α_{20}	α_{200}	u_*	T_*	G	α_G	h
14^{30}-15	14.8	14.9	13.2	.9	1.8	319	304	0.03	.01	4.3	87	-
15-15^{30}	15.2	15.2	13.4	.5	.8	218	298	.03	.00			
15^{30}-16	14.6	14.9	13.4	.7	.8	282	299	-	-	5.2	84	-
16-16^{30}	13.6	14.2	13.2	.8	1.4	100	357	-	-			
16^{30}-17	12.3	13.2	13.1	1.4	1.4	53	72	-	-	4.9	92	-
17-17^{30}	10.4	11.4	13.0	1.2	1.5	44	74	-	-			
17^{30}-18	8.7	10.0	12.8	1.0	2.1	44	62	-	-	4.5	99	-
18-18^{30}	8.4	9.6	12.9	.8	2.2	41	75	-	-			
18^{30}-19	7.5	9.1	12.8	1.2	2.6	39	74	-	-	5.8	93	-
19-19^{30}	7.1	8.1	12.7	1.3	3.2	46	75	-	-			
19^{30}-20	6.8	8.3	12.6	1.4	3.3	55	82	-	-	5.3	103	-
20-20^{30}	6.7	8.7	12.8	1.7	3.1	72	102	-	-			
20^{30}-21	6.8	8.8	12.8	1.8	3.7	83	110	-	-	5.3	110	60
21-21^{30}	8.1	9.6	12.5	1.8	4.8	99	115	.07	.05			
21^{30}-22	7.2	8.8	12.6	1.3	4.9	100	124	-	-	5.9	108	70
22-22^{30}	5.9	6.9	12.6	1.3	5.0	108	132	-	-			
22^{30}-23	5.4	6.4	12.6	1.4	4.9	105	133	-	-	5.9	106	70
23-23^{30}	5.0	6.9	12.7	1.7	5.0	104	134	-	-			
23^{30}-0	5.3	7.8	12.7	1.6	4.7	96	130	-	-	6.0	118	75
0-0^{30}	6.4	8.1	12.7	1.9	4.8	88	121	-	-			
0^{30}-1	6.4	7.6	12.7	1.5	4.6	88	115	-	-	7.5	115	70
1-1^{30}	6.6	7.9	12.6	1.8	5.3	94	114	.07	.05			
1^{30}-2	6.7	7.7	12.6	1.9	5.6	81	110	.07	.05	7.5	115	70
2-2^{30}	6.8	7.7	12.7	2.1	6.1	82	110	.10	.07			
2^{30}-3	7.3	8.0	12.6	1.9	6.1	85	112	.11	.06	7.5	106	90
3-3^{30}	7.3	8.1	12.6	1.7	5.8	93	116	.09	.05			
3^{30}-4	7.0	7.8	12.7	1.6	5.5	85	117	.07	.04	6.7	112	100
4-4^{30}	6.6	7.5	12.7	1.8	5.7	86	126	.09	.05			
4^{30}-5	6.3	7.2	12.8	1.7	5.6	79	130	.08	.04	6.5	114	100
5-5^{30}	6.6	7.2	12.9	1.8	5.8	89	139	.11	.05			
5^{30}-6	6.9	7.1	12.9	2.1	5.3	98	137	.18	.05	5.7	120	120
6-6^{30}	6.9	6.9	12.9	2.5	5.4	105	129	.25	.02			

3/4 December 1977. Sunset at 15^{31} GMT. Sunrise at 7^{29} GMT.

Time	$T_{0.6}$	$T_{1.5}$	T_{200}	U_{10}	U_{200}	α_{20}	α_{200}	u_*	T_*	G	α_G	h
13^{30}-14	2.8	2.9	1.1	3.3	7.4	99	108	.28	.02	12.9	109	-
14-14^{30}	2.4	2.6	1.1	3.1	8.1	100	110	.25	.03			
14^{30}-15	2.0	2.2	.8	3.8	8.5	91	108	.31	.04	13.1	115	-
15-15^{30}	1.9	2.1	.5	4.3	8.6	101	108	.36	.03			
15^{30}-16	1.4	1.7	.5	2.8	7.3	95	106	.23	.04	12.4	122	-
16-16^{30}	.8	1.1	.5	3.0	8.8	83	100	.23	.06			
16^{30}-17	.5	.8	.4	3.5	9.7	85	101	.28	.06	12.8	130	-
17-17^{30}	.5	.7	.2	4.4	11.9	86	101	.37	.05			
17^{30}-18	.2	.4	.7	4.3	12.3	83	107	.37	.05	13.5	132	205
18-18^{30}	.0	.2	1.4	4.2	13.7	85	114	.36	.04			
18^{30}-19	- .1	.1	1.4	4.0	15.1	88	116	.35	.05	13.8	132	200
19-19^{30}	.0	.2	1.6	3.9	15.6	90	116	.33	.05			
19^{30}-20	.0	.2	2.8	4.0	14.8	93	121	.34	.05	14.6	130	180
20-20^{30}	- .1	.2	3.3	4.2	14.3	94	125	.36	.05			
20^{30}-21	- .1	.1	3.4	4.2	13.5	95	122	.37	.05	14.6	139	150
21-21^{30}	- .1	.1	3.5	4.6	14.8	94	118	.39	.05			
21^{30}-22	- .1	.1	3.5	4.3	15.4	95	116	.37	.05	15.6	137	160
22-22^{30}	.1	.3	3.3	4.4	16.8	94	113	.38	.05			
22^{30}-23	.3	.5	3.2	4.6	18.1	92	113	.39	.05	16.4	131	205
23-23^{30}	.2	.5	3.1	4.6	17.6	92	112	.39	.05			
23^{30}-0	.2	.4	3.5	4.7	17.3	92	112	.40	.05	16.9	131	210
0-0^{30}	.4	.6	3.5	5.3	18.1	91	111	.46	.05			
0^{30}-1	.4	.7	3.1	5.1	18.9	92	109	.43	.05	18.1	128	205
1-1^{30}	.6	.8	3.7	5.3	19.0	91	111	.46	.05			
1^{30}-2	.5	.7	3.7	5.3	19.6	94	111	.45	.05	19.0	127	210
2-2^{30}	.5	.7	3.3	5.7	20.4	93	108	.49	.05			
2^{30}-3	.8	1.0	3.1	5.6	20.4	92	104	.49	.05	19.4	124	230
3-3^{30}	1.0	1.3	3.2	5.3	19.4	88	104	.46	.05			
3^{30}-4	1.3	1.5	2.7	5.5	18.8	87	102	.48	.06	20.4	119	260
4-4^{30}	1.4	1.7	2.2	5.4	18.1	83	101	.46	.06			
4^{30}-5	1.4	1.6	2.1	5.6	18.1	81	101	.47	.06	19.1	119	250
5-5^{30}	1.6	1.8	2.1	6.0	18.1	83	102	.51	.06			
5^{30}-6	1.6	1.8	1.9	5.7	17.8	92	106	.49	.06	18.8	120	240
6-6^{30}	1.2	1.4	2.3	5.9	18.6	89	110	.51	.05			
6^{30}-7	1.0	1.2	1.5	6.2	17.7	86	107	.53	.05	19.1	124	250
7-7^{30}	.7	1.0	.7	5.5	16.5	88	103	.47	.05			

4/5 December 1977. Sunset at 15^{31} GMT. Sunrise at 7^{30} GMT.

Time	$T_{0.6}$	$T_{1.5}$	T_{200}	U_{10}	U_{200}	α_{20}	α_{200}	u_*	T_*	G	α_G	h
13^{30}-14	2.7	2.9	1.3	4.7	12.2	98	108	.40	.03	16.4	140	-
14-14^{30}	2.5	2.6	1.3	5.5	13.7	93	106	.48	.03			
14^{30}-15	2.1	2.4	1.3	5.0	14.1	92	104	.43	.04	15.9	140	-
15-15^{30}	1.8	2.0	1.3	4.1	13.9	99	106	.35	.05			
15^{30}-16	1.5	1.7	1.3	4.5	14.5	92	104	.39	.05	15.3	141	-
16-16^{30}	1.4	1.6	1.5	5.2	16.0	94	107	.45	.06			
16^{30}-17	1.2	1.5	1.5	4.9	15.9	94	111	.42	.05	14.5	139	-
17-17^{30}	1.0	1.2	1.5	5.1	16.2	101	114	.43	.05			
17^{30}-18	.6	.9	1.6	4.4	16.8	98	116	.38	.05	14.2	137	280
18-18^{30}	.6	.8	1.5	4.5	16.6	98	117	.38	.05			
18^{30}-19	.3	.5	1.7	4.1	17.1	98	121	.35	.06	14.1	141	280
19-19^{30}	.3	.6	1.5	4.3	16.9	102	126	.36	.06			
19^{30}-20	.1	.4	.9	3.7	15.4	105	127	.31	.05	13.9	140	280
20-20^{30}	- .2	.1	1.0	4.6	15.9	105	130	.33	.06			
20^{30}-21	- .4	- .1	.6	4.5	15.7	104	129	.39	.06	14.9	141	290
21-21^{30}	- .4	- .1	.5	4.5	16.8	107	130	.38	.06			
21^{30}-22	- .1	.2	.3	4.6	16.9	108	128	.39	.06	13.8	148	290
22-22^{30}	- .0	.3	.1	5.4	17.2	117	128	.46	.06			
22^{30}-23	- .2	.0	.0	5.1	16.7	123	130	.43	.06	11.6	143	320
23-23^{30}	- .4	- .1	- .3	4.8	15.2	120	130	.39	.05			
23^{30}-0	- .7	- .4	- .5	4.5	14.5	118	133	.37	.06	11.9	143	380
0-0^{30}	-1.0	- .7	- .7	3.8	14.0	111	133	.31	.05			
0^{30}-1	-1.4	-1.1	- .8	3.4	13.5	102	133	.28	.05	12.2	131	390
1-1^{30}	-1.6	-1.3	- .9	3.4	12.8	100	133	.28	.05			
1^{30}-2	-1.6	-1.4	-1.0	3.5	12.4	95	131	.29	.05	13.2	122	390
2-2^{30}	-1.8	-1.6	-1.0	3.7	12.4	89	128	.30	.06			
2^{30}-3	-1.9	-1.7	- .9	4.0	12.7	94	129	.34	.05	11.2	138	390
3-3^{30}	-2.1	-1.9	- .8	4.1	13.1	98	131	.34	.05			
3^{30}-4	-2.6	-2.4	-1.1	3.5	14.1	99	133	.30	.05	10.5	140	380
4-4^{30}	-2.9	-2.7	-1.2	3.5	14.3	99	133	.29	.04			
4^{30}-5	-3.0	-2.7	-1.4	3.8	14.7	105	133	.32	.05	9.3	130	350
5-5^{30}	-2.5	-2.2	-1.4	3.9	14.5	113	134	.33	.06			
5^{30}-6	-2.3	-2.0	-1.3	4.2	13.5	116	140	.35	.05	9.4	121	300
6-6^{30}	-2.4	-2.1	-1.1	3.9	12.4	107	141	.32	.05			
6^{30}-7	-2.7	-2.4	-1.4	3.6	12.4	117	148	.29	.05	8.9	141	260
7-7^{30}	-2.9	-2.6	-0.7	3.4	12.1	112	153	.27	.05			

8/9 December 1977. Sunset at 15^{29} GMT. Sunrise at 7^{35} GMT.

Time	$T_{0.6}$	$T_{1.5}$	T_{200}	U_{10}	U_{200}	α_{20}	α_{200}	u_*	T_*	G	α_G	h
13^{30}-14	11.5	11.7	10.6	6.3	12.2	168	180	.51	.07	12.7	180	-
14-14^{30}	10.7	11.0	10.6	5.8	12.5	165	179	.45	.10			
14^{30}-15	9.8	10.2	10.7	4.7	11.8	161	180	.34	.13	17.4	188	-
15-15^{30}	9.5	10.0	10.7	4.0	11.3	155	186	.28	.11			
15^{30}-16	8.8	9.4	10.8	4.3	12.0	147	184	.30	.13	10.9	181	-
16-16^{30}	7.8	8.5	10.8	3.5	12.2	140	185	.23	.12			
16^{30}-17	7.3	8.0	10.7	3.3	12.2	134	185	.23	.11	9.4	167	180
17-17^{30}	7.2	7.8	10.8	3.6	11.5	136	191	.25	.12			
17^{30}-18	6.9	7.5	10.8	3.8	11.1	146	191	.25	.12	8.1	180	170
18-18^{30}	6.3	7.0	10.7	3.0	10.8	132	190	.20	.10			
18^{30}-19	6.5	7.0	10.5	3.5	10.9	130	186	.26	.10	8.8	178	160
19-19^{30}	6.3	6.7	10.3	3.9	11.1	136	186	.29	.11			
19^{30}-20	6.4	6.8	10.2	4.2	11.3	145	191	-	-	7.3	177	160
20-20^{30}	5.8	6.3	10.1	3.7	10.7	146	195	.25	.11			
20^{30}-21	5.4	6.0	9.9	3.1	10.5	133	194	.21	.10	8.0	176	160
21-21^{30}	5.5	5.9	9.8	3.4	10.2	134	194	.25	.10			
21^{30}-22	4.9	5.5	9.6	3.0	9.9	129	197	.20	.09	7.2	170	140
22-22^{30}	4.8	5.4	9.5	2.9	9.4	122	196	.20	.09			
22^{30}-23	4.7	5.1	9.4	3.2	9.3	125	195	.23	.09	7.3	176	140
23-23^{30}	4.4	4.8	9.4	3.5	9.5	128	195	.26	.10			
23^{30}-0	4.7	4.9	9.4	3.7	9.8	130	198	.29	.09	8.0	185	150
0-0^{30}	4.8	5.0	9.5	3.9	9.9	130	200	-	-			
0^{30}-1	4.5	4.8	9.8	3.6	9.7	130	203	.29	.08	7.8	178	170
1-1^{30}	4.1	4.4	9.3	3.2	10.6	134	207	.24	.08			
1^{30}-2	4.1	4.4	9.5	3.3	10.1	129	207	.26	.07	6.1	172	190
2-2^{30}	3.5	3.8	9.8	2.8	9.5	138	207	.24	.08			
2^{30}-3	3.1	3.5	9.6	2.8	10.2	146	212	.17	.08	6.5	175	180
3-3^{30}	2.8	3.5	9.8	2.4	9.0	148	218	.13	.07			
3^{30}-4	3.1	3.7	9.7	3.1	8.8	151	213	.17	.10	6.1	185	130
4-4^{30}	3.3	3.8	9.4	3.2	9.5	147	213	.19	.10			
4^{30}-5	2.8	3.4	9.0	2.9	11.3	157	220	.16	.09	5.2	185	140
5-5^{30}	2.1	3.1	8.4	2.0	12.1	153	223	.08	.05			
5^{30}-6	1.7	2.9	7.9	2.4	12.1	155	225	.10	.07	4.2	182	160
6-6^{30}	2.1	3.0	7.8	2.7	11.7	155	230	.13	.08			
6^{30}-7	2.5	3.2	8.2	2.8	11.0	153	231	.14	.09	5.5	194	160
7-7^{30}	2.6	3.2	8.3	2.9	10.2	154	229	.16	.09			

References

André, J.C., G. de Moor, P. Lacarrère, G. Therry and R. du Vachat, 1978: Modeling the 24-hour evolution of the mean and turbulent structures of the planetary boundary layer. J. Atmos. Sci., 35, 1861-1883.

Arya, S.P.S., 1975: Geostrophic drag and heat transfer relations for the atmospheric boundary layer. Quart. J. Roy. Meteor. Soc., 101, 147-161.

Arya, S.P.S., 1977: Suggested revisions to certain boundary layer parameterization schemes used in atmospheric circulation models. Mon. Wea. Rev., 105, 215-227.

Arya, S.P.S., 1978: Comparative effects of stability, baroclinity and scale-height ratio on drag laws for the atmospheric boundary layer. J. Atmos. Sci., 35, 40-46.

Arya, S.P.S., and J.C. Wyngaard, 1975: Effect of baroclinicity on wind profiles and the geostrophic drag law for the convective planetary boundary layer. J. Atmos. Sci., 32, 767-778.

Arya, S.P.S., and A. Sundararajan, 1976: An assessment of proposed similarity theories for the atmospheric boundary layer. Boundary-Layer Meteorol., 10, 149-166.

Barr, S. and C.W. Kreitzberg, 1975: Horizontal variability and boundary layer modeling. Boundary-Layer Meteor., 8, 163-172.

Blackadar, A.K., 1957: Boundary layer wind maxima and their significance for the growth of nocturnal inversions. Bull. Amer. Meteor. Soc., 38, 283-290.

Blackadar, A.K., 1976: Modeling the nocturnal boundary layer. Preprints 3rd symposium on atmospheric turbulence, diffusion and air quality, Rahleigh, N.C., Amer. Meteor. Soc., 46-49.

Blackadar, A.K., and H. Tennekes, 1968: Asymptotic similarity in neutral barotropic planetary boundary layers. J. Atmos. Sci., 25, 1015-1020.

Bodin, S.V., 1976: An unsteady one-dimensional atmospheric boundary layer model. Paper presented at the WMO-symposium on the interpretation of numerical weather prediction products, Warsaw, 11-16 October.

Brost, R.A. and J.C. Wyngaard, 1978: A model study of the stably stratified planetary boundary layer. J. Atmos. Sci., 35, 1427-1440.

Busch, N.E., 1973: On the mechanics of atmospheric turbulence. Workshop on Micrometeorology, Ed. D.A. Haugen, Amer. Meteor. Soc., 1-66.

Businger, J.A. and S.P.S. Arya, 1974: Height of the mixed layer in the stably stratified planetary boundary layer. Advances in Geophysics, Vol. 18A, Academic Press, 73-92.

Businger, J.A., J.C. Wyngaard, Y. Izumi and E.F. Bradley, 1971: Flux-profile relationships in the atmospheric surface layer. J. Atmos. Sci., 28, 181-189.

Carson, D.J., 1973: The development of a dry inversion-capped convectively unstable boundary layer. Quart. J. Roy. Meteor. Soc., 99, 450-467.

Cats, G.J., 1977: The calculation of the geostrophic wind. Royal Netherlands Meteorological Institute, Scientific Report, 77-2. (In Dutch).

Caughey, S.J., J.C. Wyngaard and J.C. Kaimal, 1979: Turbulence in the evolving stable boundary layer. J. Atmos. Sci., 36, 1041-1052.

Clarke, R.H., and G.D. Hess, 1974: Geostrophic departure and the functions A and B of Rossby-number similarity theory. Boundary-Layer Meteorol., 7, 267-287.

Delage, Y., 1974: A numerical study of the nocturnal atmospheric boundary layer. Quart. J. Roy. Meteor. Soc., 100, 351-364.

Djolov, G.D., 1974: Modeling of interdependent diurnal variation of meteorological elements in the boundary layer. Chidrologija i meteorologija, Sofia, 13, 3-19.

Driedonks, A.G.M., H. van Dop and W.H. Kohsiek, 1978: Meteorological observations on the 213 m mast at Cabauw in the Netherlands. Preprints 4th Symposium on Meteorological Observations and Instrumentation, Denver, Amer. Meteor. Soc., 41-46.

Elzasser, W.M. and M.F. Culbertson, 1960: Atmospheric radiation tables. Meteorological Monographs, Vol. 4, No. 23.

Frisch, A.S. and S.F. Clifford, 1974: A study of convection capped by a stable layer using Doppler Radar and acoustic echo sounders. J. Atmos. Sci., 31, 1622-1628.

Haltiner, G.J., 1971: Numerical Weather Prediction. New York, John Wiley and Sons, Inc., 317 pp.

Hess, G.D., 1973: On Rossby-number similarity theory for a baroclinic planetary boundary layer. J. Atmos. Sci., 30, 1722-1723.

Hicks, B.B., 1978: Some limitations of dimensional analysis and power laws. Boundary-Layer Meteorol., 14, 567-569.

Keller, H.B., 1971: A new difference scheme for parabolic problems. Numerical solution of partial differential equations - III, New York, Academic Presse, 327-350.

Mahrt, L., R.C. Heald, D.H. Lenshow and B.B. Stankov, 1979: An observational study of the structure of the nocturnal boundary layer. Bound.-Layer Meteor., 17, 247-264.

Mahrt, L., 1981: Modelling the depth of the stable boundary layer. Submitted to Bound.-Layer Meteor.

Melgarejo, J.W. and J.W. Deardorff, 1974: Stability functions for the boundary-layer resistance laws based upon observed boundary-layer heights. J. Atmos. Sci., 31, 1324-1333.

Nieuwstadt, F.T.M., 1978: The computation of the friction velocity u_*, and the temperature scale T_* from temperature and wind velocity profiles by least square methods. Bound.-Layer Meteor., 14, 235-246.

Nieuwstadt, F.T.M., 1980a: A rate equation for the inversion height in a nocturnal boundary layer. J. Appl. Meteor., Chapter IV of this dissertation.

Nieuwstadt, F.T.M., 1980b: The steady-state height and resistance laws of the nocturnal boundary layer: Theory compared with Cabauw observations. Bound.-Layer Meteor., Chapter III of this dissertation.

Nieuwstadt, F.T.M. and A.G.M. Driedonks, 1979: The nocturnal boundary layer: a case study compared with model calculations. J. Appl. Meteor., 18, 1397-1405, Chapter II of this dissertation.

Rao, K.S., and H.F. Snodgrass, 1979: Some parameterizations of the nocturnal boundary layer. Boundary-Layer Meteorol., 17, 15-28.

SethuRaman, S., 1977: The observed generation and breaking of atmospheric gravity waves over ocean. Boundary-Layer Meteor., 12, 331-349.

Smeda, M., 1979: Incorporation of planetary boundary-layer processes into numerical forecasting models. Bound.-Layer Meteor., 16, 115-129.

Tennekes, H., 1973a: Similarity laws and scale relations in planetary boundary layers. Workshop on Micrometeorology, D.A. Haugen, ed., Amer. Meteor. Soc..

Tennekes, H, 1973b: A model for the dynamics of the inversion above a convective boundary layer. J. Atmos. Sci., 30, 558-567.

Thorpe, A.J. and T.H. Guymer, 1977: The nocturnal jet. Quart. J. Roy. Meteor. Soc., 103, 633-653.

Ulden, A.P. van, J.G. van der Vliet and J. Wieringa, 1976: Temperature and wind observations at heights from 2 to 200 m at Cabauw 1973. Royal Netherlands Meteorological Institute, Scientific Report 76-7.

Wieringa, J., 1967: Evaluation and design of wind vanes. J. Appl. Meteor., 6, 1114-1122.

Wyngaard, J.C., 1975: Modeling the planetary boundary layer - extension to the stable case. Bound.-Layer Meteor., 9, 441-460.

Yamada, T., 1976: On the similarity functions A, B and C of the planetary boundary layer. J. Atmos. Sci., 33, 781-787.

Yamada, T., 1979: Prediction of the nocturnal surface inversion height. J. Appl. Meteor., 18, 526-531.

Yu, T.W., 1977: A comparative study on parameterization of vertical turbulent exchange processes. Mon. Wea. Rev., 105, 57-66.

Yu, T.W., 1978: Determining height of the nocturnal boundary layer. J. Appl. Meteor., 17, 28-33.

Zeman, O., 1979: Parameterization of the dynamics of stable boundary layers and nocturnal jets. J. Atmos. Sci., 36, 792-804.

Zilitinkevich, S.S., 1972: On the determination of the height of the Ekman boundary layer. Bound.-Layer Meteor., 3, 141-145.

Zilitinkevich, S.S., 1975: Resistance laws and prediction equations for the depth of the planetary boundary layer. J. Atmos. Sci., 32, 741-752.

Zilitinkevich, S.S., and J.W. Deardorff, 1974: Similarity theory for the planetary boundary layer of time-dependent height. J. Atmos. Sci., 31, 1449-1452.

Samenvatting

Het onderwerp van deze dissertatie is de atmosferische grenslaag, waaronder wordt verstaan de onderste laag van de atmosfeer. Enerzijds tracht grenslaag onderzoek een antwoord te vinden op puur meteorologische vragen, anderzijds dient het ook een meer algemeen belang. De meeste activiteiten van de mens vinden namelijk plaats in de grenslaag, zodat de resultaten van grenslaag onderzoek direct toepasbaar zijn op velerlei gebied: luchtvaart, verspreiding van luchtverontreiniging, landbouw, windhinder, windenergie, stedelijke planologie en lucht-zee interactie.

We zullen ons hier beperken tot de grenslaag tijdens een heldere nacht. Een karakteristiek kenmerk van deze nachtelijke grenslaag is een zogenaamde temperatuur inversie: d.w.z. de temperatuur neemt toe met de hoogte. Dit profiel is een gevolg van de afkoeling van het aardoppervlak tijdens de nacht door straling.

Een dergelijke temperatuur inversie heeft dynamische consequenties: de nachtelijke grenslaag is stabiel. Verstoringen in de stroming, turbulentie genoemd, worden gedempt. Dit aspect bepaalt voor het grootste gedeelte de structuur van de nachtelijke grenslaag. Een algemene bespreking van deze verschijnselen, op basis van atmosferische waarnemingen en hun fysische interpretatie, vormt het onderwerp van hoofdstuk I.

In hoofdstuk II wordt de structuur van de nachtelijke grenslaag beschreven aan de hand van een numerieke oplossing van de bewegingsvergelijkingen. De resultaten van dit model worden uitgebreid vergeleken met metingen die zijn verkregen met een 200-m hoge meteorologische meetmast. Kwalitatief zijn deze waarnemingen in overeenstemming met de modelresultaten. Met name geeft het rekenmodel een juiste beschrijving van de grenslaaghoogte.

In de volgende hoofdstukken wordt het onderzoek geconcentreerd op deze grenslaaghoogte. In hoofdstuk III wordt onderzocht of de grenslaag als stationair beschouwd kan worden. Hiertoe wordt een theoretische uitdrukking voor de stationaire grenslaaghoogte afgeleid. Een uitgebreide vergelijking met waarnemingen leert dat voor zeer stabiele omstandigheden de gevonden expressie niet geldig is. De conclusie is dat de grenslaag niet als stationair kan worden beschouwd.

In hoofdstuk III wordt tevens aandacht besteed aan een juiste definitie van de nachtelijke grenslaaghoogte. Twee definities worden in de regel gebruikt: 1) de hoogte van de inversie in het temperatuur profiel; 2) de dikte van de turbulente grenslaag. De tweede definitie verdient de voorkeur, omdat het temperatuurprofiel sterk wordt beïnvloed door niet-grenslaag processen zoals straling. Dit laatste aspect wordt nader belicht in hoofdstuk IV.

Op basis van de conclusie van hoofdstuk III wordt in hoofdstuk V een vergelijking afgeleid voor een niet-stationaire grenslaaghoogte De vorm is een lineaire relaxatie vergelijking. Deze beschrijft een proces waarbij de grenslaaghoogte tot een evenwichtshoogte nadert. De tijdschaal in dit relaxatie proces is echter zeer groot, zodat de grenslaaghoogte zich slechts zeer langzaam ontwikkelt.

De belangrijkste conclusies kunnen als volgt worden samengevat:

- Een uitdrukking voor de grenslaaghoogte gebaseerd op een hypothese van stationariteit wordt niet bevestigd door waarnemingen.
- Straling beïnvloedt het temperatuurprofiel, zodat de inversie hoogte groter wordt dan de dikte van de turbulente grenslaag.
- Het quasi-stationaire gedrag van de grenslaaghoogte, dat uit waarnemingen volgt, wordt verklaard door de grote tijdschaal die de ontwikkeling van de grenslaag beheerst.